UNIVERSITY OF CALGARY

Toward Practical Solid-State Based Quantum Memories

by

Khabat Heshami

A THESIS

SUBMITTED TO THE FACULTY OF GRADUATE STUDIES

IN PARTIAL FULFILLMENT OF THE REQUIREMENTS FOR THE

DEGREE OF DOCTOR OF PHILASOPHY

DEPARTMENT OF PHYSICS AND ASTRONOMY

CALGARY, ALBERTA

May, 2013

Abstract

Quantum information processing promises to have transformative impacts on information and communication science and technology. Photonic implementation of quantum information processing is among successful candidates for implementation of quantum computation and is an essential part of quantum communication. Linear optical quantum computation, specifically the KLM scheme [1], and quantum repeaters [2, 3] are prominent candidates for practical photonic quantum computation and long-distance quantum communication. Quantum memories for photons are key elements for any practical implementation of these schemes. Practical quantum memories require theoretical and experimental investigations into quantum memory protocols and physical systems for implementations.

The present thesis is focused on studying new approaches toward practical solid-state based quantum memories. First, I present a proposal for a new quantum memory protocol called the controllable-dipole quantum memory [4]. It represents a protocol, in a two-level system, without any optical control that is shown to be equivalent to the Raman type-quantum memory. Then I include our studies on the quantum memory based on the refractive index modulation of the host medium [5]. It is shown that it can resemble the gradient echo quantum memory without a spatial gradient in the external field. These two protocols can be implemented in rare-earth doped crystals. With regards to using new physical systems, I present a proposal based on nitrogen vacancy centers [6]. This may pave the way toward micron-scale on-chip quantum memories that may contribute to the implementation of integrated quantum photonics. Finally, I studied the precision requirements for the spin echo technique [7]. This technique is necessary to extend the storage time in solid-state quantum memories, in which the coherence times are limited by spin inhomogeneous broadening.

List of published papers and papers to be submitted

- K. Heshami, C. Healey, B. Khanaliloo, V. Acosta, C. Santori, P. Barclay and C. Simon, *Optical quantum memory in nitrogen vacancy ensemble in diamond coupled to a cavity*, In preparation (2013).

- H. Kaviani, M. Khazali, R. Ghobadi, E. Zahedinejad, K. Heshami and C. Simon, *Quantum storage and retrieval of light by sweeping the atomic frequency*, preprint arXiv:13043166 (2013).

- J. Clark, K. Heshami and C. Simon, *Photonic quantum memory in two-level ensembles based on modulating the refractive index in time: Equivalence to gradient echo memory*, Physical Review A **86**, 013833 (2012).

- K. Heshami, A. Green, Y. Han, A. Rispe, E. Saglamyurek, N. Sinclair, W. Tittel and C. Simon, *Controllable-dipole quantum memory*, Physical Review A **86**, 013813 (2012).

- K. Heshami, N. Sangouard, J. Minar, H. de Riedmatten and C. Simon, *Precision requirements for spin-echo-based quantum memories*, Physical Review A **83**, 032315 (2011).

- Y. Han, B. He, K. Heshami, C.-Z. Li and C. Simon, *Quantum repeaters based on Rydberg-blockade-coupled atomic ensembles*, Physical Review A **81**, 052311 (2010).

Acknowledgements

First, I am grateful and indebted to my supervisor, Dr. Christoph Simon, for his constant help, support and guidance in every step of my PhD studies. His guidance based on his intuition and deep insight was the key to success in every project. Discussion with him has always helped me to find the right path over the last four years. Pieces of advice that I received from Christoph will significantly impact my performance in my future career. I also would like to thank Dr. Wolfgang Tittel, Dr. Barry Sanders and Dr. Paul Barclay for their support and constructive comments to refine my approach toward a better understanding of my research.

Life of any international graduate student could have been miserable without the valuable moments with exceptional friends. I would like to thank my friends Jalal, Sadegh, Saleh, Farid, Hamidreza, Nasrin, Mahdi, Neda, Kianoosh and many others at the University of Calgary for sharing these moments with me.

I would like to acknowledge working with my collaborators, specifically Adam Green. I also have been fortunate to work with Yang Han, Arnaud Rispe, Dr. Erhan Saglamyurek, Niel Sinclair, Hamidreza Kaviani, Mohammad Khazali, James Clark, Behzad Khanaliloo, Chris Healey and Dr. Bing He at the University of Calgary. It has been a pleasant experience to work, remotely, with Dr. Nicolas Sangouard, Dr. Hugues de Riedmatten, Dr. Victor Acosta and Dr. Charles Santori.

Meeting Adam D'Souza, Dr. Daniel Oblak and Joshua Slater during my PhD have been an absolute pleasure. My pleasant experience at the Department of Physics and Astronomy at the University of Calgary could have been spoiled without constant support of the kind graduate administrator of the department, Tracy Korsgaard.

At last but not the least, I want to thank my family for all their support. Without sacrifices that have been made by my parents, Ala and Marzieh, and my sisters, Seiran and Neda, I could not pursue any of my goals in life. Above all, words cannot express my gratitude to God for the support and love that I receive, each and every day, from my wife Arina.

Table of Contents

List of Tables

List of Figures and Illustrations

List of Symbols, Abbreviations and Nomenclature

Symbol	Definition
AFC	Atomic Frequency Comb
CD	Controllable-Dipole
CRIB	Controlled Reversible Inhomogeneous Broadening
DLCZ	Duan-Lukin-Cirac-Zoller
EIT	Electromagnetically Induced Transparency
GEM	Gradient Echo Memory
KLM	Knill-Laflamme-Milburn
NV	Nitrogen Vacancy
QND	Quantum Non-Demolition

Chapter 1

Introduction

1.1 Overview

Quantum mechanics introduced a fundamental evolution to information science through quantum information processing. Quantum computation was introduced by David Deutsch in 1985 [8], in which its potential in performing certain probabilistic tasks based on the "quantum parallelism" has been discussed. The concept that has led to the invention of a quantum algorithm, by Peter Shor in 1994 [9], for factoring integer numbers on a quantum computer that takes a number of steps which is polynomial in the input size (length of the integer number). This algorithm provides an exponential speedup compared to the best classical algorithms for factoring. Earlier in 1984 [10], Bennett and Brassard introduced a protocol for secure private key distribution based on the quantum state of the photons as transmitters. In their scheme, the fundamental quantum properties of the information carriers avoid eavesdropping without inducing detectable disturbance to the quantum state of the transmitter, which is a prominent advantage compared to its classical counterpart. These steps have led to more explorations that promise striking impacts on the classical information science and established the quantum computation and communication sciences.

Demonstration of quantum computation and communication schemes yielded several implementation systems. Among these, photons have been one of the promising candidates for implementation of quantum computation and are the most natural choice for quantum communication tasks. Photons can carry information using their different degrees of freedom, such as polarization, path, frequency mode, transverse mode and temporal mode. The coherence times are long, due to the weak coupling of the photons to the environment.

Implementation of deterministic quantum computation schemes requires two-qubit gates, which they necessitate non-linear interaction between weak optical pulses in the photonic implementa-

tions. This has been a long lasting challenge in experimental quantum optics. However, in 2001, Knill, Laflamme and Milburn (KLM) introduced a scheme for quantum computation with linear optics [1]. Their scheme only requires linear optical elements, such as beam splitters and phase shifters, in addition to single-photon sources, photo-detectors for single-photons and feedback from the photo-detectors. The required non-linearity is hidden in the photo-detectors, and their techniques effectively transfer this non-linearity back to the gates. The implementation of this scheme needs reliable single-photon sources. Realizing deterministic single-photon sources is challenging. However, quantum memories for light have been proposed to realize deterministic single-photon sources, see Sec. (1.2.5).

This is not the only application of quantum memories for photons as they can be used to synchronize events in photonic quantum architectures that can result in significant improvements in performance, see [11]. In this regard, quantum memories are the key element in long-distance quantum communication based on quantum repeaters. Quantum repeaters are invented to amplify quantum communication distances as they overcome the exponential photon loss with respect to the distance [2, 3, 12]. This is achieved by generating entangled pairs between the internal links of the quantum repeater. Then one can distribute the entanglement over longer distances by applying the entanglement swapping operation between neighboring links. This cannot be implemented efficiently without quantum memories for photons to synchronize entanglement generation and distribution across different links, see Sec. (1.2.5).

Both linear optical quantum computation and long-distance quantum communication rely on the implementation of efficient quantum memories for photons. These motivated my studies that have been presented in this thesis. In the following, I introduce the quantum memory in detail and explain its applications in single-photon sources and quantum repeaters.

1.2 Quantum memories for light

A quantum memory for light is a device that can faithfully store and re-emit photons. Quantum memories are physical systems that are operating based on quantum memory protocols. The physical system can be comprised of atoms, ions or defects in solids that are able to interact with photons. Some of the properties of a quantum memory, such as storage time, are mainly determined by the coherence properties of the physical system. Other specifications, such as efficiency or multimode capacity of memory as a function of optical depth, are determined by the protocol.

The thesis contributes to the development of memory protocols and physical systems for implementations of quantum memories. To explore this in more detail I must first introduce tools to assess the performance of a quantum memory. Below, I introduce the figures of merit for quantum memories. Followed by the discussion of the quantum memory protocols, physical systems, state-of-the-art and applications for quantum memories are discussed.

1.2.1 Figures of merit

Fidelity is a commonly used criterion for assessing the performance of a quantum memory. In order to be able to define a proper measure for fidelity, one needs to understand the application of the quantum memory. Here, I focus on quantum memories for single-photons. For this purpose, conditional fidelity is a proper measure for faithfulness of the quantum memory. The conditional fidelity is the overlap of the state of the re-emitted photon with the state of the input photon that is conditioned on the successful retrieval of the single-photon. Assuming that the quantum state of the single-photon is pure, the overlap of the single-photon wave functions is equivalent to the general definition of the quantum fidelity. It has to be noted that poor fidelity due to a unitary evolution applied by quantum memories may arise in some cases. This does not rule out practicality of the quantum memory in some of applications (*e.g.* quantum repeaters).

The fidelity is mainly determined by the quantum memory protocol, and limitations that come from the physical system and implementation. I will describe these limitations when the physical

systems are discussed.

Efficiency is a key feature for quantum memories as it can affect performance of possible applications, such as single photon sources that are based on quantum memories. For single photon storage and retrieval, the efficiency can be described based on the single photon probabilities. The storage efficiency could be defined as one minus the probability of having a photon at the output during the storage, if transmission is the only loss channel. Similarly, the retrieval efficiency is the probability of retrieving a photon given that one photon is successfully stored, see chapters (2,4). High efficiency is an essential feature for quantum memories to be used as single photon sources and elements of a long-distance quantum communication.

The efficiency depends on specifications of the physical systems that are to be used for implementation of the quantum memory. For quantum memories that are based on an ensemble of atoms, increasing the optical depth enhances the coupling between the photon and the memory. Cavities also can enhance the efficiency. The efficiency with respect to optical depth scales differently in different protocols. This is further discussed with some of the examples, later in the thesis.

Storage time is one of the crucial aspects of quantum memories. Quantum memories are developed for synchronization of different events in implementations of quantum information processing. Performance of some of the applications such as quantum repeaters rely on the storage time of quantum memories. In quantum repeaters, quantum memories are crucial to store the entanglement at different links. The minimum storage time is proportional to L_0/c, where L_0 is the length of one link. It has been shown that for storage times of $T_s \ll L/c$, where L is the total communication distance, the rate of entanglement distribution degrades exponentially in $\sqrt{L}$ as opposed to the polynomial scaling with L for quantum memories with infinitely long storage time, see [13].

In general, the storage time is limited by relevant coherence times of the atomic level configuration that are used for the storage. In solid-state systems, where the optical coherence is stored in spin states, the spin inhomogeneous broadening limits the storage time [14]. In some of the

memory schemes, dynamical decoupling approaches have been used to extend the storage time. The precision requirements for one of these schemes were studied in this thesis and are presented in Chapter (5).

Multimode storage capacity can be defined as the maximum number of modes that can be stored simultaneously in a memory with a certain efficiency. Here, the focus is on quantum memories that are based on ensembles of atoms. In addition to the advantage of atomic ensembles in enhancing the photon-memory coupling, ensembles allow one to implement quantum memory protocols with large multimode storage capacity. One way of multimode storage is based on storing photons at different frequencies. This requires large memory bandwidth.

Memory bandwidth is the available spectral bandwidth for storage. This parameter is noteworthy as it sets a limit on the rate that the memory can operate.

There are other parameters such as the wavelength of the quantum memory. This can be important to match the memory wavelength with an appropriate transmission channel (optical fibers or free-space transmission) in order to optimize the performance of the communication scheme. Furthermore, for quantum memories that are used as single photon sources or in quantum repeaters, it is essential to be compatible with the available parametric down conversion sources, see Sec. (1.2.5).

In the next section, I introduce quantum memory protocols. Quantum memories inherit some of their properties from memory protocols as they determine a procedure for the operation of quantum memories. Part of my research contributes to developing new protocols and exploring the connection of these protocols with known schemes. This contribution is briefly introduced in the next sections of this chapter and is presented in detail in the following chapters.

1.2.2 Protocols

1.2.2.1 Off-resonant Raman coupling quantum memory

In 2007, in two separate works, the quantum memory protocol based on the off-resonant Raman interaction has been proposed [15, 16]. The scheme is based on an ensemble of 3-level atoms, and it

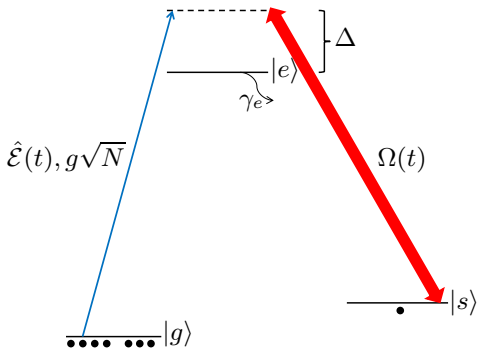

Figure 1.1: The figure shows the off-resonant Raman coupling that allows the absorption of a single-photon through the creation of a spin excitation. One can retrieve the stored photon by applying the same control field after the storage time.

operates by application of a properly shaped control field. To understand the basic principles of this protocol, one can imagine that all atoms are prepared in the ground state g, see Fig. (1.2.2.1). The purpose is to store and retrieve the single photon pulse that is characterized by $\hat{\mathscr{E}}(t)$. Coupling of the $s-e$ transition to the applied control field is determined by $\Omega_c(t)$. Both the input single photon and control field are not in resonant with the $g-e$ and $s-e$ transitions, respectively. However, two-photon resonance is necessary for an efficient coupling, such that $\omega_p - \omega_c = \delta_{gs}$.

In order to analyze this system, two paths have to be taken. First, one needs to use Maxwell's wave equation to consider the propagation of the electromagnetic fields in the medium. Second, a Hamiltonian that consists of energy of the levels and the atom-field interaction terms has to be considered. The propagation equation is a second order differential equation. The fact that the bandwidth of the pulse is much smaller than its central frequency leads to simplification of the wave equation. This derivation is explained in Chapter (4) for a more complicated case, where the refractive index of the medium is time-dependent.

The Hamiltonian can be used in the Heisenberg equation, $\dot{\hat{A}} = \frac{i}{\hbar}[\hat{H},\hat{A}] + \frac{\partial \hat{A}}{\partial t}$, to find the dynamics of any operator in this system, see [15]. The Heisenberg equation gives a set of equations for the level populations and transition operators. The point that the number of photons is much smaller than the number of atoms allows for a significant simplification, see the appendix of [15]. Finally, having Δ much larger than the bandwidth of the input pulse and the excited state broadening leads

to the elimination of the excited state from the equations of motion. It has to be noted that sources of decoherence, such as the ground-state spin broadening, can be added to the equations. These considerations provide the tools to study the properties of the Raman quantum memory.

In principle, the fidelity of the Raman quantum memory can approach the ideal fidelity. However, due to the coupling to the control field, excitation of atoms from their ground state g generate unwanted spin excitation, and consequently result in noise at the readout. This will limit the fidelity. One can avoid this process, by choosing appropriate levels with the opposite polarization selection rules. The efficiency depends on the effective optical depth. The effective optical depth is determined by the single-photon coupling, control field Rabi frequency, number of atoms, detuning and the ground state spin broadening. The efficiency in the forward direction can be limited, due to re-absorption during the read-out. The backward retrieval is not limited, and the efficiency can reach 100%, see Fig. (1.2.2.1). High efficiencies may require more control field power. This may lead to a time-dependent phase modulation that is given by $\phi(t) = \int_0^t dt' \frac{|\Omega_c(t')|^2}{\Delta}$. This effect that is called the AC Stark shift and can significantly limit the performance of the quantum memory. One can apply a proper phase modulation on the input pulse to cancel the effect of the AC Stark shift, and therefore reach the ideal efficiency.

Multimode storage capacity of quantum memories based on atomic ensembles have been studied in [17]. For quantum memories without controlled inhomogeneous broadening, including Raman-type quantum memory, the multimode storage capacity does not scale favorably with optical depth. Specifically, the studies show that the number of modes that can be stored simultaneously with an efficiency above a certain threshold, in the Raman-type quantum memory, scales with the square-root of the optical depth.

It is important to understand that the bandwidth of the Raman quantum memory is determined by the bandwidth of the control field. This allows one to implement a broadband quantum memory based on this protocol in contrast to the limited bandwidth in the electromagnetically induced transparency, see the next section.

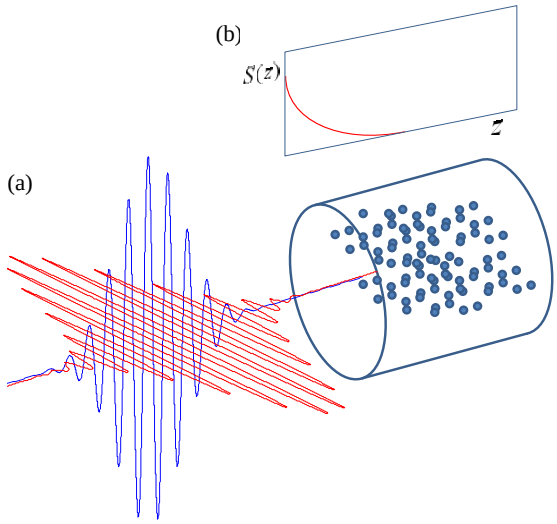

Figure 1.2: (a) Shows the control field (red) and the input single-photon pulse (blue) that are properly timed for absorption of the input pulse in the atomic ensemble. (b) Schematically shows the probability of the spin excitation that is decreasing exponentially over the length of the medium. This is the reason for the limited efficiency for the forward retrieval, as the re-emitted pulse is affected by re-absorption in the rest of the medium. The backward retrieval is experimentally more demanding, but it allows to reach 100% efficiency.

Finally, it has to be noted that the proposed protocol in Chapter (2) is equivalent to the Raman quantum memory in a 2-level system and without application of an optical control field. See new protocols in subsection 1.2.2.6 and Chapter (2) for more details.

1.2.2.2 Electromagnetically induced transparency quantum memory

Slow light has been one of the most exotic effects in optics. Electromagnetically induced transparency (EIT) is well-known to exhibit slow light effect. As it can be seen in Fig. (1.2.2.2), the imaginary part of the susceptibility that is responsible for absorption features a transparency window. Similar to Fig. (1.2.2.1), the light that propagates in a medium of three-level atoms can be controlled by applying a control field, $\Omega(t)$. In contrast to the previous scheme that is demonstrated in Fig. (1.2.2.1), when the detuning Δ approaches zero, this transparency window in Fig. (1.2.2.2) appears. This can be explained by interference between different possibilities for absorption of the probe field. For the detuning $\Delta = 0$, one can imagine that the probe field, $\hat{\mathscr{E}}(t)$, can be absorbed through the $|g\rangle - |e\rangle$ transition. For an excited state with a relatively long life time, the absorp-

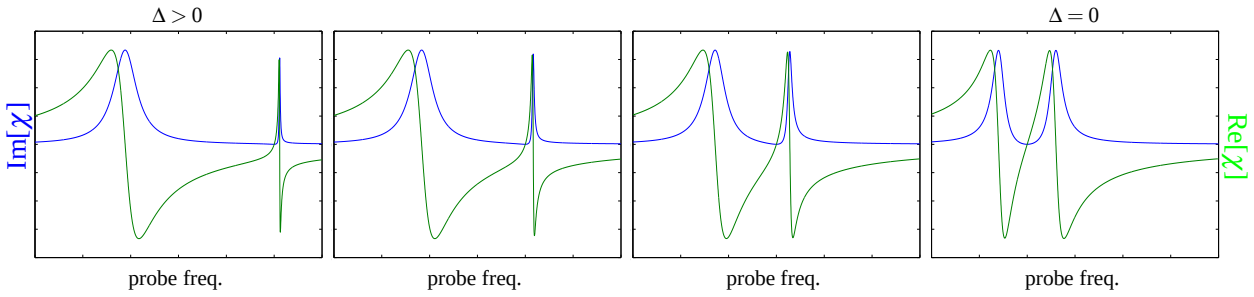

Figure 1.3: This figure shows the imaginary part (blue) and real part (green) of the susceptibility that is experienced by the probe field $\hat{\mathscr{E}}(t)$, see Fig. (1.2.2.1). In the Λ configuration in Fig. (1.2.2.1), by reducing the detuning Δ from left to the right, the scheme approaches the condition for EIT. The plot on the right presents a transparency window that is associated to a reduction in the group velocity that can be determined by the slope of the Re[χ].

tion through the $|g\rangle - |e\rangle - |s\rangle - |e\rangle$ transition destructively interferes with the aforementioned absorption process. This results in a transparency window in the absorption line. The transparency window is associated with a reduction in the group velocity that corresponds to the real part of the susceptibility for the propagating light.

The group velocity is determined by the Rabi frequency of the control field. For a weak propagating field (single-photon), it has been shown that the group velocity can be reduced to zero. In this process, by turning off the control field gradually, the optical excitation in the propagating probe field is converted to a spin excitation and is stored in the ground state of the system. By turning on the control field, the stored excitation can be read out.

The optical depth and the ground state coherence time are necessary for higher efficiency and storage time, respectively. Similar to the Raman-type quantum memory, the available bandwidth for storage is determined by specifications of the control field that results in the transparency window, see Fig. (1.3). For multimode storage, the capacity scales with the square-root of the optical depth. This is a disadvantage for non-inhomogeneously broadened ensemble memories, such as Raman-type and EIT-based quantum memories.

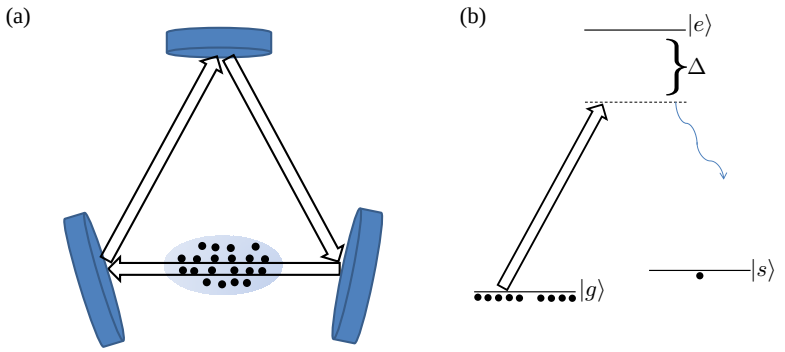

Figure 1.4: (a) Ensemble of atoms in a ring cavity that is interacting with the cavity field with a well-defined propagation direction. (b) Λ-level configuration of the atoms. All atoms are prepared in the ground state. The cavity field can result in scattering a photon and generate a collective spin excitation.

1.2.2.3 Off-resonant Raman scattering protocol (DLCZ)

As another scheme that is based on an ensemble of three-level atoms, I introduce the off-resonant Raman scattering scheme that is known as the DLCZ protocol. This protocol has been proposed in [3] by Duan, Lukin, Cirac and Zoller (DLCZ) as a part of a scheme for long-distance quantum communication. This scheme is not a quantum memory protocol in the sense that it does not allow for reversible mapping of externally provided single-photons. However, the protocol allows to generate entanglement between the atomic ensemble and a scattered photon. This can be utilized toward implementations of single-photon sources or long-distance quantum communication schemes.

Applying a detuned optical pulse to the atomic ensemble scatters one photon and generates a spin excitation. In order to avoid absorption of the pulse, the field has to be detuned by Δ from the $|g\rangle - |e\rangle$ transition. However, a greater Δ may reduce the probability of scattering a photon and generating a collective spin excitation. The use of the ring cavity is a way to enhance this probability (coupling).

The spontaneous emission from the excited state might seem to be problematic in this scheme. However, it can be shown that the spontaneous emission distributes excitation over all possible modes (wave vectors). The Raman scattering generates a collective spin excitation, where its wave vector (mode) is determined by the wave vector of the incoming and scattered photon. There-

fore, at the read out there is a preferred direction for which the read out emission is collectively enhanced by the number of atoms in the ensemble. This results in a high signal-to-noise ratio (a suppressed noise). This concept is discussed in detail in Chapter (5), and used to study the precision requirements for spin-echo quantum memories.

1.2.2.4 Controlled-reversible inhomogeneous broadening quantum memory

Controlled-reversible inhomogeneous broadening (CRIB) quantum memory has been introduced and analyzed in [18, 19, 20]. As its title suggests, it is based on controlling the inhomogeneous broadening of the relevant transition. Inhomogeneous broadening refers to the variance in energy of the atoms in an ensemble. In this protocol, the photon is stored in a collective excitation of an inhomogeneously broadened atomic ensemble. After absorption of an incoming photon, this collective atomic state can be described by $\mid \psi(t)\rangle = \frac{1}{\sqrt{N}} \sum_{j=1}^{N} e^{i\delta_j t} \mid gg..e^j g..g\rangle$, where N is the number of atoms in the ensemble and δ_j is the detuning of the central frequency of the incoming photon from the jth atom. The variance in energy (level splitting) of atoms leads to dephasing of the collective atomic state. The dephasing happens at the rate that is determined by the width of the inhomogeneous broadening. This prevents any application, including storage that requires coherence times that are longer than the inverse of the width of the broadening. However, a controlled inhomogeneous broadening allows one to rephase the collective atomic state. After some time $t = T$, using this control the inhomogeneous broadening can be reversed. Therefore, the jth atom in the ensemble will acquire a reversed detuning of $-\delta_j$. It can be seen from the collective atomic state $\mid \psi\rangle$ that the dephasing can be reversed at the time $t = 2T$, see Fig. (1.2.2.4).

The fidelity of the CRIB quantum memory can in principle approach 100%. Similar to the other protocols, the efficiency depends on the optical depth of the ensemble. As it has been discussed for the Raman-type quantum memory, the re-absorption effect in the medium limits the forward retrieval efficiency. The backward retrieval efficiency approaches 100% for high optical depths. See subsection (1.2.2.6) for a modified CRIB protocol that offers a solution to suppress the re-absorption effect in the CRIB protocol.

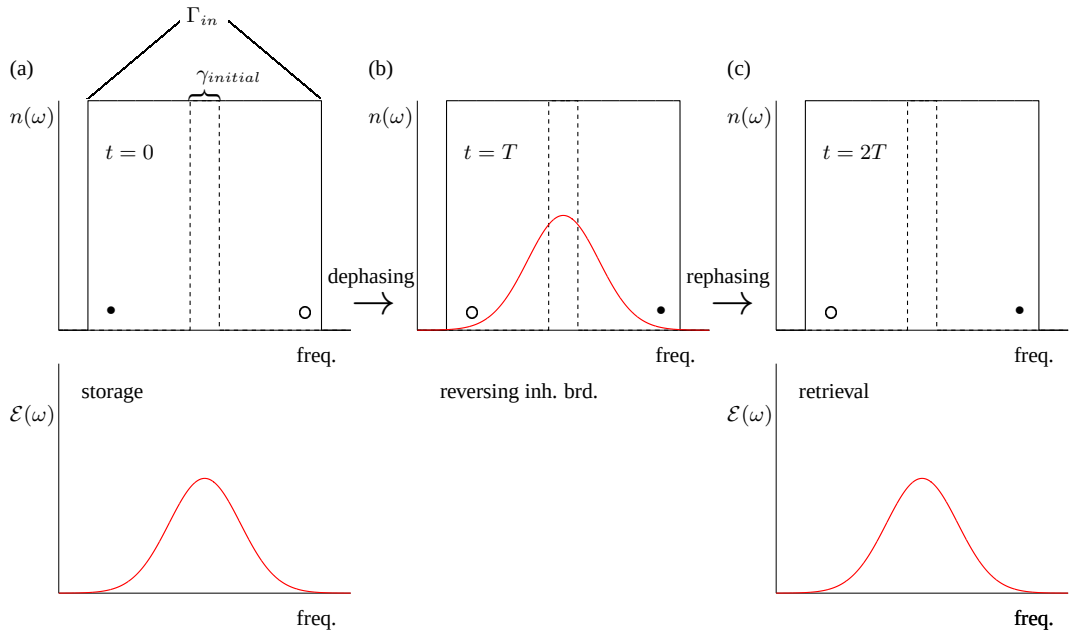

Figure 1.5: (a) A schematic absorption profile of an atomic ensemble with initial broadening of $\gamma_{initial}$ is broadened to Γ_{in} by applying an inhomogeneous external (magnetic/electric) field. This broadened ensemble allows to absorb the incoming pulse $\mathscr{E}(\omega)$. (b) The broadened ensemble dephases due to the broadening. After the time $t = T$, the external field is reversed leading to the inversion of the detuning of all absorbers, see the open and solid circles. (c) Reversing the broadening at time $t = T$ allows to get all the atoms rephased at $t = 2T$. Efficient retrieval is expected at $t = 2T$.

The limit on the storage time is determined by properties of the physical system. For a storage time of T_{stor}, one has to reverse the inhomogeneous broadening at $t = T_{stor}/2$ to achieve an efficient recall at $t = T_{stor}$, see Fig. (1.2.2.4). This property has been used for pulse sequencing in [21].

Multimode storage is one of the most important features of quantum memory protocols that are based on inhomogeneous broadening. As opposed to the protocols that are based on unbroadened atomic ensembles, the number of modes that can be stored with a certain efficiency scales linearly with the optical depth. In CRIB, depending on the physical system, the inhomogeneous broadening is produced by an external electric or magnetic field. Increasing the external field strength results in a greater inhomogeneous broadening and consequently a greater memory bandwidth. This controllable memory bandwidth can be used to store multiple input modes.

The gradient echo memory (longitudinal CRIB) is based on the CRIB protocol, where the broadening is produced by a longitudinally (along the propagation direction of the input field) varying external field. This is in contrast to the transverse CRIB, where every slice of the medium along the propagation direction contains all of the frequency components.

The most distinguishing feature of the gradient echo memory (GEM) compared to CRIB is that the forward retrieval efficiency is not limited by re-absorption as the atoms are broadened longitudinally in space that prevents re-absorption at the retrieval. The gradient echo memory protocol has led to some of the influential experimental results on quantum memories [21, 22, 23]. In Chapter (3), I present a proposal for a novel quantum memory protocol based on a different principle that resembles the gradient echo memory under certain conditions.

1.2.2.5 Atomic frequency comb quantum memory

The atomic frequency comb (AFC) quantum memory is another well-known quantum memory protocol that is based on inhomogeneous broadening, see [24]. The principle of the protocol is based on periodicity in the absorption frequency of the atomic ensemble, see Fig. (1.2.2.5). An incoming pulse interacting with an ensemble of atoms with a comb-like atomic frequency distribution generates a collective atomic state. This collective atomic state dephases as different atoms

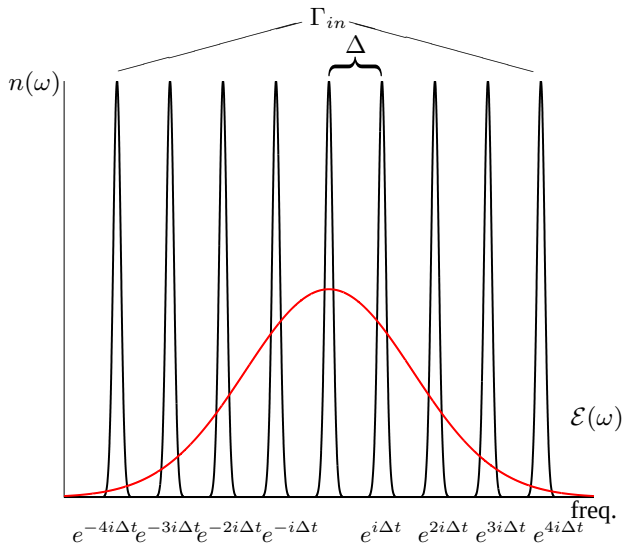

Figure 1.6: (a) The figure shows the absorption profile of inhomogeneously broadened ensemble that is prepared for the AFC protocol. The periodic absorption peaks are prepared by optical pumping. The incoming field $\mathscr{E}(\omega)$ interacts with the ensemble. The collective atomic state dephases as atoms in different absorption peaks precess at different rates. However, the collective atomic state automatically rephases (due to the periodicity) at $t = \frac{2n\pi}{\Delta}$, where $n = 1, 2, ...$

have different frequencies (detunings). However, due to the comb-like distribution (periodicity in absorption peak frequencies), the collective atomic state rephases at certain times. The rephasing times are integer multiples of $2\pi/\Delta$, where Δ is the angular frequency difference between the absorption peaks of the AFC. The storage time is determined by this dephasing-rephasing time. Therefore, once the atomic frequency comb is prepared, the storage time is fixed. Transferring the stored excitation to a third level allows one to eliminate the limitation due to the fixed storage time. In addition, for communication purposes, the functionality of the AFC quantum memory can be improved by transferring optically excited state to the collective spin ground state for longer storage times and on-demand retrieval [25].

The fidelity of the AFC has been shown to approach the ideal fidelity [26]. The efficiency in the forward direction is limited by re-absorption, see [24]. However, the backward retrieval approaches 100% efficiency for high optical depths. AFC provides multimode storage. The number of modes that can be stored is independent of the optical depth as opposed to the other protocols, see [24].

1.2.2.6 New protocols

A significant part of my research is devoted to finding new protocols for realizing quantum memories. As I discussed above, various protocols exist, and each protocol brings certain possibilities and limitations. Developing new protocols may allow to approach a more practical quantum memory protocol.

Below, I describe three new protocols that are developed by our research group and some of the new quantum memory schemes by other groups. The first two are my main contributions to the topic of quantum memory protocols, which are presented in Chapters (2) and (3). In the first two cases, these protocols are shown to be able to operate similar to the off-resonant Raman interaction quantum memory and the gradient echo quantum memory, respectively. In the first case, the controllable-dipole quantum memory possesses properties similar to the Raman-type quantum memory, but in a two-level system and without any optical control. The latter, under certain conditions, operates similar to the GEM without any spatial gradient imposed on the atomic ensemble. The third proposal has similarities to the slow-light effect in the electromagnetically induced transparency and shows connections to the gradient echo memory. These similarities and connections provide the ground-work for a better understanding of quantum memories and categorizing the schemes. This is also a step toward inventing hybrid schemes with combined features that may serve better than the current demonstrations for some of the quantum memory applications. Here, I briefly describe these protocols.

Controllable-dipole quantum memory is a protocol in an ensemble of two-level atoms that is based on the ability to control the transition dipole moment for storage in the optical coherence of the transition. There are solid-state systems, such as Tm^{+3} ions doped in YAG crystal, in which the transition dipole moments of some of the transitions can be manipulated by applying an external electric or magnetic fields. In Chapter (2), I show that this proposal is equivalent to the Raman-type quantum memory in a two-level system and with no optical control. I studied both cases of the ensemble in cavity and for atoms in free-space. The first case is treated analytically, and the

optimal solutions are found. The case of atoms in free-space is more complicated, and there has not been any optimal solution for arbitrary input pulse shapes. However, I analyzed the performance for Gaussian pulses and compared the results with the controlled reversible inhomogeneous broadening quantum memory.

Quantum memory based on the refractive index modulation is another novel scheme that utilizes a time-dependent refractive index of a medium to generate an effective longitudinal controlled reversible broadening. The time-dependent refractive index of the medium allows one to effectively modulate the frequency of the propagating pulse as a linear function of the position in the medium. This results in an effective longitudinal position-dependent detuning between the pulse and atoms. A comparison shows that this scheme is equivalent to the gradient echo memory, where the position-dependent detuning is due to an external position-dependent (electric or magnetic) field. In chapter (3), I present an implementation that is based on Tm^{+3} ion that are doped in the lithium niobate crystal (medium), in which one can modulate the refractive index of the medium by a time-dependent electric field, such that it provides enough bandwidth to store the input pulse. Reversing the time-dependent electric field allows for retrieving the stored pulse.

Quantum memory by atomic frequency sweeping is an emerging scheme that is based on modulating the transition frequency of an ensemble of two-level atoms. The protocol is developed by our group, see [27]. The results show that changing the transition frequency of a narrow atomic line from a large negative to a large positive detuning allows to store pulses that are much broader than the atomic frequency linewidth. The polaritonic description of the dynamics in this system indicates a slow-light effect that is similar to that of the electromagnetically induced transparency. There is also a correspondence between this system and an array of waveguide cavities that are interacting with side cavities. Numerical analysis also sheds light on similarities between this proposal and the gradient echo memory. Atoms in hollow-core photonic crystal fiber is a potential implementation of this scheme as the medium is required to accommodate the input pulse.

Other quantum memory protocols are also recently developed. Similar to the quantum memory

by atomic frequency sweeping, a protocol has recently been introduced that is based on a controlled homogeneous splitting, see [28]. The authors of this paper showed that one can store and retrieve a quantum state of light by controlling the homogeneous splitting between two frequency linewidth of two species in an ensemble. They also observe the slow-light effect that is not based on the ground-state coherence (as opposed to EIT), therefore it shares partial similarities with our above-mentioned protocol.

In addition to this protocol, I. Iakoupov and A.S. Sørensen in [29] presented a modified controlled reversible inhomogeneous broadening quantum memory. In contrast to CRIB, the external field that is to broaden the ensembles frequency linewidth is only turned on for the duration of the input pulse. The reversed external field is applied for the same duration at the time of retrieval. Their study shows that the forward retrieval efficiency could approach the ideal efficiency, and the re-absorption is less severe.

1.2.3 Physical systems

Any stationary quantum system that can be coupled to photons and has a coherence time that is longer than the duration of the photons can be a candidate for the implementation of a quantum memory. A trapped single-atom, or ensembles of atoms in a trap or in a gas cell, or in a crystal are other possibilities. Artificial atoms such as quantum dots and nitrogen vacancy (NV) centers in diamond are also among the possible physical systems. Coherence times vary from about 1μs in the electronic ground states of Rb atoms in a Vapour cell to over 1s in nuclear spin states of some rare-earth ion doped crystals. The efficiency of the atom-photon interface is determined by the optical depth that varies from one implementation to another.

My research is focused on the solid-state candidates. In particular, rare-earth ion doped crystals are attractive because of their properties such as relatively long optical coherence times and inhomogeneous broadening that can be engineered to be utilized in some of the protocols. In addition, NV centers in diamond possess various useful properties that propose this system as a promising candidate for photonic quantum information processing tasks. The NV centers in diamond show a

significant ground state nuclear spin coherence times even at room temperature. This has provided over a second coherence time that can be used for storage of microwave photons. Below, I provide details about these two solid-state candidates for implementations of quantum memories.

1.2.3.1 Rare-earth ion doped crystals

Rare-earth elements are already an inevitable part of the current technology. They became particularly attractive since the invention of the laser in 1960s. In industry, they are used in producing magnets and batteries. In life sciences, their fluorescence properties are used for examining biological fluids and drug research. Rare-earth elements are known to be comprised of scandium, yttrium and 15 other metallic elements that are called Lanthanides. There are four elements that are particularly appealing to the quantum memory community. These four elements are praseodymium (Pr), neodymium (Nd), erbium (Er) and thulium (Tm). These rare earth elements belong to the $4f$ block that corresponds to the filling of the $4f$ electronic shell. The $5s$, $5p$ and $6s$ shells are filled and have a larger radial distribution, which they partially shield the $4f$ electrons that results in a narrow homogeneous optical linewidth and reduces the influence of crystal strain and lattice phonons, see [30, 31].

There are few crystals, such as YAG($Y_3Al_5O_{12}$), Y_2SiO_5 or $LiNbO_3$ that are often used as the host crystals for the rare-earth ions. The wavelength of the transition is determined by the rare-earth ion. The doped ion replaces yttrium and lithium in the host crystals. The host crystal can offer crystallographically equivalent or inequivalent sites for the dopants. This may have an impact on the response to the external magnetic or electric fields. Homogeneous broadening is limited by the excited state lifetime of the relevant transition. However, depending on the temperature it is determined by phonon interactions (high temperatures) or energy exchange between spins (cryogenic temperatures). Inhomogeneous broadening, which is due to inhomogeneity in the environment of the dopants, is caused through spin-spin interaction and strain that are sources of a spatially varying potential for dopants. Therefore, the density of dopants becomes an important factor that has an impact on the inhomogeneous broadening. This is the reason that one cannot

increase the optical depth arbitrarily at a certain frequency by increasing the density of dopants. There is a chance to increase the optical density by using the stoichiometric rare-earth crystals, see [32].

In Chapter (2), the proposed implementation of the Controllable-dipole quantum memory is in Tm:YAG. The photon is stored in a two-level configuration that is based on the optical coherence of that transition. It is also noteworthy that one can control the transition dipole moment of the certain transitions of Tm^{+3} ion in Tm:YAG by applying small changes to the external magnetic field, see Chapter (2). In Chapter (3), the proposed protocol requires a host that has a variable refractive index under the external electric field. Therefore, Tm:$LiNbO_3$ is an appropriate choice of the rare-earth doped crystals to implement the protocol.

1.2.3.2 NV centers in diamond

Defects in solids are attractive due to their potential to provide atom-like properties with relatively long coherence times. The defect can be a displaced atom or a vacancy in the crystal structure. In addition to the defects, impurities exist in or can be added to the crystal structure. Depending on the impurity, it can add an excessive electron or a hole (lack of an electron) to the structure. This along with the symmetry of the defect can determine some of important properties of the impurity-vacancy centers in crystals.

Nitrogen is the most common impurity in diamond. A nitrogen vacancy (NV) center in diamond is a nitrogen that replaces a carbon , which is neighbor to a vacancy in the diamond crystal structure. A negatively charged NV center that is the focus of this study is comprised of 6 contributing electrons (3 electrons from 3 carbon atoms, 2 electron from nitrogen and 1 electron from the environment that is possibly from another single atomic nitrogen impurity). These 6 electrons are confined in the defect (vacancy) in the diamond with C_{3v} symmetry as they can not contribute in any covalent bond with a neighboring site in the lattice. The C_{3v} symmetry denotes symmetry under rotations around a vertical axis and (here it is the NV axis, see Fig. (1.2.3.2)) and 3 mirror planes. For comparison this is the same symmetry as for the NH_3 molecule. This information can

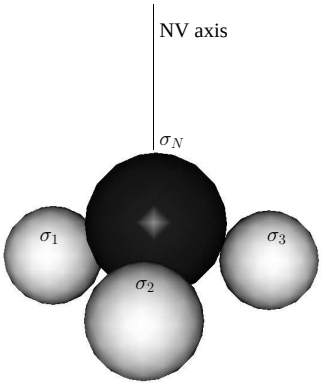

Figure 1.7: The figure shows the dangling electronic orbitals σ_1, σ_2 and σ_3 that are associated with the electrons shared by three neighboring carbons and σ_N that corresponds to electrons from the nitrogen. In the basis of the NV center the z direction is determined by a vector from the nitrogen toward the vacancy. One of the carbon's dangling electrons (for example σ_1) defines the x direction, and the y direction is correspondingly defined perpendicular to x and z.

be used to determine the electronic level configuration and energies, see [33].

There has been significant interest in NV centers for studying and utilizing their properties for various applications. NV centers have relatively long electronic spin coherence times (up to about 1ms) at room temperature. These coherence times become much longer at low temperatures. The spin state can be read optically by exciting the NV center and measure the polarization of the fluorescent emission. These properties have made NV centers an attractive tool for magnetic sensing and nano-scale nuclear magnetic resonance [34, 35].

Recently, storage of microwave photons in a single NV center or an ensemble of NV centers has been studied theoretically and experimentally [36, 37, 38]. For an NV center that is not coupled to any neighboring nuclear spin the coherence (storage) time is given by the electronic ground state T_2 time. T_2 time of about 1ms has been observed at room temperature. In [39], T_2 time of 0.5s has been reported at low temperatures around 77°K. NV centers can couple to their neighboring nuclear spins (of C^{13} or N^{15}) that are within few nm distances. This potentially allows one to take advantage of the even longer coherence time of nuclear spin that has been shown to be over one second [40]. It has also been shown that the parallel electron-nuclear coupling rate exceeds the $1/T_{1e}$, where T_{1e} is the electronic spin lifetime. This means that the flip-flop of the electronic

spin that is happening at the time scale of about 10ms leads to dephasing of the nuclear spin [40]. Therefore, the nuclear spin coherence time is limited by the electronic spin lifetime. A dynamical decoupling technique has been used to achieve over one second coherence time at room temperature [40].

Despite all these attractive properties, the storage of optical photons becomes problematic due to the short excited state lifetime of individual NVs and the broad optical linewidth (excited state inhomogeneous broadening) in NV ensembles.

In Chapter (4), a solution to these difficulties is presented, and an NV ensemble coupled to a cavity is shown to be a promising solid-state candidate for micron-scale on-chip optical quantum memories.

1.2.3.3 Other systems

Apart from the above-mentioned solid-state systems, there are other physical systems that are being used by several groups around the world. The most commonly used systems are ensemble of trapped cold atoms and hot atomic gases. A hot atomic gas cell of Rb atoms has been used for the implementation of the Raman-type quantum memory in [41] and for realizing the gradient echo memory, see [23]. Trapped cold atoms in a ring cavity have been used to implement DLCZ type protocol that resulted in a combination of high efficiency and storage time, see [42].

In addition, a cold trapped single atom in a cavity has also been shown to operate as a quantum memory, see [43].

Atoms trapped in a hollow core fiber provide a relatively large optical depth [44], which is one of the requirements for an efficient quantum memory. Hollow core photonic crystal fibers as a trap for Cs atoms have been shown to provide even higher optical depths that are promising for the Raman-type scheme [45]. Another candidate is a rare-earth ion doped fiber. Despite their small optical coherence, they can be useful for protocols that are based on inhomogeneous broadening [46]. Very recently, inhomogeneous and homogeneous optical linewidths of rare-earth ion doped transparent ceramics have been studied, see[47]. The results from this study are comparable to

rare-earth ion doped single crystals. This suggests that ceramic materials can be competitive with single crystals for applications in quantum information, including quantum memories. Further studies are required to determine their potential advantages.

1.2.4 State of the art

Quantum memory protocols and their experimental demonstrations progressed rapidly during the past decade. Various quantum memory protocols have been adapted to realize each of the quantum memory criteria in various setups. Even though high efficiency, long storage time and multimode capacity have not been achieved in one single implementation, there have been attempts to address these requirements individually.

1.2.4.1 Solid-state systems

Achieving high efficiency has been the focus of many experiments. Since the transition dipole moment in rare-earth doped solids are weak, achieving high optical depth and, consequently, high efficiency is challenging. Higher concentration of dopants could increase the inhomogeneous broadening and prevent one from arbitrarily increasing the optical depth. Isotropically pure, stoichiometric rare-earth crystals promise much higher optical depths compared to the rare-earth doped crystals, see [32].

In 2010, Pr^{3+} doped in Y_2SiO_5 crystal was used to implement the gradient echo memory (GEM) protocol. In this study, an efficiency of about 69% was achieved and currently constitutes the solid-state quantum memory with the highest efficiency, see [22]. Very recently, implementing the AFC protocol in the same material within an impedance-matched cavity resulted in about 58% efficiency, see [48, 49]. It has to be noted that this result is achieved based on a weakly absorbing sample. This promises more progress in terms of the efficiency based on impedance-matched quantum memories [49].

In 2005, Pr^{3+}: Y_2SiO_5 was used to implement EIT-based storage [14]. This experiment demonstrated storage times of over 1s. In this experiment, multiple π-pulses have been used to prevent

dephasing due to the spin inhomogeneous broadening. This technique only allowed to store strong pulses, due to a limited signal-to-noise ratio. See Chapter (5) for evaluation of the error due to the uncertainty in π-pulses.

In terms of the bandwidth, the AFC protocol in Tm^{3+} doped lithium niobate waveguide provided 5GHz memory bandwidth [50]. This also provides the potential for multimode capacity. Quantum memory based on AFC protocol in Tm^{3+}:YAG allowed storage of more than 1000 temporal modes [51].

Storage of entangled photons has been demonstrated in Tm^{3+}:$LiNbO_3$ [50] and Nd^{3+}:Y_2SiO_5 [52] based on the AFC protocol. This is important as it is a key component in long-distance quantum communication based on quantum repeaters.

1.2.4.2 Atomic gases

Some of the major achievements in developing quantum memories are based on physical realizations in atomic gases. The highest efficiency for quantum memories has been accomplished in hot atomic gas of Rb atoms in a cell. The efficiency of about 87% was achieved based on the GEM protocol, see [53]. The same protocol has been employed to use the quantum memory as an optical pulse sequencer to store and re-order multiple pulses in time [21].

In a similar setup, Raman-type quantum memory has been implemented. Despite the limited efficiency, the scheme provided one of the broadband quantum memory implementations with a bandwidth of about 1.5GHz [41].

Recently, an ensemble of cold Rb atoms in a magneto-optical trap inside a ring cavity, resulted in the best available combination of storage time and efficiency. The off-resonant Raman scattering (DLCZ) protocol has been employed in this experiment and about 73% efficiency and over 3ms lifetime have been demonstrated.

The next step is to combine the required features in one single implementation to take a step toward more practical quantum memories.

1.2.5 Applications

1.2.5.1 Deterministic single-photon sources

Immediate application of an efficient quantum memory is the implementation of a deterministic single-photon source. A parametric down-conversion source can produce photon pairs in a non-deterministic way. One can combine this source with a quantum memory. Detecting one of the photons at one arm determines the presence of another photon at the other arm to be stored in the quantum memory. Later the stored excitation can be retrieved to construct an on-demand heralded single-photon source. A highly efficient single-photon source is a crucial element in photonic quantum information processing, especially in linear optical quantum computation based on the KLM scheme [1].

In [54] the off-resonant Raman scattering approach has been used to realize a deterministic and storable single-photon source. Applying an off-resonant weak laser pulse allows to scatter one photon and create a collective spin excitation in the ground state of an atomic ensemble. Detecting the scattered photon determines the stored spin excitation and its mode (wave vector). Later, the stored excitation can be retrieved to serve as a deterministic and storable single-photon source.

1.2.5.2 Quantum repeaters for long-distance quantum communication

One of the main motivations for developing quantum memories is their use as a component in quantum repeaters. Quantum repeaters are developed to provide the possibility of distributing entanglement between distant parties. Direct transmission of photons through free space (on earth) or fiber is limited by exponential decay of transmission probability with distance.

A quantum repeater with atomic ensembles and linear optics was first proposed in 2001 by Duan-Lukin-Cirac-Zoller (DLCZ), see [3]. Their proposed scheme is as follows. Applying a weak off-resonant pulse to an atomic ensemble scatters a photon and generates a collective spin excitation, see Sec. (1.2.2.3). The scattered photon is correlated to the collective spin excitation. Having two ensembles and collecting scattered photons from both allows one to perform a Bell state measurement with the scattered photons. A successful Bell state measurement results in entanglement

generation between the collective spin excitations in the atomic ensembles. The-above mentioned setup is one link in the DLCZ quantum repeater. Having several links and generating stored entanglement in every link provides the possibility to distribute entanglement over long distances as detailed below. Consider two neighboring links that include ensembles that are labeled as A_1, B_1 and A_2, B_2 corresponding to link 1 and 2. The spin excitation in A_1 is entangled with that of B_1. Similarly, A_2 is entangled with B_2. Recalling the stored excitation from B_1 and A_2 and sending the photons to a Bell state measurement results in entanglement between A_1 and B_2. This procedure can be performed in other links and finally generate entanglement between A_1 and B_N, where N is the number of links. The loss does not scale exponentially with the total length as it is determined by the traveling distance of the scattered photons within a link.

As seen from the DLCZ quantum repeater, the proposal is not limited to only DLCZ-type quantum memory. In a similar approach, other quantum memory protocols can play a similar role as nodes in a quantum repeater, [12]. Having a source of entangled photons at each node, one can generate entangled pairs, store one photon at the node and send the other photon to a beam splitter at the middle of the link. Similar operation at the other node of the link and the Bell state measurement in the middle of the link results in entanglement generation between the stored excitations in the quantum memories. Recalling the stored excitation and performing the Bell state measurement between the neighboring links distributes entanglement over longer distances. As generating entanglement in each link is not deterministic, quantum memories are vital to keep the performance of the quantum repeater by synchronizing the links before distributing entanglement.

There are several proposal s for quantum repeater architectures with different performances and demands for quantum memories. Recently, Munro *et al.* in [55], proposed a quantum communication scheme that does not require long-lived quantum memories. The loss could be overcome by use of a redundant quantum parity code. Instead of quantum storage, efficient two-qubit gates is necessary in addition to an efficient interface between photons and stationary qubits is necess

Chapter 2

Controllable-dipole quantum memory

2.1 Preface

Quantum memories are implemented based on quantum memory protocols, see Sec. (1.2.2). The protocol specifies all the steps that have to be taken to store in and recall from a quantum memory. Taking the quantum memory protocol into account and considering the light-atom interaction allows to analyze the performance of the quantum memory.

This chapter presents a new quantum memory protocol for storage in two-level systems that is based on direct control of the transition dipole moment. Mainly, the analysis is focused on the case in which the atomic ensemble is inside a cavity. This enhances the light-atom interaction. The analysis is focused on finding the conditions for maximizing the efficiency. We could show that the optimal write process is related to the optimal read process by a reversal of the *effective time* $\tau = \int dt g^2(t)/\kappa$, where $g(t)$ is the time-dependent light-atom coupling and κ is the cavity decay rate. Then the paper shows results on the free-space case, where Maxwell equation is used for considering the propagation of the photon in the medium. A possible implementation is discussed based on Tm^{3+}:YAG. In Tm^{3+}:YAG, the transition dipole moment can be controlled by changing the direction of the external magnetic field. Finally, the performance of the controllable-dipole quantum memory is compared with that of the controlled reversible inhomogeneous broadening (CRIB) quantum memory. The proposed protocol based on the modulation of the transition dipole moment is shown to be equivalent to the Raman-type quantum memory without the requirement for application of an optical control field.

This work has been published through collaboration with several co-authors. I contributed to this publication by performing theoretical analysis for the free-space solution, preparing graphs for describing the scheme and comparisons and presenting the performance in the free-space case.

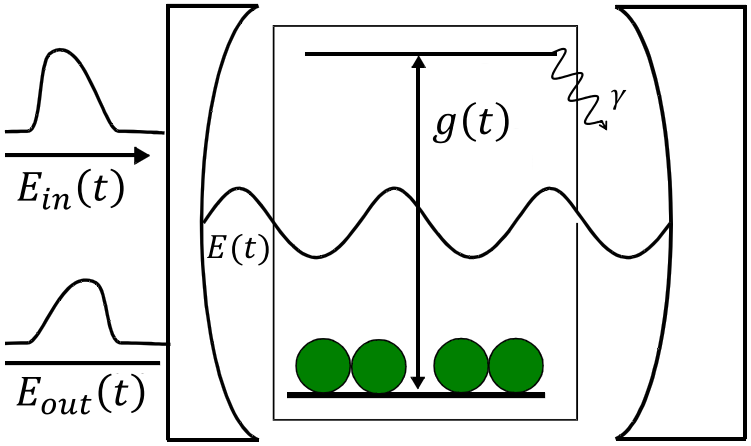

Figure 2.1: We consider an ensemble of two-level systems inside a one-sided cavity, where the time-dependence of the light-matter coupling $g(t)$ can be controlled. See also Eq. (1).

I supervised an undergraduate student for calculations regarding the analysis of the system in the cavity. Finally, I wrote a part of the manuscript and prepared responses to the referee reports.

2.2 Introduction

Quantum memories for light are devices that allow one to store and retrieve light in a way that preserves its quantum state [56, 57, 58]. They are essential components for optical quantum information processing, notably for quantum repeaters [12]. All quantum memories require a way of switching the coupling between the light and the material system (which is used as the memory) on and off in a controlled way. In the case of memories based on electromagnetically induced transparency or off-resonant Raman transitions [41, 56, 59, 60, 16] the coupling is controlled by a laser beam, which is typically much more intense than the signal that one aims to store. In contrast, in the case of photon-echo based memories [58, 30, 61] the coupling is controlled in a more indirect way via the dephasing of the atoms in the storage medium. This typically requires spectral tailoring of the medium by optical pumping before the signal can be stored.

Here we consider a way of controlling the light-matter interaction that is different from the mentioned examples, and that is particularly simple from a conceptual point of view, namely the direct control of the transition dipole element of the relevant optical transition. This is motivated

by recent demonstrations that transition dipoles can be turned on and off in certain solid-state systems, in particular in rare-earth ion doped crystals by applying magnetic fields [62, 63, 64], and for NV centers in diamond by applying electric fields [65]. We consider the case where the storage medium is placed inside an optical cavity [49, 66, 67]. This both enhances the light-matter interaction, which is desirable for achieving high efficiencies, and simplifies the equations of motion, thus clearly bringing out the basic principles of the memory dynamics. The free-space case, which is attractive from the point of view of experimental implementation, is discussed in the appendix.

2.3 Controllable-dipole quantum memory in a cavity

We consider an ensemble of two-level atoms coupled to a cavity mode, see Fig. 1. We ignore the spatial dependence of the light-matter interaction, and thus phase-matching considerations [68, 69]. The system that we consider is formally equivalent to a Raman memory in a cavity, if the excited state is adiabatically eliminated in the Raman case [66], and where the two-photon spin transition is replaced by a single-photon optical transition. There is also some similarity to Refs. [70, 71], where the light-matter coupling is controlled by tuning a cavity instead of the transition dipole moment.

2.3.1 Equations of motion

We use the usual input-output formalism for a single-sided, fairly high-finesse cavity [72]. The basic equations are then

$$\begin{aligned}\dot{\sigma}(t) &= -i\Delta(t)\sigma(t) - \gamma\sigma(t) + ig(t)E(t)\\ \dot{E}(t) &= ig(t)\sigma(t) - \kappa E(t) + \sqrt{2\kappa}E_{in}(t)\\ E_{out}(t) &= -E_{in}(t) + \sqrt{2\kappa}E(t).\end{aligned} \tag{2.1}$$

Thanks to the linearity of the dynamics, σ and E can be interpreted as the atomic polarization and cavity fields (in the semi-classical regime), but also as the probability amplitudes corresponding to a single atomic excitation in the ensemble and a single cavity photon respectively (in the quantum regime, which is our focus here) [57, 60, 66]; $E_{in}(t)$ and $E_{out}(t)$ are the incoming and outgoing fields (photon wave functions); $g(t)$ is the time-dependent light-matter coupling, which is proportional to the transition dipole matrix element between the ground and excited atomic states (and also to $\sqrt{N}$, where N is the total number of atoms); κ is the cavity decay rate; γ is the atomic decay rate; $\Delta(t)$ is a time-dependent detuning, which may arise in practice as a consequence of applying a time-dependent external field in order to control the dipole element and thus $g(t)$; γ and $\Delta(t)$ are imperfections that we will neglect at first to keep the discussion simple, but whose effect will be discussed later in the paper.

We are interested in the (realistic) situation where the cavity decay defines the shortest relevant timescale. In this case it is well justified to adiabatically eliminate the cavity field, setting $\dot{E} = 0$. This gives

$$E(t) = \frac{1}{\kappa}\left(ig(t)\sigma(t) + \sqrt{2\kappa}E_{in}(t)\right) \tag{2.2}$$

and hence

$$\begin{aligned} \dot{\sigma}(t) &= -\frac{g^2(t)}{\kappa}\sigma(t) + i\sqrt{\frac{2}{\kappa}}g(t)E_{in}(t) \\ E_{out}(t) &= E_{in}(t) + i\sqrt{\frac{2}{\kappa}}g(t)\sigma(t) \end{aligned} \tag{2.3}$$

where we have set $\Delta(t) = \gamma = 0$, as mentioned above. It is straightforward to derive the (very intuitive) continuity equation

$$\frac{d}{dt}|\sigma(t)|^2 = |E_{in}(t)|^2 - |E_{out}(t)|^2. \tag{2.4}$$

2.3.2 Read process

We now discuss quantum memory operation, starting with a discussion of the read process. (The motivation for this approach will become clear in the following.) The read process corresponds to

a situation where there is no incoming photon, $E_{in} = 0$. The continuity equation (2.4) implies

$$|\sigma(0)|^2 = |\sigma(t)|^2 + \int_0^t dt' |E_{out}(t')|^2, \tag{2.5}$$

which motivates the definition of the read efficiency η_r as

$$\eta_r = \frac{\int_0^\infty dt |E_{out}(t)|^2}{|\sigma(0)|^2}. \tag{2.6}$$

Here we have defined $t = 0$ as the starting time of the read process.

The solution of Eq. (2.3) with $E_{in} = 0$ is given by

$$\begin{aligned} \sigma(t) &= \sigma(0) e^{-\int_0^t dt' g^2(t')/\kappa} \\ E_{out}(t) &= i\sqrt{\frac{2}{\kappa}} g(t)\sigma(t). \end{aligned} \tag{2.7}$$

Using Eqs. (2.6) and (2.7) one finds

$$\eta_r = 1 - e^{-2\int_0^\infty dt g^2(t)/\kappa}. \tag{2.8}$$

Eq. (2.8) motivates the introduction of the effective time variable

$$\tau = \int_0^t dt' g^2(t')/\kappa, \tag{2.9}$$

see also Ref. [16], giving the simple expression $\eta_r = 1 - e^{-2\tau_r}$, where $\tau_r = \int_0^\infty dt g^2(t)/\kappa$ is the total effective time that elapses during the read process. This means that in order to maximize the read efficiency one simply has to maximize τ_r. The shape of $g(t)$ has an impact on the form of the output field, but the efficiency only depends on τ_r.

In order to rewrite the whole dynamics in terms of the effective time variable τ, we furthermore introduce effective input, output and cavity fields,

$$\mathscr{E} = \frac{\kappa}{g} E, \mathscr{E}_{in} = \frac{\sqrt{\kappa}}{g} E_{in}, \mathscr{E}_{out} = \frac{\sqrt{\kappa}}{g} E_{out}. \tag{2.10}$$

One then finds the new equations of motion (after adiabatic elimination of $\mathscr{E}$)

$$\begin{aligned} \frac{d}{d\tau}\sigma(\tau) &= -\sigma(\tau) + i\sqrt{2}\mathscr{E}_{in}(\tau) \\ \mathscr{E}_{out}(\tau) &= \mathscr{E}_{in}(\tau) + i\sqrt{2}\sigma(\tau). \end{aligned} \tag{2.11}$$

The read efficiency can be rewritten as

$$\eta_r = \frac{\int_0^{\tau_r} d\tau |\mathscr{E}_{out}(\tau)|^2}{|\sigma(0)|^2}. \tag{2.12}$$

The solution of Eq. (2.11) in the read case ($\mathscr{E}_{in} = 0$) is simply

$$\sigma(\tau) = \sigma(0)e^{-\tau}, \mathscr{E}_{out}(\tau) = i\sqrt{2}\sigma(\tau). \tag{2.13}$$

Eq. (2.13) shows that in terms of the effective time (and of the effective fields) the read process is a simple exponential decay - a remarkable simplification considering that the time dependence of $g(t)$ (and hence $E_{out}(t)$) is completely arbitrary.

2.3.3 Write process

We are now ready to discuss the write process. We will immediately use the effective variables. Solving Eq. (2.11) for non-zero $\mathscr{E}_{in}$ one finds

$$\sigma(0) = i\sqrt{2}\int_{-\tau_w}^{0} d\tau' e^{\tau'} \mathscr{E}_{in}(\tau'), \tag{2.14}$$

where τ_w is the total elapsed effective time for the write process and $\sigma(-\tau_w) = 0$. Note that no effective time elapses during times when the transition dipole is zero (i.e. during storage). We define the write efficiency as

$$\eta_w = \frac{|\sigma(0)|^2}{\int_{-\tau_w}^{0} d\tau |\mathscr{E}_{in}(\tau)|^2}. \tag{2.15}$$

2.3.3.1 Optimal input field

Our goal is to find the form of $\mathscr{E}_{in}(\tau)$ that maximizes η_w. Since the solution for σ is linear in $\mathscr{E}_{in}$, maximizing η_w corresponds to maximizing $|\sigma(\tau_w)|^2$ for a normalized input field satisfying $\int_{-\tau_w}^{0} d\tau |\mathscr{E}_{in}(\tau)|^2 = 1$.

Before discussing the formal optimization, let us take a step back and try to make a guess for the optimum input field. We have seen that when expressed in terms of effective time rather than real time, the read process simply corresponded to an exponential decay, see Eq. (2.13). It is

natural to suspect that inverting this decay (in effective time) will give the optimum effective input field. This means that our guess for the optimum solution is $\mathscr{E}_{in}(\tau) \propto e^{\tau}$.

This can be proved by functional differentiation. The optimum solution has to satisfy

$$\frac{\delta}{\delta \mathscr{E}_{in}^{*}(\tau)} \left[|\sigma(0)|^2 + \lambda \left(\int_{-\tau_w}^{0} d\tau |\mathscr{E}_{in}(\tau)|^2 - 1 \right) \right] = 0, \tag{2.16}$$

where λ is a Lagrange multiplier, and $\mathscr{E}_{in}(\tau)$ and $\mathscr{E}_{in}^{*}(\tau)$ are independent variables for each τ. Solving this equation using Eq. (2.14) gives $\mathscr{E}_{in}(\tau) \propto e^{\tau}$, confirming the intuitive guess, see also Fig. 2.

For this optimal solution the write efficiency is analogous to the read efficiency,

$$\eta_w = 1 - e^{-2\tau_w}. \tag{2.17}$$

The total efficiency (ignoring losses during storage) is then

$$\eta_{tot} = \eta_w \eta_r = (1 - e^{-2\tau_w})(1 - e^{-2\tau_r}), \tag{2.18}$$

which can obviously be simplified further if $\tau_w = \tau_r$. Provided that the optimum input field is chosen for the write process, the efficiency is thus maximized by maximizing τ_w and τ_r.

In real time the input field for the write process and the output field for the read process satisfy

$$\begin{aligned} E_{in}(t) &\propto g_w(t) e^{\int_{-\infty}^{t} dt' g_w^2(t')/\kappa} \\ E_{out}(t) &\propto g_r(t) e^{-\int_{0}^{t} dt' g_r^2(t')/\kappa}, \end{aligned} \tag{2.19}$$

where $g_w(t)$ and $g_r(t)$ are the light-matter coupling for the write and read processes respectively, and the proportionality constants are such that $\int_{-\infty}^{0} dt |E_{in}(t)|^2 = 1$ and $\int_{0}^{\infty} dt |E_{out}(t)|^2 = \eta_{tot}$. Eq. (2.19) shows that if the light-matter couplings are simple square functions in time, then the input and output fields are growing and declining exponentials in real time, respectively. However, there is no general requirement to choose the couplings in this way. On the one hand, one can achieve optimal write efficiency for any form of g_w, as long as the input field satisfies the above equation; on the other hand, the form of the output field can be tailored by choosing the form of g_r.

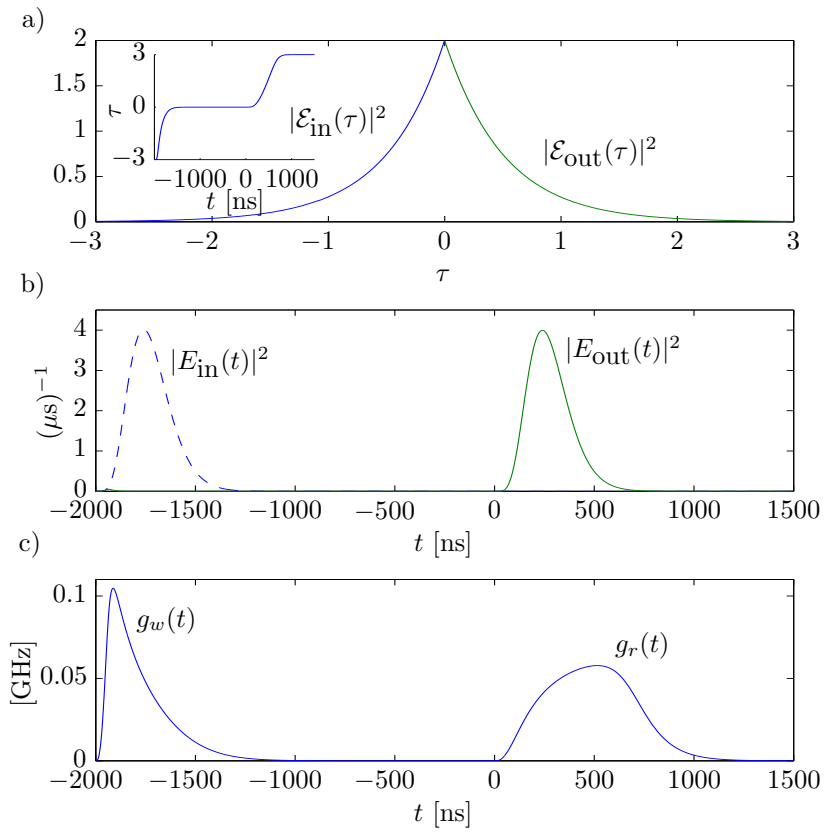

Figure 2.2: (a) The effective input and output fields $\mathscr{E}_{in}(\tau)$ and $\mathscr{E}_{out}(\tau)$ of Eq. (2.10) in terms of the effective time τ of Eq. (2.9). The inset shows the effective time versus real time. It can be seen that the effective time elapses only when the coupling is on. (b) An example for the possible time dependence of the real fields $E_{in}(t)$ and $E_{out}(t)$. (c) The corresponding write and read couplings $g_w(t)$ and $g_r(t)$. Any $E_{in}(t)$ can be absorbed with the optimal efficiency $\eta_w = 1 - e^{-2\tau_w}$ for $g_w(t)$ satisfying Eq. (2.20); and $E_{out}(t)$ can, for example, be chosen to be proportional to $E_{in}(t-T)$ (where T is the storage time) for $g_r(t)$ satisfying Eq. (2.20).

2.3.3.2 Optimal coupling

This means in particular that memory performance can be optimal even if the input and output fields are not related by time reversal in real time. For example, let us suppose that we want the input and output fields to have the same temporal shape, $E_{out}(t) = -\sqrt{\eta_w \eta_r} E_{in}(t-T)$, where T is the storage time, while still satisfying Eq. (2.19). By inverting Eq. (2.19) one can show that this can be achieved by choosing the following time-dependent couplings for the write and read

processes:

$$g_w(t) = \sqrt{\frac{\kappa\eta_w|E_{in}(t)|^2}{2(1-\eta_w+\eta_w\int_{-\infty}^{t}dt'|E_{in}(t')|^2)}}$$
$$g_r(t) = \sqrt{\frac{\kappa\eta_r|E_{in}(t-T)|^2}{2(1-\eta_r\int_{-\infty}^{t}dt'|E_{in}(t'-T)|^2)}}. \tag{2.20}$$

This choice of $g_w(t)$ achieves the optimal write efficiency $\eta_w = 1-e^{-2\tau_w}$ for any input field $E_{in}(t)$ and any value of $\tau_w = \int_{-\infty}^{0}dt g_w^2(t)/\kappa$. On the other hand, the above choice of $g_r(t)$ ensures that the output field is proportional to the input field (shifted in time by T). We have seen that the read efficiency always satisfies $\eta_r = 1-e^{-2\tau_r}$ with $\tau_r = \int_0^{\infty}dt g_r^2(t)/\kappa$. Note that arbitrary output field shapes are possible for appropriately chosen $g_r(t)$, see also Fig. 2.

2.3.3.3 Imperfections

So far we have neglected the spontaneous decay rate γ. It is not difficult to include in the above approach, but it obviously leads to somewhat lower efficiencies, because its effect is irreversible. The optimum input field can still be found by functional differentiation. To discuss the simplest example, let us consider square coupling pulses of strength $g_{w(r)}$ and duration $t_{w(r)}$. Then the optimized input field for writing satisfies $E_{in}(t) \propto g_w e^{\frac{g_w^2 t}{\kappa}+\gamma t}$ and the output field from the read process fulfills $E_{out}(t) \propto g_r e^{-\frac{g_r^2 t}{\kappa}-\gamma t}$, while the efficiencies satisfy

$$\eta_{w(r)} = \frac{\frac{g_{w(r)}^2}{\kappa}}{\frac{g_{w(r)}^2}{\kappa}+\gamma}\left(1-e^{-2\left(\frac{g_{w(r)}^2}{\kappa}+\gamma\right)t_{w(r)}}\right). \tag{2.21}$$

One can see that for large effective times the efficiencies tend towards $\frac{C}{C+1}$ [66], where $C = \frac{g^2}{\kappa\gamma}$, which is essentially the optical depth in the presence of the cavity. High efficiencies require large C. For a given decay rate, C can in principle always be increased by increasing g (which requires increasing the dipole moment or the number of atoms), or by decreasing κ (which requires increasing the finesse of the cavity, i.e. the number of roundtrips).

The general case also includes a time-dependent detuning $\Delta(t)$. By functional differentiation one finds that the optimum input field has a phase dependence that exactly compensates the detun-

ing. If this is not possible, the achievable efficiencies will again be reduced. However, in analogy to the case of spontaneous decay, the effect will be small as long as the ratio $\frac{g^2}{\kappa\Delta}$ is large.

2.4 Implementation

We will now discuss potential experimental implementations of the proposed protocol. In certain rare-earth ion doped crystals optical transitions can be switched on and off by changing the applied magnetic field [62, 63, 64]. This is due to the coupling of the electronic Zeeman and hyperfine interactions in the presence of the crystal field. This coupling yields a substantial contribution to the overall nuclear Zeeman effect which is different for the ground and excited states, allowing one to control the branching ratios of optical transitions. For example, in Tm:YAG adding a field of order 80 mT transversally to a static applied field of 1 T will turn on a previously forbidden transition to a point where its optical depth d is of order 1/cm [62, 63]. It is possible to control magnetic fields of this order (tens of mT) on ns timescales [73], making it possible to store light pulses whose duration is on these timescales. See also the appendix for more details on the proposed implementation. In practice the spectral width of the pulses is more likely to be limited by nearby transitions. The optical depth will be enhanced by the cavity, one has $C \approx dF$ for the ratio C defined above, where F is the cavity finesse. Based on Eq. (2.21) high efficiencies should thus be achievable combining crystals of typical dimensions (say 1 cm in length) with moderate-finesse cavities. We have focused on the case of a memory inside a cavity. However, good memory performance based on the same principle is possible without a cavity as well, see the appendix. In particular, we show that the present protocol outperforms memories based on controlled reversible inhomogeneous broadening (CRIB) [19] in terms of efficiency for a given optical depth.

The described memory could be attractive from a practical point of view as a solid-state Raman-like memory that does not require an optical control field, thus avoiding spurious signal detections (i.e. noise) due to the presence of the strong control beam [41]. Implementations in systems other than rare-earth ion doped crystals may be possible, for example using electric control fields for NV

centers in diamond [65].

More conceptually, the present protocol has the potential to provide insight into the basic principles underlying quantum memories for light in general. As a first example, we have seen that the optimal write process is related to the read process by a reversal of effective, but not necessarily real, time. Because of the mentioned formal equivalence of the considered system to off-resonant Raman memories, this result applies to the latter as well. It is an interesting question whether the same also holds for other memory protocols for appropriately defined effective variables. See Refs. [19, 60, 74, 75] for related discussions in real time. Even more generally, the present protocol seems well placed to serve as an "archetype" for quantum memories, because, as discussed above, in all memory protocols the light-matter interaction is controlled in some fashion. Mapping various protocols onto the controllable-dipole memory discussed here may be a good way of analyzing their similarities and differences.

2.5 Appendix A1: Solution of the Maxwell-Bloch equations in free space

The equations of motion in free space are given by

$$\begin{aligned} \partial_t \sigma(z,t) &= -(\gamma + i\Delta(t))\sigma(z,t) + ig(t)E(z,t) \\ \partial_z E(z,t) &= i\frac{g(t)}{c}\sigma(z,t), \end{aligned} \tag{2.22}$$

where $\sigma(z,t)$ can be interpreted as the wave function for a single atomic excitation, and $E(z,t)$ as the wave function for a single photon; γ, $\Delta(t)$ and $g(t)$ are the same as in the paper and it can be represented by $g(t) \equiv \sqrt{\omega_0/2\varepsilon_0\hbar V}\wp(t)$, where $\wp(t)$ is the controllable transition dipole moment, ω_0 is central frequency of the incident light pulse, and V is the quantization volume; c is the speed of light. These equations are valid if saturation can be neglected, which is guaranteed if the number of atoms N is much greater than one. Moreover it is assumed in the derivation that the length of the medium L is much smaller than the characteristic length of the pulse, such that the difference between the real time t and retarded time $t - z/c$ is negligible.

We define $S(z,t) = e^{i\chi(t)}\sigma(z,t)$, $\mathscr{E}(z,t) = \frac{cE(z,t)}{ig(t)}e^{i\chi(t)}$ and $\tau(t) = \int_0^t dt' \frac{g(t')^2}{c}$, where $\chi(t) = \int_0^t dt'(\Delta(t') - i\gamma)$, see also Ref. [16]. Substituting these variables in the Eq. (2.22) gives

$$\begin{aligned} \partial_\tau S(z,\tau) &= -\mathscr{E}(z,\tau) \\ \partial_z \mathscr{E}(z,\tau) &= S(z,\tau). \end{aligned} \tag{2.23}$$

Using a proper Laplace transformation, $\mathscr{L}\{\mathscr{E}(z,\tau)\} = e(s,\tau) = \int_0^\infty dz e^{-sz}\mathscr{E}(z,\tau)$ and $\tilde{S}(s,\tau) = \int_0^\infty dz e^{-sz}S(z,\tau)$, one can convert the set of differential equations in Eq. (2.23) to a differential equation and an algebraic equation, namely

$$\begin{aligned} \partial_\tau \tilde{S}(s,\tau) &= -e(s,\tau) \\ \tilde{S}(s,\tau) &= -\mathscr{E}(0,\tau) + se(s,\tau). \end{aligned} \tag{2.24}$$

One can easily find $\tilde{S}(s,\tau) = -\frac{1}{s}\int_0^\tau d\tau' e^{(\tau'-\tau)/s}\mathscr{E}(0,\tau') + e^{-\tau/s}\tilde{S}(s,0)$. Plugging this result into the second equation in Eq. (2.24) gives $e(s,\tau) = s^{-1}\mathscr{E}(0,\tau) + s^{-1}e^{-\tau/s}\tilde{S}(s,0) - s^{-2}\int_0^\tau d\tau' e^{(\tau'-\tau)/s}\mathscr{E}(0,\tau')$. Using $\mathscr{L}\{(z/a)^{n/2}I_n(\sqrt{4az})\} = s^{-(n+1)}e^{a/s}$ and the convolution theorem [76] the solution is as follows,

$$\begin{aligned} \mathscr{E}(z,\tau) &= \mathscr{E}(0,\tau) + \int_0^z dz' S(z',0) I_0(\sqrt{4\tau(z'-z)}) \\ &+ \int_0^\tau d\tau' \mathscr{E}(0,\tau')\sqrt{\frac{z}{\tau'-\tau}} I_1(\sqrt{4(\tau'-\tau)z}), \\ S(z,\tau) &= S(z,0) - \int_0^\tau d\tau' \mathscr{E}(0,\tau') I_0(\sqrt{4z(\tau'-\tau)}) \\ &- \int_0^z dz' S(z',0)\sqrt{\frac{\tau}{z'-z}} I_1(\sqrt{4\tau(z'-z)}), \end{aligned} \tag{2.25}$$

where I_n is the nth modified Bessel function, see also [77]. One can simply use the above-mentioned definitions for $\mathscr{E}(z,\tau)$, $S(z,\tau)$ and $\tau(t)$ to convert the result in Eq. (2.25) to the actual optical field.

This solution allows one to analyze both the storage (write) and retrieval (read) process, depending on the initial conditions. In the next section it is used to determine the efficiency of the controllable-dipole memory in free space.

2.6 Appendix A2: Efficiency analysis and comparison with the controlled reversible inhomogeneous broadening quantum memory protocol

In this section we study the efficiency of the controllable-dipole quantum memory and we compare its performance to that of the controlled reversible inhomogeneous broadening (CRIB) protocol [84]. In the free-space case, in contrast to the cavity case discussed in the paper, we do not know the exact conditions for $E_{in}(t)$ and $g(t)$ which maximize the total efficiency for the controllable-dipole protocol. In spite of this, we show that it is still possible to achieve very good memory performance under realistic conditions. We have chosen an incident light pulse that is a Gaussian with full width at tenth of maximum (FWTM) $T_{pulse} = 300$ ns, and a Gaussian profile for $g(t)$, which is displaced in time relative to the pulse, see Fig. 2.3. We also choose $\gamma = 50$ kHz, and assume that $\Delta(t)$ has the form shown in the inset of Fig. 2.3. All of these choices are motivated by the implementation considerations discussed in the next section. We are interested in the efficiency of the memory as a function of the optical depth. In our model, the optical depth $D(t) = \frac{g(t)^2 L}{\gamma c}$ is a function of time. In order to facilitate the comparison with CRIB we define $d = \max D(t)$ to indicate the effective optical depth of our system when the dipole has its maximum value.

Fig. 2.4(a) shows the efficiency of the controllable-dipole memory for the above-mentioned parameters as a function of d, for retrieval in the backward and in the forward direction. As for other memory protocols including CRIB, the efficiency in the forward direction is limited by reabsorption, see Ref. [20]. In the backward direction, the achievable maximum efficiency is mainly limited by the decay rate γ. Note that backward retrieval requires transferring the atomic excitation to an extra level using an optical control field. Here we have assumed that the pulse is retrieved immediately after having been stored. Otherwise the storage time also has to be taken into account.

Fig. 2.4(b) shows the efficiency as a function of d for the CRIB memory protocol, based on the results of Ref. [20]. In order to make a meaningful comparison, we choose the same initial linewidth $\gamma = 50$ kHz for CRIB as for the controllable-dipole memory. In the CRIB protocol the initial line is broadened through the application of an external field in order to accomodate the

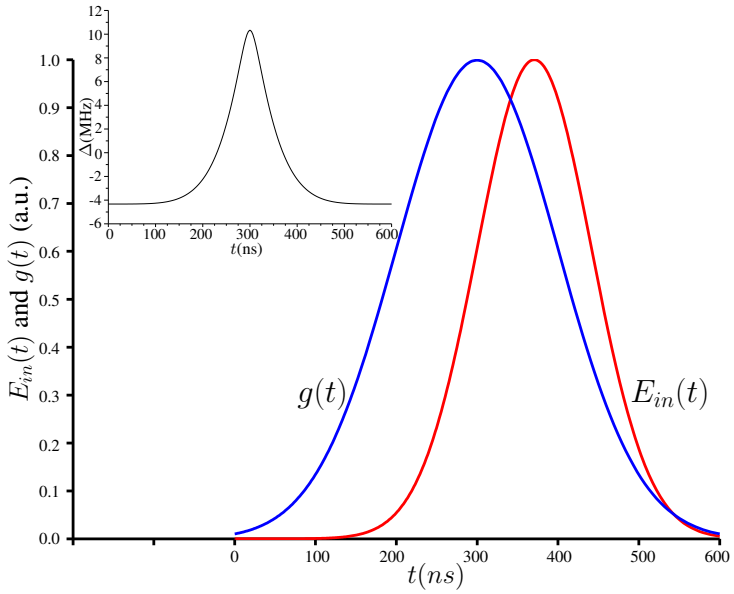

Figure 2.3: The time-dependent coupling $g(t)$ and input field $E_{in}(t)$ used in our examples. The inset shows the time-dependent detuning $\Delta(t)$. See text for a more detailed discussion.

spectrum of the input pulse. This can be seen as analogous to the effective spectral broadening that happens in the controllable-dipole protocol as a consequence of the time dependence of the transition dipole, making CRIB a natural point of comparison for the present protocol. The input pulse of Fig. 2.3 has a frequency FWTM of 9.8 MHz. Since broadening the initial line lowers the optical depth, it is advantageous to choose the width of the broadened line somewhat smaller than this value. This cuts off the outermost frequency components of the pulse, but enhances the efficiency for the most important components. In Fig. 2.4(b) we show the efficiency of CRIB for two different choices of the broadened width. The first (8 MHz) is chosen such that the maximum achievable efficiency is the same as for the controllable-dipole memory. One can see that in this case the efficiency for the CRIB memory increases significantly more slowly with d. On the other hand, for the second choice of broadened linewidth (3.5 MHz) the efficiency initially increases similarly quickly for CRIB. But then the achievable maximum efficiency is reduced, because a significant fraction of the input pulse is cut off. Taking these observations together, one can see that the controllable-dipole memory shows better efficiency performance than the CRIB protocol, even without full optimization of the pulse shapes. It should be noted that the shape of the broadened

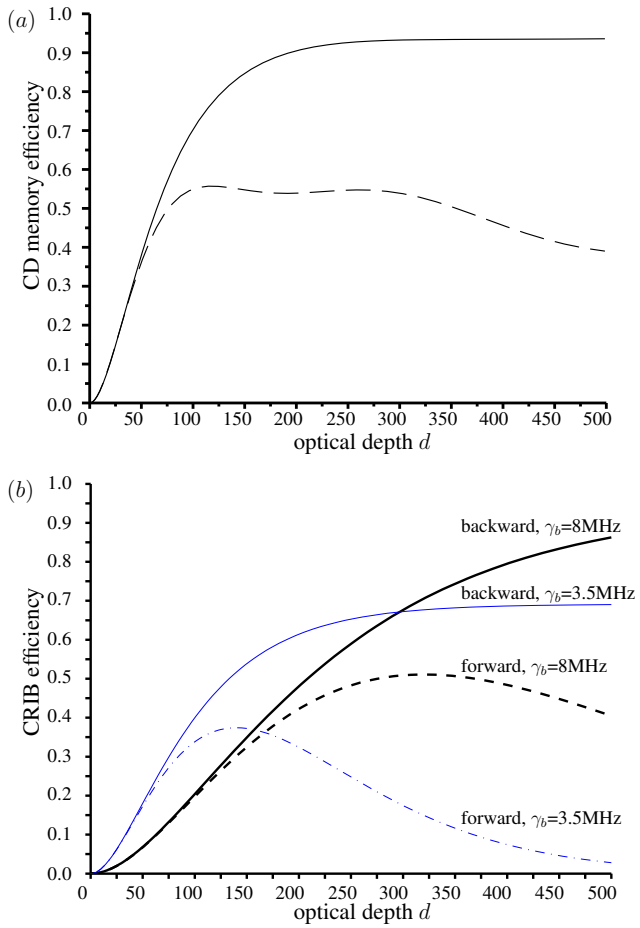

Figure 2.4: (a) Efficiency of the controllable-dipole memory in free space for readout in the backward (solid line) and forward (dotted line) direction. In analogy with other quantum memory protocols such as AFC or CRIB, the forward retrieval efficiency is limited due to re-absorption. (b) Efficiency for a CRIB memories with two different values for the broadened linewidth, also in backward and forward direction. See text for a more detailed discussion.

absorption line in CRIB has not been optimized for a Gaussian pulse.

2.7 Appendix A3: Implementation in Tm:YAG

In the following we discuss a potential implementation of the controllable-dipole quantum memory protocol in a Tm:YAG crystal. We focus on the first crystal-field states of the ${}^3H_6(0)$ and ${}^3H_4(0)$ multiplets, with a transition at 793 nm [63], see Fig. 2.5(a). For a magnetic field in x direction, the states $|2\rangle$ and $|3\rangle$, which are employed as ground and excited states in our memory scheme, are eigenstates of the nuclear spin in x direction with eigenvalues M_I of $1/2$ and

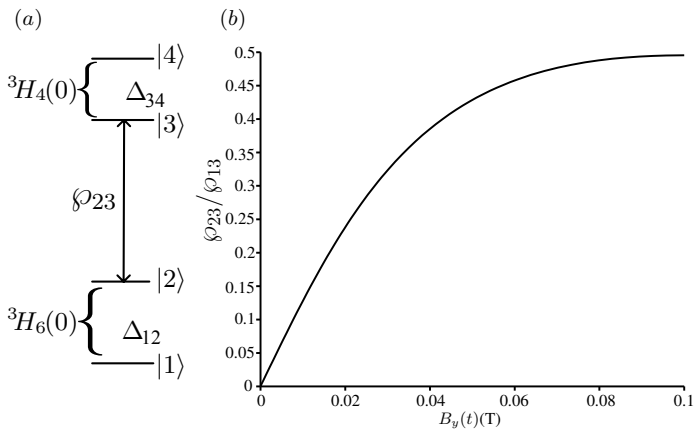

Figure 2.5: (Color online)(a) Transition used for the proposed implementation. (b) The corresponding transition dipole moment as a function of the applied magnetic field. See text for a more detailed discussion.

$-1/2$ respectively. According to the nuclear spin selection rule $\Delta M_I = 0$ the dipole moment $\wp_{23} = \langle 2, M_I = -1/2| - er|3, M_I = 1/2\rangle \equiv 0$ and the transition $|2\rangle \leftrightharpoons |3\rangle$ is forbidden. This corresponds to $g(t) = 0$. When an additional magnetic field is applied in the y direction, the states $|2\rangle$ and $|3\rangle$ become superpositions of the nuclear spin states corresponding to $M_I = 1/2, -1/2$. Perturbative treatment of the electronic Zeeman effect and hyperfine interaction shows that the first order of perturbation is zero. However, in the second order of perturbation, cross coupling of the electronic Zeeman effect and hyperfine interaction is taking place, which leads to nuclear spin state mixing for certain directions of the magnetic field, see [62]. This yields a considerable transition dipole moment between $|2\rangle$ and $|3\rangle$ and thus non-zero $g(t)$.

The sensitivity to the direction of the magnetic field is due to the anisotropic gyromagnetic ratio in Tm:YAG [62]. Based on the crystal-field Hamiltonian approach, one can completely calculate the magnetic interactions from the crystal-field wave functions. Fig.2.5(b) shows a particular case of the dependence of $\wp_{23}$ on the direction of B. Using the same definition of local crystal-field axes as in Ref.[63], we fix $B_x = 1T, B_z = 0T$, and let B_y vary from 0T to 0.10T. As a consequence, $\wp_{23}$ varies from 0 to $0.44\wp_{13_0}$, where $\wp_{13_0} \equiv \wp_{13}|_{(B_y=0)}$ is the transition dipole moment of $|1\rangle \leftrightharpoons |3\rangle$ when $|B_y| = 0$. Note that $\wp_{13}$ also varies slightly under the same modulation of the direction of the magnetic field, see Fig. 2.5. Therefore, with a magneto-dependent transition dipole moment and

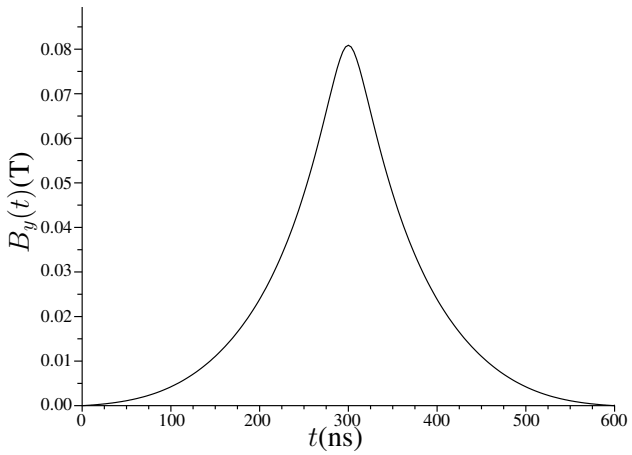

Figure 2.6: Time dependence of the applied magnetic field B_y in order to obtain $g(t)$ as shown in Fig. 2.3; this field dependence also leads to a time-dependent detuning $\Delta(t)$ as shown in the inset of Fig. 2.3.

long-lived upper level (coherence times of order 100 μs have been reported [78]), the transition $|2\rangle \leftrightharpoons |3\rangle$ is an excellent candidate for the present scheme. The initial narrow line can be prepared by spectral tailoring, see e.g. [79].

The speed of controlling $g(t)$ is limited by how fast one can control the magnetic field. Ref. [73] demonstrated a device composed of an electronic circuit and a low inductance coil capable of producing rapidly switched magnetic fields with a speed of 0.02T/10ns. Noticing the variation range of B_y in Fig.2.5(b), this speed would enable us to control $\wp_{23}$, and consequently change the coupling $g(t)$, on a time scale of 100ns, which sets a lower bound for the input pulse duration T_{pulse}. This motivates the choice of $g(t)$ and $E_{in}(t)$ shown in Fig. 2.3. Fig.2.6 shows the time-dependent magnetic field B_y that has to be applied in order to produce that form of $g(t)$. This field also leads to a time-dependent detuning $\Delta(t)$ as shown in the inset of Fig. 2.3.

Chapter 3

Photonic quantum memory in two-level ensembles based on modulating the refractive index in time

3.1 Preface

Inventing new quantum memory protocols and studying similarities and differences between the quantum memory protocols is an important step toward a better understanding of the protocols and categorizing them. This provides the opportunity to combine different schemes to satisfy several criteria in one implementation. Such theoretical investigations may lead to a versatile quantum memory with simpler implementations.

This chapter presents studies of a new quantum memory protocol that allows storing light in ensembles of two-level atoms by modulating the refractive index of the host medium. One can imagine an ensemble of atoms in a host, *e. g.* rare-earth ions doped in a crystal. Results in this paper show that linear modulation of the refractive index of the host medium in time induces a position-dependent detuning between the photon and the atoms. This can be used to store and recall photons. Under certain conditions that are explained in the manuscript, the dynamics of the proposed system is shown to be equivalent to that underlying the gradient echo memory protocol. It has to be noted that the gradient echo memory is based on a position-dependent modulation on the transition energy of the atoms. The experimental implementation is proposed based on the Tm^{3+} ions doped in lithium niobate waveguide. A proper external electric field can modulate the refractive index of the lithium niobate without affecting the transition energy of the thulium ions. Since this scheme is based on the application of a time-dependent electric field, it could introduce simplicity in practice compared to the requirement for a position-dependent magnetic or electric field in the implementation of GEM.

This work is published based on an undergraduate project. I supervised calculations that have been done by the undergraduate student. I refined the calculations and derivations. I analyzed the proposed physical system for the implementation. Finally, I wrote the manuscript and prepared responses to the referee reports.

3.2 Introduction

Quantum memory for light is an essential element for the photonic implementation of quantum communication and information processing [80, 12]. In recent years there has been a lot of work both on theoretical proposals and on experimental implementations [56, 58]. Thus far optical control, using relatively strong laser pulses, has been exploited for electromagnetically induced transparency and off-resonant Raman-type storage [81, 82] in ensembles of three-level systems. More recently, a direct control of the transition dipole-moment has been proposed that emulates Raman-type quantum memories in a two-level atomic configuration [83].

In photon-echo based memories [30], the light-matter coupling is controlled in a more indirect way by exploiting the dephasing and rephasing of inhomogeneously broadened atomic ensembles. This includes the controlled reversible inhomogeneous broadening protocol [84], the atomic frequency comb protocol [24], and the gradient echo memory (GEM) protocol [85]. The GEM protocol has allowed the demonstration of the highest memory efficiency (in the quantum regime) so far [23].

Recently Ref. [86] proposed a quantum memory protocol based on controlling the refractive index. Considering an ensemble of three-level atoms inside a host medium (e.g. rare-earth ions doped into a crystal), which is located in a circular optical cavity, the authors showed that a continuous change of the refractive index of the host medium during an off-resonant Raman interaction between a single photon, a classical control pulse and the atomic ensemble allowed mapping the state of the single photon into a collective atomic excitation.

Here we consider storing quantum states of light in an ensemble of two-level atoms in a host

medium, where the refractive index of the medium can be modulated during the interaction of the light with the atoms. In contrast to Ref. [86] here there is no optical control pulse (which is related to the fact that we consider two-level instead of three-level atoms) and no cavity. Interestingly, we find that under certain conditions the considered system leads to dynamics that are equivalent to those of the GEM protocol; controlling the refractive index of the host medium *in time* can mimic the effect of the *spatial* frequency gradient present in GEM.

This paper is organized as follows. In Sec. 3.3 we derive the dynamical equations for our system under certain conditions, which we discuss in detail. In Sec. 3.4 we compare these results to the GEM protocol. In Sec. 3.5 we discuss a possible experimental implementation of our protocol. Sec. V contains our conclusions.

3.3 Maxwell-Bloch equations

Here we study the propagation of the light and its interaction with two-level atoms inside a host medium whose refractive index varies in time. We show that in a certain parameter regime the time-dependent refractive index does not play a role in the propagation equation for the light. In contrast, it plays an essential role in the dynamics of the atomic polarization. For simplicity, we assume the field is propagating in a certain direction with a fixed linear polarization. (This is well justified for our choice of possible implementation in a waveguide, see below.) The wave equation for the electric field operator is analogous to the classical equation, namely

$$\frac{\partial^2 E}{\partial z^2} = \mu_0 \frac{\partial^2 D}{\partial t^2} = \mu_0 \frac{\partial^2}{\partial t^2}(\varepsilon E + P), \tag{3.1}$$

where E is the electric field, z is the direction of propagation, μ_0 is the vacuum permeability, D is the electric displacement field, ε is the permittivity of the propagation medium and P is the polarization of the embedded two-level atoms. There are thus two fundamentally different contributions to D. The εE term is due to the permittivity of the host medium, whereas P describes the polarization of the two-level atoms that are the actual memory system for the light.

Consider the case where ε is time-dependent. The permittivity of the medium is related to its refractive index as $\varepsilon(t) = n^2(t)\varepsilon_0$. We consider a medium with a linearly changing refractive index, $n(t) = n_i + \dot{n}t$. Based on this, only the first derivative of the refractive index remains in the Eq. (3.1), giving

$$(\frac{\partial^2}{\partial z^2} - \frac{n^2(t)}{c^2}\frac{\partial^2}{\partial t^2})E = \frac{1}{c^2}(2\dot{n}^2 E + 4n(t)\dot{n}\dot{E}) + \mu_0\ddot{P}, \tag{3.2}$$

where c is the speed of light. We now introduce the slowly varying components of the signal field E and the atomic polarization P, $E = \mathscr{E}e^{-i(\omega_0 t - k_0(t)z)}$ and $P = \mathscr{P}e^{-i(\omega_0 t - k_0(t)z)}$. Here the wave vector $k_0(t) = k_i + \dot{k}t = (n_i + \dot{n}t)\frac{\omega_0}{c}$ is a function of time and $\dot{k} = \frac{\dot{n}\omega_0}{c}$, where ω_0 is the central frequency of the signal.

The wave equation can be greatly simplified provided that a number of (realistic) conditions are fulfilled (see also the appendix). The second-order spatial derivative for $\mathscr{E}$ can be dropped provided that the field amplitude changes appreciably over the length of the medium (such that the derivative is comparable to $\mathscr{E}/L$) and $k_0(t) \gg 1/L$. Similarly, the second order time-derivative can be ignored if $\omega_0 \gg 1/\tau$, where τ is the duration of the pulse. The same conditions also allow one to drop the first and second order derivatives of the slowly varying polarization operator. We are interested in the regime where the extent of the pulse in space (outside the medium), $\mathscr{L} = c\tau$, is much greater than the length of the medium, L [24]. This is a realistic condition which is satisfied even in experiments with broadband pulses [50]. This allows one to drop the first-order time derivative of $\mathscr{E}$ compared to the first-order spatial derivative. Note that this condition is not crucial; the time derivative can also be eliminated by transforming the equation to the co-propagating frame as in Ref. [87], provided that $\Delta n \ll n_i$, where Δn is the total change in the refractive index.

Finally, by assuming $\Delta n \ll n_i$ and $\dot{k}L \ll \frac{2c}{nL}$ one obtains the simplified propagation equation

$$\frac{\partial \mathscr{E}}{\partial z} = \frac{i\mu_0\omega_0^2}{2k_i}\mathscr{P}. \tag{3.3}$$

This shows that, under the above conditions, the propagation equation remains unchanged compared to that of systems with constant refractive index ($\dot{k}$ does not play an appreciable role in the propagation), see e.g. [87, 24]. The derivation of Eq. (3) from Eq. (2) is discussed in detail in the

appendix.

We now derive the dynamics of the polarization of the dopant atoms. The polarization of the j-th atom is $P^j = \langle g^j|\hat{d}|e^j\rangle\sigma_{ge}^j$, where $\sigma_{ge}^j = |g^j\rangle\langle e^j|$ and $\langle g^j|\hat{d}|e^j\rangle$ is the matrix element of the corresponding dipole moment component between the ground and excited states. The collective atomic polarization at a certain position z is the sum over the individual atoms in a slice of width Δz. The slow component of this collective operator is given by

$$\mathscr{P} = \frac{1}{A\Delta z}\langle g|\hat{d}|e\rangle \sum_{j=1}^{N_z} \sigma_{ge}^j e^{i(\omega_0 t - k_0(t) z_j)} \equiv \langle g|\hat{d}|e\rangle \frac{N}{V}\tilde{\sigma}_{ge}, \tag{3.4}$$

where we assume equivalent dipole moment for all of the atoms; A and V are the cross-section area and volume of the light-atom interface; N is the number of the dopant atoms and $\tilde{\sigma}_{ge} = \frac{1}{N_z}\sum_{j=1}^{N_z} \sigma_{ge}^j e^{i(\omega_0 t - k_0(t) z)}$ is the average atomic polarization at position z. The Hamiltonian of the ensemble of the dopant atoms interacting with the light field can be written as

$$\begin{aligned} H &= H_0 + H_{int} \\ &= \sum_{j=1}^{N} \hbar\Omega\sigma_{ee}^j - \langle e|\hat{d}|g\rangle \sum_{j=1}^{N} \sigma_{eg}^j E(z_j,t) + h.c., \end{aligned} \tag{3.5}$$

where we assume uniform excited state energy $\hbar\Omega$ for all of the atoms. We can now derive the dynamics of the slowly varying collective atomic polarization using

$$\frac{d\tilde{\sigma}_{ge}}{dt} = -\frac{i}{\hbar}[\tilde{\sigma}_{ge}, H] + \frac{\partial\tilde{\sigma}_{ge}}{\partial t}. \tag{3.6}$$

For the next step we assume that all of the atoms are initialized in the ground state and the number of atoms $N \gg 1$. For weak (quantum) signals one can then ignore the change in the excited state population.

Using Eqs. (3.3,3.4,3.5,3.6), the above definition of the slowly varying field, and including the atomic excited state linewidth γ, one finds the Maxwell-Bloch equations describing the interaction of the light with the collective atomic polarization in a medium with linearly time-varying

refractive index,

$$\begin{aligned} \frac{d\tilde{\sigma}_{ge}(z,t)}{dt} &= -(\gamma + i(\Delta + \dot{k}z))\tilde{\sigma}_{ge}(z,t) + ig\tilde{\mathscr{E}}(z,t), \\ \frac{\partial\tilde{\mathscr{E}}(z,t)}{\partial z} &= i\frac{nNg}{c}\tilde{\sigma}_{ge}(z,t), \end{aligned} \tag{3.7}$$

where $\tilde{\mathscr{E}} = \sqrt{\frac{\hbar\omega_0}{2\varepsilon_i V}}\mathscr{E}$ and $\Delta = \Omega - \omega_0$ is the detuning. The coupling constant $g = \langle e|\hat{d}|g\rangle\sqrt{\frac{\omega_0}{2\hbar\varepsilon_i V}}$, where ω_0 is the central frequency of the pulse and $\varepsilon_i = n_i^2\varepsilon_0$ is the initial refractive index of the medium. Note that the time dependence of the permittivity can be ignored in the definitions of $\tilde{\mathscr{E}}$ and g because we are interested in the regime where $\Delta n \ll n_i$.

The above set of equations shows the role of the linearly changing refractive index of the host medium in the regime that we have discussed. One sees that the linear change of the refractive index in time results in a space-dependent frequency shift given by the $\dot{k}z$ term in Eq. (3.7), see also Fig. 3.1(b). The above Maxwell-Bloch equations are identical to those underlying the GEM quantum memory protocol [85]. In the next section we therefore discuss in detail how the present proposal compares to GEM.

3.4 Comparison with Gradient Echo Memory

The dynamical equations (8) derived in the previous section (under a number of realistic conditions) are exactly equivalent to those underlying the GEM quantum memory protocol [85]. In the GEM protocol, an initially narrow atomic absorption line is broadened by applying an external (longitudinal) field gradient. This longitudinal broadening allows one to accommodate all frequency components of the incoming pulse, see Fig. 3.1(a). Once the pulse is absorbed, the produced collective atomic excitation starts to dephase due to the position-dependent detuning. By inverting the external field that is used to generate the gradient, one can rephase the collective atomic excitation, which leads to the re-emission of the light.

At first sight it may seem surprising that a time variation of the refractive index leads to a spatial gradient in the detuning. This can be understood in the following way. In the definition

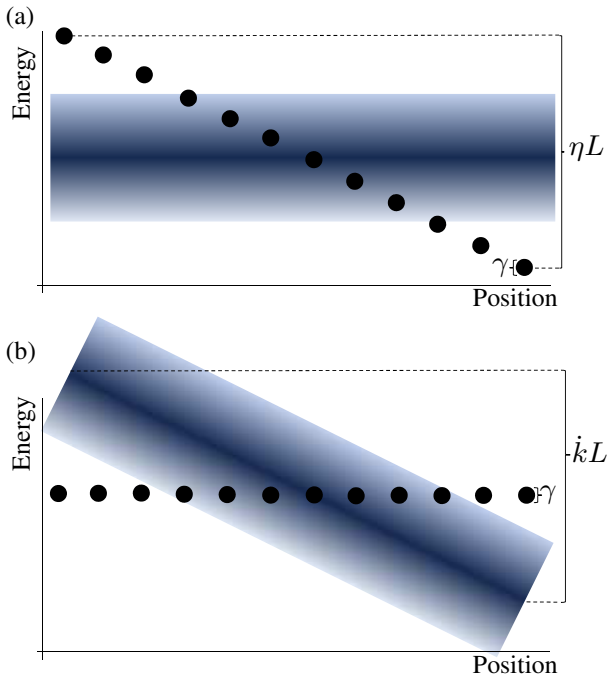

Figure 3.1: (Color online) (a) In the GEM protocol, a longitudinal energy shift in the atoms (solid dots) allows one to cover all of the frequency components of the incoming light. (b) In the protocol proposed here, due to the linear change of the refractive index in time, the light experiences an effective position-dependent frequency shift $\dot{k}z$. This allows different frequency components of the light to interact on resonance with a spectrally narrow line of atoms.

for the slow-varying field $\mathscr{E}$, $E = \mathscr{E}e^{-i(\omega_0 t - k_0(t)z)}$, the fast-varying phase $-i(\omega_0 t - k_0(t)z)$ has a temporal and a spatial part. One can define an effective frequency for the light by taking the time derivative of the phase, $\omega_{eff} = \omega_0 - \dot{k}z$. One can see that this corresponds to a spatial gradient in the frequency of the light, leading to a spatial gradient in the light-atom detuning, see Fig. 3.1(b). A quantum memory can then be realized in analogy with GEM. The light is absorbed while the refractive index is changing linearly in time. Then the refractive index is kept constant for storage. The light can be retrieved by changing the refractive index linearly in time again, but with the opposite sign to before. As for other two-level memory protocols including GEM, the storage time can be increased if necessary by transferring the population (after the absorption has been completed) from the excited state to a long-lived third state.

The total shift in the effective frequency over the length of the medium is $\dot{k}L$. In order to accommodate all frequency components of the signal $\dot{k}L$ has to be larger than the frequency band-

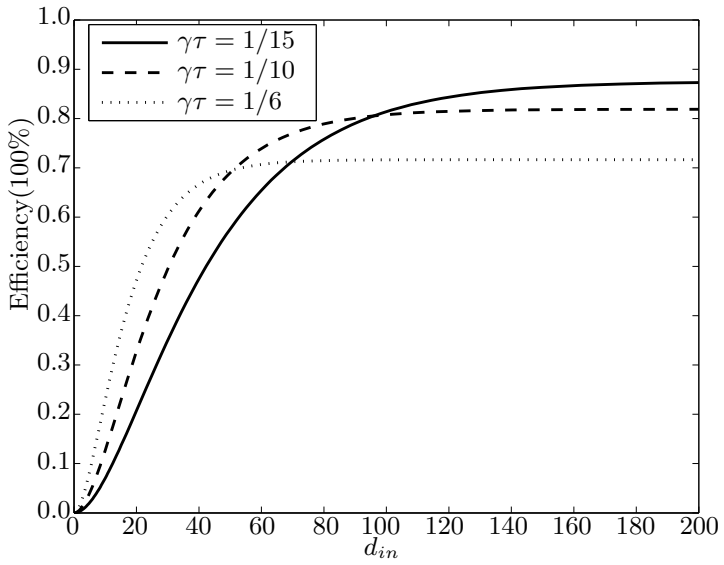

Figure 3.2: The efficiency of the proposed memory protocol based on refractive index modulation in terms of the initial optical depth d_{in}. The efficiency is given by $e^{-2\gamma\tau}(1-\exp(-d_{in}\gamma/\dot{k}L))^2$. The figure shows the efficiency for different pulse durations τ, relative to the excited state line width, γ. We assume $\dot{k}L\tau = 2$. Depending on the available optical depth, one can optimize the achievable efficiency by choosing an appropriate pulse duration.

width of the signal, $\Delta\omega \equiv 1/\tau$. Therefore, $\dot{k}L$ can be understood as the memory bandwidth. This is equivalent to the role of ηL in GEM, see Fig. 3.1 and [87].

The efficiency of the present quantum memory proposal can be found by analogy to GEM, see Eqs. (3, 4) in [87]. Converting the equations of motion to the frequency domain, one finds that the transmitted pulse is attenuated by a factor of $\exp(-\beta\pi)$, where $\beta = \frac{nNg^2}{c\dot{k}}$. This implies that the optical depth of the system is $d = 2\beta\pi = 2\pi\frac{nNg^2}{c\dot{k}} = d_{in}\frac{\gamma}{\dot{k}L}$. Here d is the optical depth that is associated with the effectively broadened line, with the initial optical depth $d_{in} \equiv 2\pi\frac{nNg^2L}{c\gamma}$. The retrieval efficiency is then given by $(1-\exp(-d))^2 e^{-2\gamma\tau}$, see Fig. 3.2. Here we have assumed that the decay of the excited state only has an effect during absorption and retrieval, but not during storage. As mentioned before, this can be achieved e.g. by transferring the excitation to a third, longer-lived state. Hyperfine ground states in rare-earth doped crystals can have coherence times of many seconds [88].

3.5 Possible implementation

We now discuss a potential experimental implementation of our proposed protocol. We propose to use thulium ions doped into a lithium niobate waveguide. This system was used in a recent implementation of an atomic frequency comb memory [50]. Lithium niobate is an attractive host for the present proposal because of its electro-optic properties, see below. The thulium ions interact with near-infrared light at a wavelength of 795 nm. The transition is naturally inhomogeneously broadened. We propose to prepare an initial atomic linewidth of $\gamma = 10$ MHz by optical pumping, which is very realistic. We consider the case where $\dot{k}L\tau = 2$. This assures that the memory bandwidth is large enough that it can accommodate the incoming pulse. Assuming $L = 3$ cm this leads to the requirement $\Delta n \approx 1.5 * 10^{-5}$. We choose the pulse duration $\tau = 1/6\gamma$. The above values assure that $\omega_0 \gg 1/\tau$, $L \ll \mathscr{L} = c\tau$, $\dot{k}L \ll \frac{2c}{nL}$, $\Delta n \ll n_i$ and $k_0(t) \gg 1/L$, as required for the derivation in section II. The given length corresponds to an optical depth $d_{in} \approx 18$ (at the peak) for a doping concentration of $1.35 * 10^{20}$ cm^{-3}, see the supplementary information of Ref. [50, 89]. For the given parameter values one would achieve about 43% efficiency, see Fig. 3.2, which would be largely sufficient for a proof of principle experiment. Much larger optical depths, which would allow greater efficiencies (see Fig. 3.2), have already been achieved in other crystals doped with rare-earth-ions, see [22].

We consider the refractive-index modulation of the ordinary optical axis of lithium niobate by a fast varying electric field. We consider the case where the crystal is clamped (spatially confined) and the temperature is a few Kelvin. Under these conditions the refractive index of the ordinary axis $n_o \approx 2.26$ [90]. The change in the refractive index through the electro-optical effect is governed by $\Delta(\frac{1}{n^2})_{ij} = \sum_k r_{ijk}E_k$, where $i, j = 1$ is associated with the refractive index change of the ordinary axis. This means that a time-dependent external field in a certain direction, E_k, can impose a time-dependent refractive index for the ordinary axis if there exists a non-zero linear electro-optical coefficient for that direction, r_{11k}. For lithium niobate $r_{113} \approx 10 * 10^{-12}$m/V and $r_{112} \approx -3 * 10^{-12}$m/V [90, 91]. This leads to $\Delta n \approx 1.8 * 10^{-5}$ under $0.3 * 10^6 - 1.0 * 10^6$V/m electric field,

depending on the direction of the field in the 2-3 plane. This is equivalent to applying $3-10$V to a system that has 10μm thickness, comparable to the waveguide used in Ref. [50]. The maximum change in the refractive index in lithium niobate is expected to be 10^{-3}, which is limited by the breakdown electric field [92].

Applying the external electric field to change the refractive index is potentially accompanied by level shifts, due to the linear Stark shift, for the atomic ground and excited states. On the other hand, for a certain type of dopant, by having the external electric field orthogonal to the difference between the permanent electric dipole moment of the ground and excited states, one can keep the resonant frequency between these states unchanged. In our proposed system the permanent dipoles are aligned with the 3-axis [93, 94], therefore the electric field should be applied along the 2-axis in order to avoid level shifts.

3.6 Conclusion

We have proposed a memory protocol based on varying the refractive index of the host medium in time, and shown that in a certain regime it is equivalent to the GEM protocol, even though the latter is based on a spatial frequency gradient. One may wonder why no similar spatial gradient was seen in the protocol of Ref. [86], which also considered a time-varying refractive index, but in a Raman-type system, in contrast to the two-level ensemble considered by us. This can be understood by noting that in the scheme of Ref. [86] the refractive index modulation causes a spatial gradient in the frequencies for both the signal and the control fields, such that the two-photon transition frequency remains unchanged. This holds for co-propagating signal and control. It might be interesting to consider counter-propagating signal and control fields in this context, for which no such cancelation would occur. This might result in a protocol similar to Raman-GEM [21].

We found that a relatively small modulation of the refractive index should be able to provide sufficient memory bandwidth. We proposed a potential implementation in lithium niobate waveg-

uides doped with rare-earth ions. However, other implementations could also be considered. In general, it may be easier to control the behavior of the refractive index in time, compared to the spatial control of the atomic transition frequencies required in standard GEM experiments.

3.7 Appendix: Wave equation simplification

Here we explain in more detail how to obtain Eq. (3) from Eq. (2). Substituting $E = \mathscr{E} e^{-i(\omega_0 t - k_0(t) z)}$ and $P = \mathscr{P} e^{-i(\omega_0 t - k_0(t) z)}$ into Eq. (3.2) and canceling the fast varying phase gives

$$\begin{aligned} &(\partial_z^2 + 2ik_0(t)\partial_z - k_0^2(t))\mathscr{E} \\ &-\frac{n^2(t)}{c^2}(\partial_t^2 - 2i(\omega_0 - \dot{k}z)\partial_t - (\omega_0 - \dot{k}z)^2)\mathscr{E} \\ &= \frac{1}{c^2}(2\dot{n}^2 - 4in(t)\dot{n}(\omega_0 - \dot{k}z) + 4n(t)\dot{n}\partial_t)\mathscr{E} \\ &+\mu_0(\partial_t^2 - 2i(\omega_0 - \dot{k}z)\partial_t - (\omega_0 - \dot{k}z)^2)\mathscr{P}. \end{aligned} \tag{3.8}$$

In the left hand side of the equation, the term $k_0^2(t)\mathscr{E}$ cancels $\frac{n^2(t)}{c^2}\omega_0^2\mathscr{E}$. The second order spatial derivative of the field can be dropped compared to the first order, assuming that the field changes appreciably over the length of the medium, L, and $k_0(t) \gg \frac{1}{L}$. Similarly, the second order time derivative of the field and the first and second order time derivative of the polarization operator can be ignored compared to the first order derivatives if $\omega_0 \gg \frac{1}{\tau}$. This simplification is valid as long as $\omega_0 \gg \dot{k}L$. These conditions lead to

$$\begin{aligned} &(2ik_0(t)\partial_z + \frac{n^2(t)}{c^2}(2i\omega_0\partial_t - 2\omega_0\dot{k}z))\mathscr{E} \\ &= \frac{1}{c^2}(2\dot{n}^2 - 4in(t)\dot{n}\omega_0 + 4n(t)\dot{n}\partial_t)\mathscr{E} - \mu_0\omega_0^2\mathscr{P}. \end{aligned} \tag{3.9}$$

One can rewrite this equation and use $k_0(t) = n(t)\omega_0/c$ to simplify it to

$$\begin{aligned} &(\partial_z + \frac{n(t)}{c}(\partial_t + i\dot{k}z))\mathscr{E} \\ &= (-\frac{i\dot{n}^2}{c^2 k_0(t)} - \frac{2\dot{n}}{c} - \frac{2in(t)\dot{n}}{c^2 k_0(t)}\partial_t)\mathscr{E} + \frac{i\mu_0\omega_0^2}{2k_0(t)}\mathscr{P}. \end{aligned} \tag{3.10}$$

Provided that $\Delta n \ll n(t)$ (and using again $\omega_0 \gg 1/\tau$), one has $\frac{i\dot{n}^2}{c^2 k_0(t)}\mathscr{E} \ll \frac{2in(t)\dot{n}}{c^2 k_0(t)}\partial_t\mathscr{E} \ll i\frac{n(t)\dot{k}z}{c}\mathscr{E}$. The condition $\Delta n \ll n(t)$ also allows one to drop $\frac{2\dot{n}}{c}\mathscr{E}$ compared to $\frac{n(t)}{c}\partial_t\mathscr{E}$. This simplifies the

wave equation to

$$(\partial_z + \frac{n(t)}{c}(\partial_t + i\dot{k}z))\mathscr{E} = \frac{i\mu_0\omega_0^2}{2k_0(t)}\mathscr{P}. \tag{3.11}$$

Provided that the extent of the pulse in space, $\mathscr{L} = c\tau$, is much larger than the length of the medium, L, one can ignore $\frac{n(t)}{c}\partial_t\mathscr{E}$ in comparison with $\partial_z\mathscr{E}$, which is the dominant term for the slowly varying component of the field. Finally, assuming that $\dot{k}L \ll \frac{2c}{nL}$ the term $\frac{in(t)\dot{k}z}{c}\mathscr{E}$ also can be dropped compared to the dominant term, leading to

$$\partial_z\mathscr{E} = \frac{i\mu_0\omega_0^2}{2k_0(t)}\mathscr{P}. \tag{3.12}$$

The coefficient of $\mathscr{P}$ can be rewritten as,

$$\frac{i\mu_0\omega_0^2}{2k_i(1+\frac{\dot{k}t}{k_i})} \approx \frac{i\mu_0\omega_0^2}{2k_i}(1-\frac{\dot{k}t}{k_i}). \tag{3.13}$$

Under the condition $\Delta n \ll n_i$ this can be well approximated by $\frac{i\mu_0\omega_0^2}{2k_i}$, which leads to

$$\partial_z\mathscr{E} = \frac{i\mu_0\omega_0^2}{2k_i}\mathscr{P}, \tag{3.14}$$

which is the standard wave equation under similar (realistic) conditions in the absence of a time variation of the refractive index.

Chapter 4

Raman-type optical quantum memory based on an ensemble of nitrogen-vacancy centers in a cavity

4.1 Preface

Future photonic quantum technology requires miniaturized quantum memories that can be integrated with other element from photon sources to the detection. Current quantum memories that are implemented in atomic gas cells have over 10cm length. Rare-earth doped crystals are at about 1cm length. The recent impedance-matched quantum memory has about 2mm length. These sizes are far beyond the required sizes for integrated quantum photonics. Nitrogen vacancy (NV) centers in diamond is an attractive candidate as it can be fabricated in sizes that are comparable with the wavelength of light. Coherence properties of these artificial atoms suggest that NVs could be the next implementations of the quantum memories.

In this chapter, a scheme to realize the Raman-type optical quantum memory has been proposed that is based on an ensemble of nitrogen vacancy centers in a diamond that are coupled to a cavity. The scheme allows generating a collective spin excitation in the presence of the excited state inhomogeneous broadening through the off-resonant Raman coupling. We present the requirements for achieving high efficiency and high fidelity.

The manuscript has not been published yet. The work is based on collaboration with several co-authors. I performed the theoretical analysis and used numerical methods to predict the results based on the available realistic parameters. Finally, I wrote the manuscript.

4.2 Introduction

Quantum memories for light [58] are known to be vital for photonic quantum information processing, specifically in long-distance quantum communications based on quantum repeaters [3, 12]. An efficient quantum memory can be utilized as a deterministic single photon source [54]. The highest available efficiency is $> 80\%$ that is achieved in a warm Rb vapor cell and is based on gradient echo memory protocol in a Λ-system [53]. The similar protocol in a two-level atomic configuration allowed about 69% efficiency in a highly absorptive rare earth ion doped crystal [22]. These crystals combined with an impedance-matched cavity have been shown to reach 58% efficiency with much shorter crystal length (about 2mm length) [48]. However, none of the present implementations of the quantum memory is suitable to be integrated with other elements for an on-chip quantum information processing architecture with multiple operant quantum memories. In this regard, nitrogen vacancy (NV) centers in diamond are attractive systems to be exploited as quantum memories for photons due to their spin coherence time and efficient light-NV coupling. The electronic spin coherence time of 0.5s has recently been observed in NV ensembles that opens a path toward long storage times in electronic spins of NV ensembles, see [95]. NV ensembles have been used for storage and retrieval of microwave fields, see [96].

In contrast to the rare earth ion doped crystals [22, 97], the large intractable excited state inhomogeneous broadening of the NV ensembles in addition to their short excited state lifetimes prevents storage based on the optical coherence. Electromagnetically induced transparency has been observed in the NV ensemble, where 17% transparency has been achieved [98]. The large inhomogeneous optical linewidth affects the efficiency of this scheme that prevents quantum storage for optical photons. However, off-resonant Raman coupling approach allows to circumvent the excited state inhomogeneous broadening and store optical photons in the collective spin coherence [16, 99].

4.3 The scheme

Each negatively charged NV consists of 6 contributing electrons in the C_{3v} symmetry that is imposed by the environment (diamond) [33]. Fig. 4.1 shows the ground and excited states triplets, where the ground state splitting of $m_s = \pm 1$ is due to an external background magnetic field. There are four different orientations for the NV centers in the ensemble. Applying the external magnetic field allows to select a subgroup of NV centers that are aligned with the magnetic field [40].

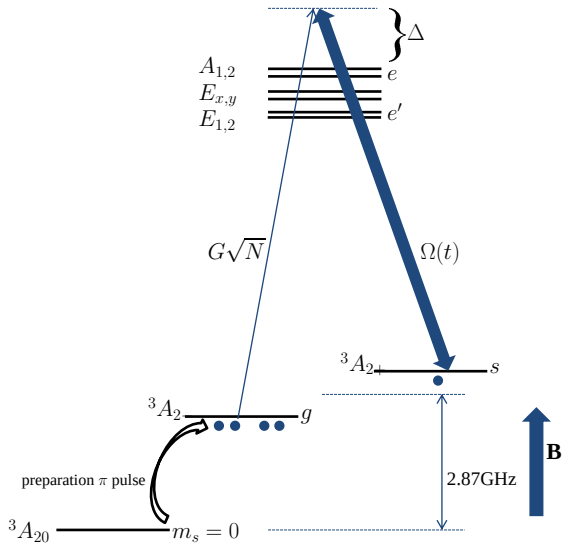

Figure 4.1: (Color online) The figure shows the ground and excited states triplet for a negatively charged NV center in diamond. Initially, a microwave π-pulse transfers the population to the ground state g. The ground states g and s are coupled to the excited state e, where the couplings are $G\sqrt{N}$ and $\Omega(t)$. The excited state detuning, Δ, allows off-resonant Raman optical storage in the presence of the excited state inhomogeneous broadening.

Originally, all NV centers are initialized in the $^3A_{20}$ ground state with electronic spin of $m_s = 0$. A preparation microwave π-pulse prepares all NVs in $m_s = -1$ ground state, see below for further discussion. As shown in Fig. 4.1, the cavity field and the classical control field are both interacting with NV centers. For storage, the input field is coupled to the cavity and the control field with the perpendicular polarization is simultaneously applied to the ensemble. This requires a cavity bandwidth that is larger than the input field's bandwidth. This allows to store the input field in the

ground state coherence of NV ensemble. For retrieval, one applies a similar control field to read the stored pulse out.

It is crucial to consider selection rules in order to recognize active transitions and construct a proper Hamiltonian for studying the dynamics in this setup. Under the low magnetic field and low strain condition only spin-conserving transitions are allowed. Therefore, transitions from ${}^3A_{20}$ ground state to the $E_{x,y}$ excited states are cyclic and do not allow a Λ-level configuration with ${}^3A_{2\pm}$. Here, all NVs are prepared in ${}^3A_{2-}$ ground state and we consider coupling of the ${}^3A_{2\pm}$ and the excited states triplets to realize the Λ configuration. This is similar to the Λ system that has been employed in [100] to generate entanglement between an optical photon and a solid-state spin. For practical reasons we choose to study this system in high strain regime (due to linearity of the polarizations and the increased excited state splitting, see below for more details). In the high strain regime the excited state triplets split into two branches, where each branch consists of 3 states. In the upper branch $A_{1,2}$ excited states are coupled to ${}^3A_{2-}({}^3A_{2+})$ ground states with $\hat{x}(\hat{y})$ linear polarizations, where $\hat{x}$ and $\hat{y}$ are determined by the direction of the strain in the xy-plane of the NV. In the lower branch $E_{1,2}$ excited states show the opposite polarizations of $\hat{y}(\hat{x})$ to the ${}^3A_{2-}({}^3A_{2+})$ ground states. In the high strain regime, in the lower branch the non-spin-preserving transition appears that in [101] led to realizing a Λ-level configuration that includes the ${}^3A_{20}$ ground state, see [102, 103, 104]. In our model, since the population is transferred to the ${}^3A_{2-}$ ground state, we consider the coupling between ${}^3A_{2\pm}$ ground states and the $A_{1,2}$ and $E_{1,2}$ excited states in the upper and lower branches. As the excited state inhomogeneous broadening is larger than the splitting between A_1 and A_2 (and also E_1 and E_2) we treat the upper and lower branches as two inhomogeneously broadened excited state with the opposite polarization selection rules, which leaves us with a 4-level system. These conditions are studied in [33] under the $\delta^a_{E_1}$ strain.

Let us describe the dynamics for this system, where the input and the control field are interacting with an ensemble of four-level artificial atoms (NVs). The following Hamiltonian shows the

free evolution and the interaction terms for the proposed scheme.

$$
\begin{aligned}
&H = H_0 + V, \\
&= \hbar \sum_{j=1}^{N} \delta_g \hat{\sigma}_{ss}^{j} + (\omega_p - \Delta)\hat{\sigma}_{ee}^{j} + (\omega_p - \Delta - \delta_e)\hat{\sigma}_{e'e'}^{j}, \\
&-\hbar \sum_{j=1}^{N} \hat{\mathscr{E}} G e^{-i\omega_p(t-z_j/c)} \hat{\sigma}_{eg}^{j} + \hat{\mathscr{E}} G' e^{-i\omega_p(t-z_j/c)} \hat{\sigma}_{e's}^{j} \\
&+\Omega(t) e^{-i\omega_c(t-z_j/c)} \hat{\sigma}_{es}^{j} + \Omega'(t) e^{-i\omega_c(t-z_j/c)} \hat{\sigma}_{e'g}^{j} + h.c.,
\end{aligned}
\tag{4.1}
$$

where e, e', s and g represent $A_{1,2}$, $E_{1,2}$, $^3A_{2+}$ and $^3A_{2-}$ states, respectively, see Fig. (4.1). The excited state inhomogeneous broadening that we consider later is larger than the energy splitting between A_1 and A_2, which justifies to treat these two levels as one that is labeled as e. The same assumption holds for E_1 and E_2. In the above Hamiltonian, ω_p and ω_c are the input and the control field frequencies; δ_g and δ_e are the ground and excited states splittings and Δ is the input and the control field detuning from the $A_{1,2}$ excited states. $\hat{\mathscr{E}}$ is the cavity field annihilation operator with coupling $G = \langle e|\hat{d}.\hat{\varepsilon}_p|g\rangle\sqrt{\frac{\omega_p}{2\hbar\varepsilon_0 V}}$ and $\Omega(t) = \langle e|\hat{d}.\hat{\varepsilon}_c|g\rangle E_c(t)/2\hbar$ is the Rabi frequency describing coupling of the control field to the $e-s$ transition. The G' and $\Omega'(t)$ are the similar quantities for the unwanted coupling to the e' excited state.

We are interested in analyzing the collective spin $\hat{S} = \frac{1}{\sqrt{N}}\sum_{j=1}^{N} \hat{\sigma}_{gs}^{j} e^{i(\omega_p-\omega_c)(t-z_j/c)}$ based on dynamics of the collective polarizations $\hat{P} = \frac{1}{\sqrt{N}}\sum_{j=1}^{N} \hat{\sigma}_{ge}^{j} e^{i\omega_p(t-z_j/c)}$ and $\hat{P}' = \frac{1}{\sqrt{N}}\sum_{j=1}^{N} \hat{\sigma}_{ge'}^{j} e^{i\omega_c(t-z_j/c)}$ and coupling to the cavity field $\hat{\mathscr{E}}$. Assuming that the number of NVs, N, is much larger than the number of input photons leads to simplification of the dynamics of the level populations. In addition, having $\Delta \gg 1/\tau$, where τ is the input pulse duration, results in adiabatic elimination of the excited states, see [105, 106]. These give

$$
\begin{aligned}
&\dot{\hat{S}} = -(\gamma_s + \frac{G^2 \hat{\mathscr{E}}^{\star}\hat{\mathscr{E}}}{\Gamma + i\Delta} + \frac{|\Omega(t)|^2}{\Gamma' + i(\delta_e + \delta_g + \Delta)})\hat{S} \\
&+iG'\hat{\mathscr{E}}^{\star}(\frac{iG\hat{\mathscr{E}}\hat{S}}{\gamma' - i(\delta_e - \delta_g + \Delta)} + \frac{i\sqrt{N}\Omega'(t)}{\gamma' - i(\delta_e - \delta_g + \Delta)}) \\
&+i\Omega^{\star}(\frac{iG\sqrt{N}\hat{\mathscr{E}}}{\gamma - i\Delta} + \frac{i\Omega(t)\hat{S}}{\gamma - i\Delta}),
\end{aligned}
\tag{4.2}
$$

where γ_s, γ and γ' are the ground state spin and the excited states (e,e') inhomogeneous broadening. Γ and Γ' are the excited states lifetimes for e and e'. The cavity field dynamics can be simplified to

$$\hat{\mathscr{E}}(t) = \left(\frac{G'\sqrt{N}\Omega(t)\hat{S}^{\star}}{\Gamma' - i(\delta_g + \delta_e + \Delta)} - \frac{G\sqrt{N}\Omega(t)\hat{S}}{\gamma - i\Delta} + \sqrt{2\kappa}\hat{\mathscr{E}}_{in}\right) \times \frac{1}{\kappa + \frac{G^2 N}{\gamma - i\Delta}}. \tag{4.3}$$

We find the later by assuming that the cavity decay rate, κ, is faster than the cavity field dynamics that is determined by the input pulse duration, τ. Here, we also replaced $\hat{P}$ that is found based on adiabatic elimination of the excited state dynamics. $\hat{\mathscr{E}}_{in}(t)$ represents the input quantum field. The cavity input-output equation, $\hat{\mathscr{E}}_{out}(t) = -\hat{\mathscr{E}}_{in}(t) + \sqrt{2\kappa}\hat{\mathscr{E}}(t)$, in combination with Eqs. (4.2,4.3) allows to analyze the proposed memory and study the performance in terms of fidelity and efficiency, see Sec. (4.6) for a detailed derivation.

We use the above equations to numerically evaluate the single excitation wavefunctions for the spin and the fields (input, output and cavity fields). In a separate evaluation, we consider a three-level configuration that only includes e' as the excited state. Based on this we predict how much spin excitation (during read-in) and consequently optical noise (in read-out) is generated due to the unwanted coupling to e' ($E_{1,2}$). This is justified as the noise that is generated through the above-mentioned process is not coherently interfering with the single-photon wave function, which is evaluated to predict the signal intensity, see Sec. (4.7).

Fig. (4.2) shows our results in which one can compare the retrieved pulse with the input field. Thanks to the increased excited state splitting (due to strain) the noise is suppressed. The total efficiency is found based on $\eta_{tot} = \frac{\int |\mathscr{E}_{out}(t)|^2 dt}{\int |\mathscr{E}_{in}(t)|^2 d}$, where $\mathscr{E}_{in/out}(t) = \langle 0|\hat{\mathscr{E}}_{in/out}(t)|1\rangle$ is the single excitation wave function that is defined based on its corresponding operator. One can compare the probabilities for reading out the signal and the noise to estimate the fidelity based on $1 - \frac{P_{noise}}{P_{sig}}$. In the following we explain physical requirements for a proper NV ensemble in order to provide a satisfying performance for optical storage in the electronic spin coherence of the NV ensemble.

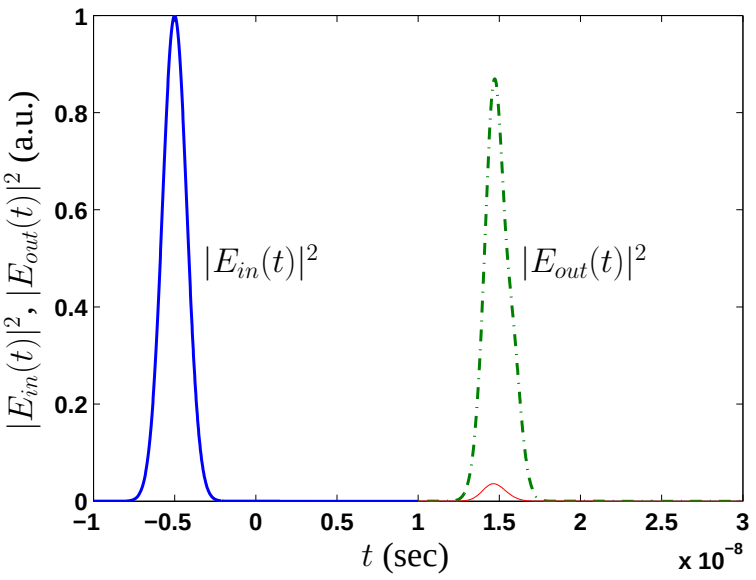

Figure 4.2: (Color online) The figure shows the input signal pulse (blue solid line) that is being stored and after 20ns is retrieved. The pulse bandwidth $\Delta\omega$ is about 1.9GHz, the excited state inhomogeneous broadening, γ_e is 10GHz, the spin inhomogeneous broadening, γ_s, is 200kHz. δ_e is 50GHz and δ_g is chosen to be 1GHz. The control Rabi frequency is about 3GHz, which corresponds to applying of about 0.24mW power. The detuning from the excited state, $\Delta = 16$GHz. These results in about 88% absorption efficiency and about 84% total efficiency. The red thin line is associated with the predicted noise that contains less than 5% energy of the input light. This results in about 94% fidelity, see below for more details.

4.4 Implementation

Ideally, one requires an ensemble of NV centers with high density of NVs and low excited state inhomogeneous broadening (optical linewidth). A sample that is prepared by using a dose of $4*10^{16}$ electrons/cm^{-3} electron irradiation and annealing at 800°C for 4-5 hours has 10-50 ppb NV density with FWHM optical linewidth of 15-20GHz. This density of NVs gives 1.755×10^3-8.775×10^3 NV/$(\mu m)^-3$, see [101]. Here, we assume the NV ensemble density of 440 NV/$(\mu m)^-3$ that is about twenty times smaller. Based on this, a smaller optical linewidth and spin inhomogeneous broadening is expected. Here, we assumed the excited state optical linewidth of 10GHz. It has to be noted that our proposal requires implementation at cryogenic temperatures.

Based on specifications of the cavity, one can estimate number of NVs by assuming that NVs are in a volume that is equivalent to the cavity mode volume. Here, we require a microcavity with

cavity linewidth of at least 2GHz in order to accommodate the signal. Coupling a linearly polarized light is a practical advantage to work at the high strain regime compared to the circular polarization at zero strain. Opposite polarizations for the input and control field is beneficial to the scheme as it prevents four-wave mixing due to exciting NVs with the control field.

The cavity quality factor ranges between $Q = 10^4$ to $Q = 10^6$, see [109, 110, 111]. Here, we assume $Q = 10^4$ which results in cavity amplitude decay rate of $\kappa = \frac{\omega_p}{2Q} = 1.48 * 10^{11}$Hz. The mode volume is $V = 100(\lambda/n_d)^3$, where λ is the wavelength and n_d is diamond's refractive index. Considering the fact that only a quarter of the NVs contributes in the scheme, this cavity volume allows to have an ensemble of about $N = 80$ NV centers in our system. A Rabi frequency of about $\Omega_0/2\pi$=1GHz per 1mW power with the beam waist of 10μm can be reached. This allows us to determine the maximum possible two-photon coupling strength. The result in Fig. (4.2) is based on applying the control field with about 0.24mW power for both the read-in and read-out processes.

The transition dipole moment in NVs are strong compared to that of rare-earth ion doped crystals. In general, this provides a more efficient photon-atom interface. The excited state lifetime is known to be 12ns. Assuming that only 3.5% of the light goes to the zero phonon line, the single-photon coupling is about $G/2\pi = 0.9$GHz. Even though G' is expected to be lower than G (which results in a better fidelity), for simplicity, we assume $G = G'$. Note that the broad phonon sidebands are not affecting the proposed process as they are relatively far from the inhomogeneously broadened zero phonon line.

We described all the requirements and specifications of the NV ensemble and the cavity. In Fig. 4.2, we show the input signal intensity, $|\mathscr{E}_{in}(t)|^2$, which has $\Delta\omega$=1.9GHz, where $\Delta\omega$ is the full width at $1/e$ of the maximum of the intensity. Numerical solution of the differential equation for the single collective spin excitation is performed based on Eqs. (4.2,4.3) and assuming that there is no initial excitation stored in the NVs. First, this results in evaluation of the stored excitation and the part of the input signal that leaks out of the cavity without being stored. Therefore, one can find the storage efficiency by using, $\eta_s = 1 - \frac{\int dt|\mathscr{E}_{outs}(t)|^2}{\int dt|\mathscr{E}_{in}(t)|^2}$, where $\mathscr{E}_{outs}(t)$ is the field that is lost

during storage. For retrieval, there is an excitation stored in the spin ensemble and there is no input field present. Using the control field, $\Omega(t)$, we can read the stored pulse out. We show that this 1ns input pulse is being stored with an absorption efficiency of $\eta_s \approx 88\%$ and retrieved after 20ns with total efficiency of $\eta_{tot} \approx 84\%$. The efficiency can be increased by increasing the control field strength. The output field can get affected due to the AC Stark shift that is caused by the control field. The AC Stark shift can be compensated by a proper phase modulation on the input pulse. This allows to approach 100% efficiency.

4.5 Conlusion and outlook

The electronic spin inhomogeneous broadening of as low as 200kHz has been observed, see [108]. This relatively narrow spin inhomogeneous broadening provides storage time of 100ns without a significant impact on the efficiency (reduces to about 81%) without application of any rephasing π-pulse. Applying series of rephasing π-pulses eliminates the limit that is due to the spin inhomogeneous broadening, see [14, 106]. Therefore, storage times in our proposal is only limited by the electronic spin coherence time. The electronic spin coherence times (T_2) has been improved to about 0.5s at 77°K by application of the dynamical decoupling to suppress the NV spin decoherence that is due to magnetic noise, see [95].

In conclusion, we proposed a scheme for storage of optical photons in an ensemble of NV centers that are coupled to a microcavity. The scheme shows that high efficiencies are possible with realistic parameters. Thanks to dynamical decoupling techniques long storage times can be achieved. Coupling to the nuclear spins may allow to increase the storage time even further and approach the nuclear spin life time of many seconds [40]. Therefore, realization of the on-chip, efficient and long storage time optical quantum memory becomes plausible due to recent advances in NVs and the development of the proposed scheme.

4.6 Appendix A1: Raman couplings for the NV ensemble in a cavity

In this section, I derive the equations of motion for an ensemble of NVs that are interaction with a single mode cavity field and the control field in order to realize a quantum memory for light. As it is explained in this chapter and schematically presented in Fig. (4.1), the system can be modeled as a 4-level system. The cavity field is interacting with ${}^3A_{2-} \rightarrow A_{1,2}(\mid g\rangle - \mid e\rangle)$ transition, where the coupling is given by G. Due to the opposite polarization selection rule the cavity field also couples to the ${}^3A_{2+} \rightarrow E_{1,2}(\mid s\rangle - \mid e'\rangle)$ transition, where its coupling is denoted by G'. The Rabi frequency $\Omega(t)$ shows the control field coupling to ${}^3A_{2+} \rightarrow A_{1,2}(\mid s\rangle - \mid e\rangle)$ and $\Omega'(t)$ denotes the opposite interaction with ${}^3A_{2-} \rightarrow E_{1,2}(\mid g\rangle - \mid e'\rangle)$ transition. The Hamiltonian in Eq. (4.1) is to consider these interactions and consequently find the dynamics. Using this Hamiltonian and the Heisenberg equation, $\frac{d\hat{\mathcal{O}}}{dt} = \frac{i}{\hbar}[\hat{H}, \hat{\mathcal{O}}] + \frac{\partial \hat{\mathcal{O}}}{\partial t}$, one can find the dynamics for population and transition operators as below,

$$
\begin{aligned}
\dot{\hat{\sigma}}_{gg} &= \gamma_{eg}\hat{\sigma}_{ee} + \gamma_{e'g}\hat{\sigma}_{e'e'} - i\hat{\mathscr{E}}G\hat{\sigma}_{eg} + i\hat{\mathscr{E}}^{\dagger}G\hat{\sigma}_{ge} - i\Omega'(t)\hat{\sigma}_{e'g} + i\Omega'^{\star}(t)\hat{\sigma}_{ge'}, \qquad (4.4)\\
\dot{\hat{\sigma}}_{ss} &= \gamma_{es}\hat{\sigma}_{ee} + \gamma_{e's}\hat{\sigma}_{e'e'} - i\hat{\mathscr{E}}G'\hat{\sigma}_{e's} + i\hat{\mathscr{E}}^{\dagger}G'\hat{\sigma}_{se'} - i\Omega(t)\hat{\sigma}_{es} + i\Omega^{\star}(t)\hat{\sigma}_{se},\\
\dot{\hat{\sigma}}_{ee} &= -\gamma_{e}\hat{\sigma}_{ee} + i\hat{\mathscr{E}}G\hat{\sigma}_{eg} - i\hat{\mathscr{E}}^{\dagger}G\hat{\sigma}_{ge} + i\Omega(t)\hat{\sigma}_{es} - i\Omega^{\star}(t)\hat{\sigma}_{se},\\
\dot{\hat{\sigma}}_{e'e'} &= -\gamma_{e'}\hat{\sigma}_{e'e'} + i\hat{\mathscr{E}}G'\hat{\sigma}_{e's} - i\hat{\mathscr{E}}^{\dagger}G'\hat{\sigma}_{se'} + i\Omega'(t)\hat{\sigma}_{e'g} - i\Omega'^{\star}(t)\hat{\sigma}_{ge'},\\
\dot{\hat{\sigma}}_{ge} &= -(\gamma - i\Delta)\hat{\sigma}_{ge} + i\hat{\mathscr{E}}G(\hat{\sigma}_{gg} - \hat{\sigma}_{ee}) + i\Omega(t)\hat{\sigma}_{gs} - i\Omega'(t)\hat{\sigma}_{e'e},\\
\dot{\hat{\sigma}}_{ge'} &= -(\gamma' - i(\delta_e - \delta_g + \Delta))\hat{\sigma}_{ge'} - i\hat{\mathscr{E}}G\hat{\sigma}_{ee'} + i\hat{\mathscr{E}}G'\hat{\sigma}_{gs} + i\Omega'(t)(\hat{\sigma}_{gg} - \hat{\sigma}_{e'e'}),\\
\dot{\hat{\sigma}}_{es} &= -(\Gamma + i\Delta)\hat{\sigma}_{es} - i\hat{\mathscr{E}}^{\dagger}G\hat{\sigma}_{gs} + i\hat{\mathscr{E}}^{\dagger}G'\hat{\sigma}_{ee'} + i\Omega^{\star}(t)(\hat{\sigma}_{ee} - \hat{\sigma}_{ss}),\\
\dot{\hat{\sigma}}_{e's} &= -(\Gamma' + i(\delta_e + \delta_g + \Delta))\hat{\sigma}_{e's} - i\hat{\mathscr{E}}^{\dagger}G(\hat{\sigma}_{e'e'} - \hat{\sigma}_{ss}) - i\Omega'^{\star}(t)\hat{\sigma}_{gs},\\
\dot{\hat{\sigma}}_{gs} &= -\gamma_s\hat{\sigma}_{gs} - i\hat{\mathscr{E}}G\hat{\sigma}_{es} + i\hat{\mathscr{E}}^{\dagger}G'\hat{\sigma}_{ge'} + i\Omega^{\star}(t)\hat{\sigma}_{ge} - i\Omega'(t)\hat{\sigma}_{e's}.
\end{aligned}
$$

It has to be noted that the above operators are the collective operators that are defined based on the single atomic operators as the following,

$$\hat{\sigma}_{\mu\mu} = \sum_{j=1}^{N} \hat{\sigma}_{\mu\mu}^{j}, \text{where } \mu = \{g, s, e, e'\}, \tag{4.5}$$

$$\hat{\sigma}_{se} = \sum_{j=1}^{N} \hat{\sigma}_{se}^{j} e^{i\omega_c(t-z_j/c)},$$

$$\hat{\sigma}_{se'} = \sum_{j=1}^{N} \hat{\sigma}_{se'}^{j} e^{i\omega_p(t-z_j/c)},$$

$$\hat{\sigma}_{ge} = \sum_{j=1}^{N} \hat{\sigma}_{ge}^{j} e^{i\omega_p(t-z_j/c)},$$

$$\hat{\sigma}_{ge'} = \sum_{j=1}^{N} \hat{\sigma}_{ge'}^{j} e^{i\omega_c(t-z_j/c)},$$

$$\hat{\sigma}_{gs} = \sum_{j=1}^{N} \hat{\sigma}_{gs}^{j} e^{i(\omega_p-\omega_c)(t-z_j/c)}.$$

In the above equations, ω_p is the resonant frequency of the cavity and ω_c is the central frequency of the control field pulse. Γ and Γ' are the radiative decay rate of the excited states e and e'. $\gamma = \gamma'$ are the excited states inhomogeneous broadening and γ_s is the ground state spin inhomogeneous broadening. δ_g and δ_e denote the ground state and excited state splittings, see Fig. (4.1). As it is defined above, $G = \langle e|\hat{d}.\hat{\varepsilon}_p|g\rangle\sqrt{\frac{\omega_p}{2\hbar\varepsilon_0 V}}$ is the single-photon coupling of the cavity field and $\Omega(t) = \langle e|\hat{d}.\hat{\varepsilon}_c|g\rangle E_c(t)/2\hbar$ is the Rabi frequency of the control field. G' and $\Omega'(t)$ are defined similarly for the other excited state and are assumed to be equal to G and $\Omega(t)$ correspondingly.

There are simplifications that can be done based on some of the features of the system. As the number of NVs are much larger than the number of photons, one can assume $\hat{\sigma}_{gg} \approx N$ and $\hat{\sigma}_{ee} \approx \hat{\sigma}_{e'e'} \approx \hat{\sigma}_{e'e} \approx 0$. In addition, having $\Delta \gg \Delta\omega$, where $\Delta\omega$ is the input field bandwidth, one

can assume that $\dot{\hat{\sigma}}_{ge} \approx \dot{\hat{\sigma}}_{ge'} \approx 0$. Similarly, I assume $\dot{\hat{\sigma}}_{se} \approx \dot{\hat{\sigma}}_{se'} \approx 0$. These assumptions results in

$$\begin{aligned} \hat{P} &= \frac{i\hat{\mathscr{E}} G\sqrt{N}}{\gamma - i\Delta} + \frac{i\Omega(t)\hat{S}}{\gamma - i\Delta}, \\ \hat{P}' &= \frac{i\hat{\mathscr{E}} G'\hat{S}}{\gamma' - i(\delta_e - \delta_g + \Delta)} + \frac{i\Omega'(t)\sqrt{N}}{\gamma' - i(\delta_e - \delta_g + \Delta)}, \end{aligned} \tag{4.6}$$

where $\hat{P} = \frac{\hat{\sigma}_{ge}}{\sqrt{N}}$, $\hat{P}' = \frac{\hat{\sigma}_{ge'}}{\sqrt{N}}$ and $\hat{S} = \frac{\hat{\sigma}_{gs}}{\sqrt{N}}$.

A similar approach can be taken to find the dynamics of the cavity field $\hat{\mathscr{E}}$ at below,

$$\dot{\hat{\mathscr{E}}} = -\kappa\hat{\mathscr{E}} + iG\hat{\sigma}_{ge} - iG'\hat{\sigma}_{se'} + \sqrt{2\kappa}\hat{\mathscr{E}}_{in}, \tag{4.7}$$

where $\hat{\mathscr{E}}_{in}$ is the input single-photon field that is to be stored and $\kappa = \frac{\omega_p}{2Q}$ is the cavity decay rate and Q is the cavity quality factor. The fact that $\kappa \gg \Delta\omega$ allows to assume $\dot{\hat{\mathscr{E}}} \approx 0$. These considerations results in Eqs. (4.2,4.3).

In order to find the quantum memory performance, I first consider the storage of the $\hat{\mathscr{E}}_{in}$ field. The above-mentioned equations and the input-output equation allows to evaluate the $\mathscr{E}_{out} = \langle 0|\hat{\mathscr{E}}_{out}|1\rangle$ that is the single-photon wavefunction of the output field. Then the storage efficiency can be determined as it is mentioned in this chapter. After the storage time the stored excitation in the collective spin of the NV ensemble can be read out by applying the same control field. This allows to calculate the total efficiency of the quantum memory.

4.7 Appendix A2: Evaluation of the noise

The coupling of the control field to the ${}^3A_{2-} \rightarrow E_{1,2}$ ($g \rightarrow e'$) is the source of noise in this scheme. This coupling may lead to the spin excitation by off-resonant excitation of an NV and scattering a photon to the cavity. This spin excitation can be read out at the retrieval stage and generate optical noise in the output field. Therefore, here I study the noise by considering the scheme when there is no input field present. Similar to the previous section one can derive the cavity field and spin

dynamics as below,

$$\hat{\mathscr{E}} = \frac{G'\Omega\sqrt{N}\hat{S}^{\dagger}}{\kappa(\Gamma' - i(\delta_g + \delta_e + \Delta))},$$
$$\dot{\hat{S}} = -(\gamma_s + \frac{\mathscr{E}^{\dagger}\mathscr{E}G'^2}{\gamma' - i(\delta_e - \delta_g + \Delta)} + \frac{|\Omega|^2}{\Gamma' + i(\delta_e + \delta_g + \Delta)})\hat{S} - \frac{\mathscr{E}^{\dagger}G'\Omega'\sqrt{N}}{\gamma' - i(\delta_e - \delta_g + \Delta)}. \tag{4.8}$$

Application of the control field for the read-out process results in generating field in the cavity and consequently output field. This is governed by the following equations, where

$$\hat{\mathscr{E}} = -\frac{1}{\kappa + \frac{G^2N}{\gamma - i\Delta}}\frac{G\Omega\sqrt{N}\hat{S}}{\gamma - i\Delta},$$
$$\dot{\hat{S}} = -(\gamma_s + \frac{\mathscr{E}^{\dagger}\mathscr{E}G^2}{\Gamma + i\Delta} + \frac{|\Omega|^2}{\gamma - i\Delta})\hat{S} - \frac{\mathscr{E}G\Omega^{\star}\sqrt{N}}{\gamma - i\Delta}. \tag{4.9}$$

Thanks to the strain the splitting between the lower and upper branches of the excited state can be increased from $\delta_e = 14$GHz to over $\delta_e = 50$GHz. Having $\delta_e > \Delta$ one can suppress the effect of the noise that is due to the opposite coupling of the control field to the lower branch.

It has to be noted that in the numerical calculations the Rabi frequency of the control field is calculated by

$$\Omega_0 = \frac{d_{zpl}}{\hbar}\sqrt{\frac{4P}{c\varepsilon_0 n_d \pi W^2}}, \tag{4.10}$$

where W is the control field beam waist, $n_d = 2.4$ is the refractive index of diamond, ε_0 is the vacuum permittivity and c is the speed of light. d_{zpl} is the transition dipole moment of the zero phonon line of the negatively charged NV that is given by,

$$d_{zpl} = 0.035d = 0.035\sqrt{\frac{3\pi^2\varepsilon_0\hbar c^3\Gamma}{n_d\omega_p^3}}, \tag{4.11}$$

where Γ is the excited state lifetime and d_{zpl} is defined based on the transition dipole moment and the fact that about 3.5% of the coupling is to the zero-phonon line.

Chapter 5

Precision requirements for spin-echo-based quantum memories

5.1 Preface

Electronic or nuclear spin ground states correspondingly provide few or many seconds lifetime that could be used for storage. However, spin inhomogeneous broadening in solid-state ensembles significantly limits the available storage time. Storage of a photon in a spin ensemble generates a collective spin excitation. The spin inhomogeneous broadening results in the dephasing of this collective excitation in time scales that are orders of magnitude shorter than the individual spins coherence time. In order to overcome this limitation, the spin echo technique has to be used. In the spin echo technique, one uses pairs of π-pulses to invert the spin population before the dephasing happens. Every pair of π-pulses allows to prevent dephasing due to the spin inhomogeneous broadening.

Here, the effects of pulse imperfections are studied in detail, using both a semi-classical and a fully quantum-mechanical approach. The results show that high efficiencies and low noise-to-signal ratios can be achieved for the quantum memories in the single-photon regime for realistic levels of the control pulse precision. Errors due to imperfect initial state preparation (optical pumping) are also studied. It can be shown that they are likely to be more influential than control pulse errors in many practical circumstances. These results are crucial for future developments of solid state quantum memories.

This publication has been done through collaboration with several co-authors. I performed the quantum mechanical treatment and re-derived the semi-classical calculations. I also wrote the manuscript and provided a response to the referee reports.

5.2 Introduction

Quantum memories for light [113, 58] are key elements of quantum repeaters [3, 12], which are necessary to distribute entanglement over long distances for future quantum networks [114]. Quantum memories based on atomic ensembles [3, 22, 24, 14, 61, 113, 58, 115, 116, 117, 118, 119] are particularly attractive in practice because the light-matter coupling is enhanced by the large number of atoms and by collective interference effects. In the retrieval process collective interference can strongly enhance the re-emission of the stored light in a well-defined direction, compared to the non-directional background emission. This makes it possible to achieve high retrieval efficiencies [22, 120, 121, 122] and small noise-to-signal ratios.

For long-distance applications such as quantum repeaters it is essential for the memories to allow long storage times. This can be achieved by using low-lying atomic states (spin states) for storage [3, 24, 14, 113, 58, 115, 116, 119]. However, spin states are typically affected by inhomogeneous broadening, i.e. different atoms in the ensemble have slightly different energies. For atomic gases this can be due to residual external magnetic fields or intensity-dependent light shifts (for optical dipole traps). In atomic gases it is possible to work with field-insensitive clock transitions [123, 124] to suppress inhomogeneous broadening due to magnetic fields.

Solid-state atomic ensembles, such as rare-earth ion doped crystals, are attractive because there are no unwanted effects due to atomic motion and because solid-state systems promise enhanced scalability. However, they also have inhomogeneous broadening of the spin transitions. For example, in rare-earth doped crystals the rare-earth ions themselves produce a spatially varying potential due to spin-spin interactions [31, 125].

Inhomogeneous broadening is important because in the absence of control techniques it limits the coherence time of collective memory excitations to the inverse of the inhomogeneous linewidth, which is typically in the tens of microseconds range and is much shorter than the desired storage times. This effect can be compensated using spin-echo techniques, such as the application of a single or a pair of π pulses. The coherence time can be further extended even beyond the single-

atom T_2 time by applying chains of π pulses (bang-bang control) [14, 126].

In practice the control pulses are never perfect. In a recent experiment [127] the most important imperfection was shown to be an inhomogeneity in the rf intensity across the sample, leading to a variation of about 1% in the total pulse area seen by individual atoms.

In Ref. [128] the authors argued that for successful operation in the quantum regime (i.e. when single atomic excitations are stored) the π pulses would have to be precise to of order $1/N$, where N is the number of atoms. Typically, solid-state ensembles contain of order 10^7 to 10^9 atoms, such a level of precision would thus be completely out of reach. The arguments of Ref. [128] were criticized in Ref. [14], but to our knowledge the question has not been fully resolved until now.

In the present paper we study this problem in detail. The argument of Ref. [128] was based on the fact that imperfect π pulses will lead to unwanted atomic excitations, which will cause background emissions. However, we will see that these emissions are non-collective and hence non-directional. As a consequence, good memory operation is achievable with realistic π pulses.

There are several different ensemble-based quantum memory protocols. For definiteness, in the following we focus on the well-known Duan-Lukin-Cirac-Zoller (DLCZ) protocol [3]. However, with small modifications our results apply to many other protocols, including storage based on electromagnetically induced transparency [115], off-resonant Raman transitions [116], controlled reversible inhomogeneous broadening [117], and atomic frequency combs [24].

In the DLCZ quantum memory protocol, as shown in Fig.5.1(a), an off-resonant write pulse undergoes Raman scattering, leading to the creation of a single photon and a single collective excitation in the state s. This collective excitation dephases due to inhomogeneous broadening of the $g-s$ transition, but the application of a π pulse in the middle of the storage time, see Fig.5.1(b), can prepare a rephased atomic collective excitation at the time of retrieval. A read pulse can now be applied, which leads to the directional emission of the read photon, see Fig. 5.1(c).

We study the effects of spin-echo related imperfections in the described protocol. We begin with a semi-classical treatment for uniform errors in the π pulses in section II. Then we give a

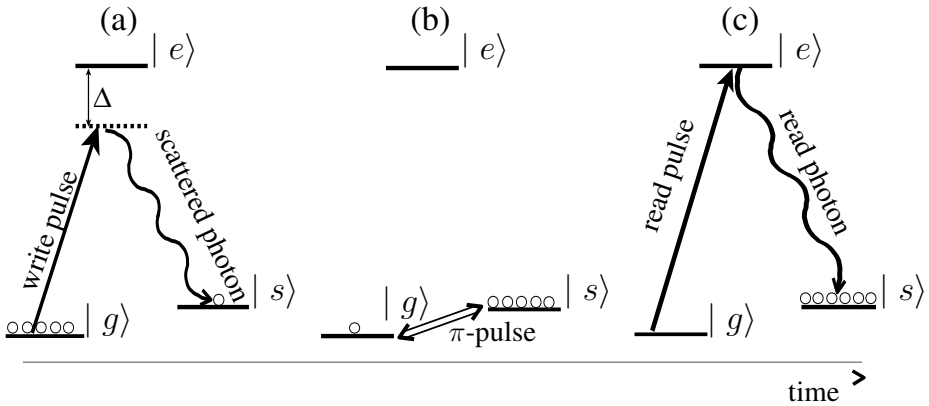

Figure 5.1: Basic level scheme in the Duan-Lukin-Cirac-Zoller protocol [3]. (a) The far detuned write pulse scatters a write photon and creates a single collective atomic excitation (spin-wave) in the state s. (b) Applying a π pulse on the $g-s$ transition in the middle of the process interchanges the roles of g and s, leading to rephasing at the end of storage period. (c) Shining the read pulse transforms the single collective atomic excitation in g into a read photon.

fully quantum-mechanical treatment for the (most relevant) case of small π pulse errors in section III, and we show that its results agree with the semi-classical approach. We treat the case of non-uniform π pulse errors in appendix A. In section IV we consider the effects of imperfect optical pumping, i.e. an imperfect initial state. In section V we use the semi-classical approach to discuss the application of multiple π pulses (bang-bang control). In section VI we give our conclusions.

5.3 Semi-classical approach

We start with a semi-classical approach. Here the collective atomic state is treated as a tensor product of single-atom states. The single-excitation component of this tensor product corresponds to the true quantum state, which is why the two approaches give equivalent results in the single-photon regime, cf. section III below.

Consider an ensemble of Λ type three-level atoms with two slightly split ground states g and s, and an excited state e. At the beginning, all of the atoms are ideally pumped into the ground state g. Applying the write pulse that scatters a (Stokes) photon, transforms the state of the k^{th} atom at the position X_k into,

$$\mid \psi^{(k)}(t_0)\rangle = \mid g\rangle - i\xi e^{i\vec{\Delta k}_1.\vec{X}_k} \mid s\rangle, \tag{5.1}$$

where ξ represents the contribution of each atom to the collective excitation, and $\vec{\Delta k}_1 = \vec{k}_w - \vec{k}_s$, where $\vec{k}_w$ is the $\vec{k}$-vector of the write pulse and $\vec{k}_s$ that of the scattered (Stokes) photon. For single-photon storage using an ensemble with N atoms, $N\xi^2 = 1$. The total atomic state, as the product of single atomic states, implies that in the limit of $\xi \to 0$ the semi-classical atomic state tends to quantum mechanical state, see below. For weak light storage this limit is equivalent to limit of large number of atoms, $N \gg 1$.

Now, let us consider the effect of inhomogeneous broadening and the π pulse. In the semi-classical picture one can easily use unitary evolution of a single atom in absence of the electromagnetic field to represent the dephasing (rephasing) before (after) applying the π pulse. The propagator is given by,

$$U^{\Delta_k}(t_f, t_i) = \begin{pmatrix} 1 & 0 \\ 0 & e^{-i\Delta_k(t_f - t_i)} \end{pmatrix}, \tag{5.2}$$

where Δ_k is the detuning from the central transition for the k^{th} atom. The Δ_k have an inhomogeneous distribution with a width Γ. Then, the state of an atom after the time interval $\tau_1 = t_1 - t_0$ is $\mid \psi^{(k)}(t_1)\rangle = U^{\Delta_k}(t_1, t_0) \mid \psi^{(k)}(t_0)\rangle$. An efficient retrieval is impossible for long storage times such that $\Gamma\tau \gtrsim 1$, since the readout amplitude is governed by the average atomic polarization, which is greatly reduced by the dephasing that takes place due to the temporal phase factors $e^{-i\Delta_k(t_f - t_i)}$ that vary from atom to atom. Applying the rf π pulse, which is tuned to the central frequency of the $g - s$ transition, can bring this random phase into a negligible global phase at a certain time. In order to represent the π pulse, let us recall the expression of the propagator of two levels of the atom under a pulsed excitation with the Rabi frequency Ω_i in the rotating wave approximation,

$$U^{\theta}(T) = \begin{pmatrix} \cos(\theta_i/2) & -i\sin(\theta_i/2) \\ -i\sin(\theta_i/2) & \cos(\theta_i/2) \end{pmatrix}, \tag{5.3}$$
$$\theta_i = \Omega_i T,$$

where T is the temporal duration of the pulse.

The final state after applying a π pulse at $t = t_1$ and waiting the time interval $\tau_2 = t_2 - t_1$

is $\mid \psi^{(k)}(t_2)\rangle = U^{\Delta_k}(t_2,t_1)U^{\theta}(T)U^{\Delta_k}(t_1,t_0) \mid \psi^{(k)}(t_0)\rangle$, where $\theta = \pi \pm \varepsilon$ and $\theta = \pi$ represents a perfect π pulse and ε is the error. One can now retrieve the read photon by applying the read pulse. Hence, we need to consider the spatial phase that comes from the read pulse to find the direction of the read photon. The spatial phase dependence due to the rf pulse can be ignored, because $\vec{k}_{rf}.\vec{X}_N \ll 1$ for realistic sample dimensions. Considering this fact, the final state after applying the read pulse is given by,

$$\begin{aligned} \mid \psi_f^{(k)}\rangle &= e^{i\vec{k}_r.\vec{X}_k}(\cos(\theta/2) - \xi \sin(\theta/2)e^{-i\Delta_k\tau_1}e^{i\vec{\Delta k}_1.\vec{X}_k}) \mid e\rangle \\ &- ie^{-i\Delta_k\tau_2}(\sin(\theta/2) + \xi e^{-i\Delta_k\tau_1}\cos(\theta/2)e^{i\vec{\Delta k}_1.\vec{X}_k}) \mid s\rangle, \end{aligned} \tag{5.4}$$

where $\vec{k}_r$ is the $\vec{k}$-vector of the read pulse.

By transferring the population of the state g into an excited state, the spin coherence transforms into an optical coherence, which leads to emission of the optical echo. The following shows how the atomic polarization would serve as the source of the echo signal,

$$\begin{aligned} I_{echo} &= I_0\frac{|P_f|^2}{\mu^2}, \\ P_f &= \sum_{k=1}^{N} \mu\langle e \mid \psi_f^{(k)}\rangle\langle\psi_f^{(k)} \mid s\rangle, \end{aligned} \tag{5.5}$$

where, μ is the electric dipole moment and I_0 is the radiation intensity of one isolated atom. It can be seen from eq. (5.4) that terms with atom-dependent temporal phases appear in the atomic polarization in the eq. (5.5). Since the emission is governed by the average over single atomic polarizations, only those terms for which these phases are canceled contribute significantly to the echo intensity. Analyzing different terms in $\langle e \mid \psi_f^{(k)}\rangle\langle\psi_f^{(k)} \mid s\rangle$ one finds that the term $i\xi \sin^2(\theta/2)e^{i\Delta_k(\tau_2-\tau_1)}e^{i(\vec{\Delta k}_1+\vec{k}_r).\vec{X}_k}$ is the only one for which one can exclude the atom-dependent temporal phase, which is called rephasing. This can take place under the condition $\tau_1 = \tau_2$, which implies that the π pulse has to be applied at the middle of the process.

The dipole moment of each single atom serves as a source of radiation. In the far field approximation and under the rephasing condition ($\tau_1 = \tau_2$), one can show that the amplitude of the readout from the whole ensemble in the direction $\vec{k}_{ro}$ is proportional to $\sum_{j=1}^{N} e^{i(\vec{\Delta k}_1+\vec{\Delta k}_2).\vec{X}_j}\sin^2\theta/2$,

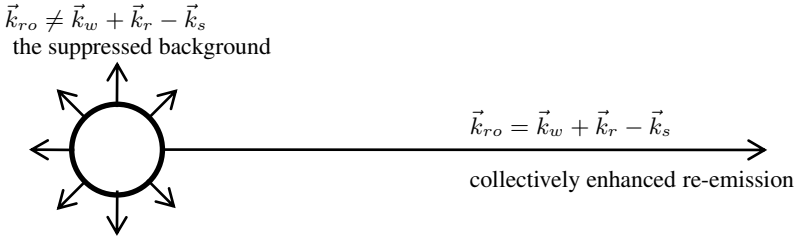

Figure 5.2: A schematic representation of the collective enhancement at a certain direction that is given by the phase-matching condition. Non-directional re-emission is suppressed by a factor $1/N$, where N is the number of atoms.

where $\vec{\Delta k}_2 = \vec{k}_r - \vec{k}_{ro}$. Hence, for $\vec{\Delta k}_1 + \vec{\Delta k}_2 = 0$ the readout intensity is proportional to N^2. This corresponds to constructive interference of the re-emission from all of the atoms at a certain direction $\vec{k}_{ro} = \vec{k}_w + \vec{k}_r - \vec{k}_s$. However, even by applying an ideal π pulse the radiation at other directions is not zero. The background re-emission (non-directional) intensity is proportional to $\langle \sum_{j,k=1}^{N} e^{i(\vec{\Delta k}_1 + \vec{\Delta k}_2).(\vec{X}_j - \vec{X}_k)} \rangle = N$, where $\vec{\Delta k}_1 + \vec{\Delta k}_2 \neq 0$. Accordingly, the intensity ratio of the collectively enhanced re-emission (directional) and the randomly distributed background re-emission (non-directional) is N, see Fig. (5.2). For example, for counter-propagation of the write and read pulses the phase-matching condition gives $\vec{k}_{ro} = -\vec{k}_s$.

However, the error in the π pulse prevents achieving the highest possible the echo amplitude and presents a source of noise.

Efficiency reduction. By considering these points one can calculate the atomic polarization, $P_f = -iN\xi\mu\cos^2(\varepsilon/2)$, because $\theta = \pi \pm \varepsilon$. Consequently, the intensity of the echo is,

$$I_{echo} = I_0 N^2 \xi^2 \cos^4(\varepsilon/2), \tag{5.6}$$

where I_0 has the same definition as in eq. (5.5). Eventually, the total efficiency of any process depends on the optical depth, performance of the experimental facilities and other theoretical and experimental details which are related to the protocol and the experimental setup. However, the present result allows to find the efficiency reduction due to the error in the π pulse that is important in our analysis.

Noise-to-signal ratio. Due to error in the rephasing pulse ($\varepsilon \neq 0$) there is a noise in the re-

emission. It is important to analyze the intensity of the noise, because for high memory fidelity the noise to echo ratio has to be small.

A single π pulse interchanges the states of the atoms from s to g and vice versa. However, an error in the π pulse produces population in the ground state g even without applying write pulse at the beginning. This would lead to fluorescent radiation. Hence, it can be distinguished by the non-zero terms in $\mid \psi_f^{(k)} \rangle$ for $\xi = 0$, which means even with no write pulse the error by itself can produce population in g. Quantitatively, the fluorescent radiation can be specified by $\mid \langle g \mid \psi_f^{(k)^{\xi=0}} \rangle \mid^2 = \cos^2(\theta/2)$ which is the term in $\mid \psi_f \rangle$ that does not originate from the read-in process ($\xi = 0$), but gives a non-zero projection on $\mid g \rangle$. Therefore, the intensity of the noise that originates from error in the π pulse can be given by,

$$\begin{aligned} I_{noise} &= I_0 \sum_{k=1}^{N} \mid \langle g \mid \psi_f^{(k)^{\xi=0}} \rangle \mid^2 \\ &= I_0 N \sin^2(\varepsilon/2). \end{aligned} \tag{5.7}$$

Obviously, the fluorescent radiation as the source of the noise has the spatial dependence of a single photon radiation. Consequently, the semi-classical picture yields an equally distributed noise (non-directional) that comes from single atom radiation of ensemble of the atoms, because of error in the rephasing pulse.

In order to analyze the effect of an imperfect π pulse on the fidelity, it is important to study the noise-to-signal ratio. The following presents the noise-to-signal ratio,

$$r = \frac{I_{noise}}{I_{echo}} = \frac{\sin^2(\varepsilon/2)}{\cos^4(\varepsilon/2)}, \tag{5.8}$$

keeping in mind that $N\xi^2 = 1$ for single-photon storage. The higher the noise-to-signal ratio, the less fidelity we have. In [127], 1% variation has been realized in the intensity of the rf pulse that causes the same error in the pulse area. Such error gives quite low noise-to-signal ratio of 0.25×10^{-4} and only wastes 0.1% of the efficiency. The semi-classical calculation suggests that the typical 1% error in the π pulse which is far beyond the $1/N$ precision, does not impose a major constraint on the efficiency and fidelity. In addition to the semi-classical calculations, it

is interesting to reconsider the problem using the quantum mechanical description. In the next section, we perform fully quantum mechanical investigation for the same question.

5.4 Quantum mechanical treatment

In this section, we perform fully quantum mechanical analysis on a global error in the π pulse. We consider an ideal initial state where all the atoms have been pumped into the ground state.

5.4.1 Ideal Protocol

As we discussed before, the large detuning of the write laser from $g-e$ leads to scattering of a photon and creating a collective atomic excitation. The theory of light-atom interaction is well established to describe interaction between the field and the atomic dipole moment. In general, one can represent the interaction Hamiltonian as,

$$H_{int} = \sum_{j=1}^{N} G \int d\vec{k}\hat{a}(\vec{k})e^{i\vec{k}.\vec{X}_j}\hat{\sigma}^j_{\rho\nu} + h.c., \tag{5.9}$$

where $G = \langle\rho|\hat{\mu}_j.\vec{\varepsilon}|\nu\rangle\sqrt{\frac{\hbar\omega}{2\varepsilon_0 V}}$ and $\hat{\sigma}^j_{\rho\nu} = |\rho\rangle_{jj}\langle\nu|$, where ρ and ν denote atomic levels g, e and s. This Hamiltonian shows the interaction between a field and the dipole moment of the j^{th} atom, $\hat{\mu}_j$. For simplicity, we assume the dipole-field coupling is identical for all the atoms and we have not considered the transverse profile. One can extract the interaction Hamiltonian for the write laser and the scattered photon from eq. (5.9), see FIG.5.1(a). By combining the interaction Hamiltonians and considering adiabatic elimination of the excited, e, one can describe the read-in part of the process as follows,

$$H^{eff}_{int} = \sum_{j=1}^{N} G' \int d\vec{k}_s\hat{a}^{\dagger}_s(\vec{k}_s)e^{i(\vec{k}_w-\vec{k}_s).\vec{X}_j}\hat{\sigma}^j_{sg} + h.c., \tag{5.10}$$

where $G' = \langle s|\hat{\mu}_j.\vec{\varepsilon}_s|e\rangle\langle e|\hat{\mu}_j.\vec{\varepsilon}_w|g\rangle\sqrt{\frac{\hbar\omega_s}{2\varepsilon_0 V}}\varepsilon_w(\tau)$ and $\Omega_w(\tau) = \langle e|\hat{\mu}_j.\vec{\varepsilon}_w|g\rangle\varepsilon_w(\tau)$ is the Rabi frequency of the classical write field.

The unitary evolution under this effective interaction Hamiltonian describes the creation of a Stokes photon via Raman scattering, which is accompanied by the creation of a collective atomic

state. The collective state is

$$\mid \psi(t_0)\rangle \quad = \quad \frac{1}{\sqrt{N}} \sum_{k=1}^{N} e^{i\vec{\Delta k}_1 . \vec{X}_k} \mid g...s^{(k)}...g\rangle, \tag{5.11}$$

where $\mid g...s^{(k)}...g\rangle$ shows all atoms in the ground state and the k^{th} atom in the spin state s and $\vec{\Delta k}_1 = \vec{k}_w - \vec{k}_s$. Here, we neglect the terms with more than one excitation, because we are interested in single photon storage. The interaction Hamiltonian governs the evolution of the atomic and the photonic state of the system. Our analysis follows the evolution of the atomic state. However, later in this section, we will refer to the above discussion in order to find the intensity of the readout based on the norm of the final atomic state.

One can find the state $\mid \psi(t_0)\rangle$ in eq. (5.11) by applying the Schwinger bosonic creation operator or equally weighted superposition of $\sigma_+ = \mid s\rangle\langle g \mid$ operators, $J_+(\vec{\Delta k}_1) = \sum_{k=1}^{N} e^{i\vec{\Delta k}_1 . \vec{X}_k} \sigma_+^{(k)} \otimes \mathbb{1}$. The inhomogeneous spin broadening implies that each atom has a slightly different energy than the other atom's spin level that indicates any atom will evolve based on its small energy detuning specified by Δ_n. After the time interval $\tau_1 = t_1 - t_0$ the state $\mid \psi(t_0)\rangle$ will be evolved to $\mid \psi(t_1)\rangle = \frac{1}{\sqrt{N}} \sum_{k=1}^{N} e^{i\Delta_k \tau_1} e^{i\vec{\Delta k}_1 . \vec{X}_k} \mid g...s^{(k)}...g\rangle$. The effect of dephasing as a result of inhomogeneous spin broadening can be described as an atom-dependent phase accumulation of the single collective atomic excitation.

The Following operator is appropriate to mathematical modeling of the dephasing after the time t,

$$e^{i\hat{\Omega}t} = \otimes_{k=1}^{N} e^{i\Delta_k t |s\rangle_k \langle s|}, \tag{5.12}$$

where $\hat{\Omega} = \sum_{k=1}^{N} \Delta_k \mid s\rangle_k \langle s \mid \otimes \mathbb{1}$, see [130], where the operator $\mathbb{1}$ shows the identity operator that acts on the rest of the atoms. The operator in Eq. (5.12) can be used to show the rephasing after applying the π pulse. Hence, one can represent the dephased state as $\mid \psi(t_1)\rangle = \frac{1}{\sqrt{N}} e^{i\hat{\Omega}\tau_1} J_+(\vec{\Delta k}_1) \mid gg...g\rangle$.

At first let us recall how an ideal π pulse treat the atoms, which it swaps g to s and vice versa.

One can describe that as $e^{i\pi/2J_x} = e^{i\pi/2\sum_{j=1}^{N}\sigma_x^{(j)}\otimes\mathbb{1}}$, where $e^{i\pi/2J_x} = \otimes_{k=1}^{N} i\sigma_x^{(k)}$, see [130].

After applying the π pulse, the operator $e^{i\hat{\Omega}t}$ leads to a rephasing of the collective excitation because for each term in the collective state the previously non-excited atoms now acquire phases whereas the previously excited atom doesn't. Finally, the stored pulse will be retrieved by applying the read field, leading to the emission of the readout photon, see FIG.5.1(c). The readout part of the process can be represented by the operator $J_+(\vec{\Delta}k_2) = \sum_{k=1}^{N} e^{i\vec{\Delta}k_2.\vec{X}_k}\sigma_+^{(k)} \otimes \mathbb{1}$, that is based on the same discussion as for the read-in. Eventually, the whole process comprised of creation of collective excitation, dephasing, π pulse, rephasing and the read pulse that leads to the final state can be described as $\mid \psi_f(\vec{\Delta}k_1, \vec{\Delta}k_2)\rangle = \frac{1}{\sqrt{N}} J_+(\vec{\Delta}k_2) e^{i\hat{\Omega}\tau_2} e^{i\pi/2J_x} e^{i\hat{\Omega}\tau_1} J_+(\vec{\Delta}k_1) \mid gg...g\rangle$.

Using Eq. (5.10) and the analogous Hamiltonian for the readout process it is straightforward to include the quantum states of the light field for the Stokes and readout photons into the description. One sees that the emission amplitude for the readout photon can be obtained directly from the norm of the atomic state $\mid \psi_f(\vec{\Delta}k_1, \vec{\Delta}k_2)\rangle$. Note that there is no preferred direction for the Stokes photon emission [131]. As before, we are not really interested in the absolute emission probability, but in how the probability varies as a function of the direction of emission for the read photon, and under the influence of errors in the control pulses. The collective enhancement happens again under the phase-matching condition $\vec{\Delta}k_1 + \vec{\Delta}k_2 = 0$.

In the ideal case, considering these conditions one can easily derive that

$$\langle \psi_f(\vec{\Delta}k_1, \vec{\Delta}k_2) | \psi_f(\vec{\Delta}k_1, \vec{\Delta}k_2)\rangle = N.$$

The later result is based on considering an ideal π pulse in the calculations and it takes place under the phase-matching condition, $\vec{\Delta}k_1 + \vec{\Delta}k_2 = 0$. As we studied in the semi-classical approach, the re-emission in other directions ($\vec{\Delta}k_1 + \vec{\Delta}k_2 \neq 0$) is negligible for the case with large number of atoms in the ensemble.

Our discussion here was focused on the case of the DLCZ protocol, but the evolution of the atomic state is identical in the other quantum memory protocols mentioned in the introduction. The only difference is that in those protocols the creation of the initial atomic excitation is accompanied

by the absorption of a single photon rather than its emission.

5.4.2 Global error in the rephasing pulse

We now study the effect of imperfect π pulse as one of the sources of error in the spin echo memories. The most general error in the π pulse can be considered as a small rotation ε_k around a random direction $\hat{n}_k$ for each atom that can be represented by the operator $e^{\sum_{k=1}^{N} i\varepsilon_k/2\vec{\sigma}^{(k)}.\hat{n}^{(k)}\otimes\mathbb{1}}$. This operator can show the effect of the inhomogeneity in the intensity of the π pulse across the sample [127]. For simplicity, we first consider a global error that can be interpreted as lack of accuracy in pulse shaping. The most general error that affects each atom differently is studied in the appendix. The corresponding operator for such error which is equally distributed over all atoms is $e^{i\varepsilon/2J.\hat{n}} = e^{i\varepsilon/2\sum_{k=1}^{N}\vec{\sigma}^{(k)}.\hat{n}\otimes\mathbb{1}}$.

Essentially, the question of studying the effect of the error in the π pulse is reduced to the problem of analyzing norm of the state

$$\mid \psi_f(\vec{\Delta}k_1,\vec{\Delta}k_2,\varepsilon)\rangle = \frac{1}{\sqrt{N}}J_+(\vec{\Delta}k_2)e^{i\hat{\Omega}\tau_2}e^{i\pi/2J_x}e^{i\varepsilon/2J.\hat{n}}e^{i\hat{\Omega}\tau_1}J_+(\vec{\Delta}k_1)\mid gg...g\rangle. \tag{5.13}$$

In order to facilitate analyzing the norm of the state $\mid \psi_f(\vec{\Delta}k_1,\vec{\Delta}k_2,\varepsilon)\rangle$ we now simplify the final state. Since we are only interested in its norm, any unitary operator can be used to simplify the state. By applying the unitary operator $e^{-i\pi/2J_x}$ from the left and adding the identity $e^{i\pi/2J_x}e^{-i\pi/2J_x}$, one can represent the final state up to a unitary and a global phase as,

$$\frac{1}{\sqrt{N}}J_-(\vec{\Delta}k_2)e^{-i\hat{\Omega}\tau_2}e^{i\varepsilon/2J.\hat{n}}e^{i\hat{\Omega}\tau_1}J_+(\vec{\Delta}k_1)\mid gg...g\rangle, \tag{5.14}$$

where $J_-(\vec{\Delta}k_2) = \sum_{k=1}^{N} e^{i\vec{\Delta}k_2.\vec{X}_k}\sigma_-^{(k)}\otimes\mathbb{1}$. Under the condition $\tau=\tau_1=\tau_2$ and by conducting some algebra one can derive that $e^{-i\hat{\Omega}\tau}e^{i\varepsilon/2J.\hat{n}}e^{i\hat{\Omega}\tau} = e^{\sum_{k=1}^{N} i\varepsilon_k/2\vec{\sigma}^{(k)}.\hat{n}'^{(k)}\otimes\mathbb{1}}$, which shows rotation in a new direction $\hat{n}'^{(k)} = (n_x\cos\Delta_k\tau + n_y\sin\Delta_k\tau)\hat{x} + (-n_x\sin\Delta_k\tau + n_y\cos\Delta_k\tau)\hat{y} + n_z\hat{z}$. Finally, by applying the unitary $e^{\sum_{k=1}^{N} -i\varepsilon_k/2\vec{\sigma}^{(k)}.\hat{n}'^{(k)}\otimes\mathbb{1}}$ the final state can be simplified to $\hat{\mathcal{O}}J_+\mid gg...g\rangle$ where the operator $\hat{\mathcal{O}}$ is given by,

$$\hat{\mathcal{O}} = \frac{1}{\sqrt{N}}\sum_{k=1}^{N} e^{i\vec{\Delta}k_2.X_k}(\alpha\sigma_-^{(k)} + \beta e^{i\Delta_k\tau}\sigma_z^{(k)} + \gamma e^{2i\Delta_k\tau}\sigma_+^{(k)})\otimes\mathbb{1}, \tag{5.15}$$

where $\alpha = \cos^2(\varepsilon/2) + 2i\sin(\varepsilon/2)\cos(\varepsilon/2) - {n_z}^2\sin^2(\varepsilon/2)$, $\beta = -i\sin(\varepsilon/2)\cos(\varepsilon/2)(n_x - in_y) + n_z\sin^2(\varepsilon/2)(n_x - in_y)$ and $\gamma = \sin^2(\varepsilon/2)(n_x - in_y)^2$. This simplification allows us to distinguish three different terms in the final state based on the effect of $\hat{\mathscr{O}}J_+$ on the $\mid gg...g\rangle$. The first term corresponds to $\sigma_-^{(k)}\sigma_+^{(j)} \mid gg...g\rangle$ which gives $\delta_{jk} \mid gg...g\rangle$. The other combination $\sigma_z^{(k)}\sigma_+^{(j)}$ in $\hat{\mathscr{O}}J_+$ yields $(-1)^{\delta_{jk}} \mid g..s^{(j)}..g\rangle$.The later gives N^2 terms that contains one excitation. Finally, the $\sigma_+^{(k)}\sigma_+^{(j)}$ leads to $N(N-1)$ terms with two excitations. One can benefit from these terms to represent the final state as

$$\alpha \mid \psi_1\rangle + \beta \mid \psi_2\rangle + \gamma \mid \psi_3\rangle, \tag{5.16}$$

where $\mid \psi_1\rangle = \frac{1}{\sqrt{N}}\sum_{j=1}^{N} e^{i(\vec{\Delta k}_1 + \vec{\Delta k}_2).\vec{X}_j} \mid g..g\rangle$, $\mid \psi_2\rangle = \frac{1}{\sqrt{N}}\sum_{j,k=1}^{N}(-1)^{\delta_{jk}} e^{i\Delta_k\tau} e^{i\vec{\Delta k}_1.\vec{X}_j} e^{i\vec{\Delta k}_2.\vec{X}_k} \mid g..s^{(j)}..g\rangle$ and $\mid \psi_3\rangle = \frac{1}{\sqrt{N}}\sum_{j,k=1, j\neq k}^{N} e^{2i\Delta_k\tau} e^{i\vec{\Delta k}_1.\vec{X}_j} e^{i\vec{\Delta k}_2.\vec{X}_k} \mid g..s^{(j)}..s^{(k)}..g\rangle$. Obviously, because of different number of excitations, these terms are perpendicular. Thus, one can study the norm of the final state, easily.

As it can be seen from the eq. (5.16), because of δ_{jk}, the first term corresponds to the directional emission of the readout photon. As we discussed in the previous section, see FIG. (5.2), the readout is strongly peaked around the direction for which all of the single-atom re-emissions can constructively interfere with each other. The readout intensity at the other directions (the non-directional background) is suppressed by the ratio $1/N$ that is a quite small number for a typical $N \sim 10^7 - 10^9$. Hence, the α term determines the intensity of the echo. In other words, shining the read laser with $\vec{k}_r = -\vec{k}_w$ result in the emission of a readout photon that its intensity is peaked around $\vec{k}_{ro} = -\vec{k}_s$. The non-directional noise in the re-emission can be attributed to the terms that correspond to β and γ coefficients, because taking average over position of the atoms leads to randomly distributed re-emission from each single atom. It can be shown that the norm of the state in Eq. (5.16) is

$$\frac{|\alpha|^2}{N}\Big|\sum_{j=1}^{N} e^{i(\vec{\Delta k}_1 + \vec{\Delta k}_2).\vec{X}_j}\Big|^2 + \frac{|\beta|^2}{N}\sum_{j=1}^{N}\Big|\sum_{k=1}^{N}(-1)^{\delta_{jk}} e^{i\Delta_k\tau} e^{i(\vec{\Delta k}_1).\vec{X}_j} e^{i(\vec{\Delta k}_2).\vec{X}_k}\Big|^2 + \frac{1}{N}\sum_{j,k=1, j\neq k}^{N}|\gamma|^2. \tag{5.17}$$

Efficiency reduction. In order to study the worst case scenario, upper bound of the noise strength and lower bound of the echo intensity have to be studied separately. Considering the

phase-matching condition it can be shown that $I_{echo} \propto N|\alpha|^2$. For small errors, $\varepsilon \ll 1$ and keeping terms up to $\mathscr{O}(\varepsilon^3)$, it can be shown that the following lower bound can be achieved for $n_z = 0$,

$$|\alpha|^2 \leq (1 - 2(\varepsilon/2)^2). \tag{5.18}$$

As in the ideal case the signal intensity is proportional to 1, one can analyze the efficiency reduction. So from quantum mechanical point of view the efficiency reduction factor is given by $1 - 2(\varepsilon/2)^2$ that gives the same results for the typical 1% error as the semi-classical calculation.

Noise. With the aim of studying the intensity of the noise that is proportional to the

$$\frac{1}{N}|\beta|^2 \sum_{j=1}^{N} |\sum_{k=1}^{N} (-1)^{\delta_{jk}} e^{i\Delta_k \tau} e^{i\vec{\Delta k}_1 . \vec{X}_j} e^{i\vec{\Delta k}_2 . \vec{X}_k}|^2 + \frac{1}{N} \sum_{j,k=1, j\neq k}^{N} |\gamma|^2$$

in the limit of the small errors, $\varepsilon \ll 1$, we need to discuss the effect of $e^{i\Delta_k \tau}$. For long enough times that τ is comparable with $\frac{1}{\Gamma}$, where Γ is the inhomogeneous linewidth, the $e^{i\Delta_k \tau}$ becomes a completely random phase. It can be shown that for random phases ϕ_k, $|\sum_k e^{i\phi_k} c_k|^2 = |\sum_{k,l} c_k c_l^* e^{i(\phi_k - \phi_l)}| = \sum_k |c_k|^2$, because $\langle e^{i(\phi_k - \phi_l)} \rangle = \delta_{kl}$. Hence we can treat the term that corresponds to β as

$$\frac{1}{N}|\beta|^2 \sum_{j,k=1}^{N} |(-1)^{\delta_{jk}} e^{i\vec{\Delta k}_1 . \vec{X}_j} e^{i\vec{\Delta k}_2 . \vec{X}_k}|^2 = N|\beta|^2.$$

Taking these considerations into account shows that the intensity of the noise is proportional to

$$\begin{aligned} &\frac{1}{N}|\beta|^2 \sum_{j=1}^{N} |\sum_{k=1}^{N} (-1)^{\delta_{jk}} e^{i\Delta_k \tau} e^{i(\vec{\Delta k}_1) . \vec{X}_j} e^{i(\vec{\Delta k}_2) . \vec{X}_k}|^2 + \frac{N(N-1)}{N}|\gamma|^2 \\ &\leq N(\varepsilon/2)^2 \max(n_z^2 (n_x^2 + n_y^2)(\varepsilon/2)^2 + n_x^2 + n_y^2) + \frac{N^2 - N}{N}(\varepsilon/2)^4 \max |(n_x - i n_y)^2|^2 \\ &\approx N(\varepsilon/2)^2 + \mathscr{O}(\varepsilon^4). \end{aligned} \tag{5.19}$$

So the choice of uniformly directed error with $n_z = 0$ gives the upper bound for the noise. Obviously, the second term in the noise intensity is proportional to ε^4 that is negligible for the small errors. Then it leads to $I_{noise} \propto N(\varepsilon/2)^2$. These results allow us to find the upper bound for the noise-to-signal ratio.

Let us recall the results for the noise and the echo from the semi-classical approach in eqs. (5.6,5.7). Obviously, the Taylor expansion of the results obtained in semi-classical treatment and

eliminating the terms $\mathcal{O}(\varepsilon^4)$ and higher, demonstrates the agreement between the results of the both approaches in the limit of small errors ($\varepsilon \ll 1$).

In the quantum mechanical approach the noise is proportional to the term given in eq. (5.19). The amplitude of the noise shows a correspondence with the fluorescent radiation in the semi-classical approach. Indeed the spatial phase dependence implies that the direction of the emission of the noise from each atom varies from one to another, leading to a non-directional noise. Thanks to collective enhancement, the non-directional noise will not swamp the echo signal, for realistic control pulse accuracy [127].

5.5 Imperfect initial state and rephasing pulse

An imperfection in the π pulse is not the only source of inefficiency in the spin echo memories. In our calculations so far we have assumed an ideal situation where all the atoms are initially in the ground state. Our quantum mechanical approach allows us to study the effect of an imperfect initial state with n atoms excited to the state s. This can happen in experiments as a result of an imperfect optical pumping in the initialization of the atomic ensemble. Without loss of generality, we can consider the initial state $\mid g..gs..s\rangle$ that has n sorted excited atoms instead of randomly positioned excited atoms. Applying the operator $\mathcal{O}J_+$ gives the final state. We expect the directional echo as result of applying $\sum_{j,k=1}^{N} \sigma_-^{(k)}\sigma_+^{(j)}$ on the initial state $\mid g..gs..s\rangle$. In contrast to the perfect initial case, this will lead to $N-n$ terms with n excitations correspond to $\mid g..gs..s\rangle$, and also $(N-n)n$ terms connected with $\mid g..s^{(j)}..gs..g^{(k)}..s\rangle$ which has n excitations. By conducting some algebra, one can easily show that only the first case gives δ_{jk} which leads to directional (collectively enhanced) re-emission under the phase-matching condition. This implies that by considering imperfection in both the initial state and the π pulse, intensity of the echo is proportional to

$$I_{echo} \propto \frac{(N-n)^2}{N}(1-2(\varepsilon/2)^2). \tag{5.20}$$

The imperfection in the initial state reduces the intensity of the echo and also introduces a new source of the non-directional noise. Previously, we analyzed the noise that corresponds to $\mid$

$\psi_2\rangle$ and $|\ \psi_3\rangle$ by finding the upper bound for β and γ. Now, the $(N-n)n$ terms of the form $|\ g..s^{(j)}..gs..g^{(k)}..s\rangle$ also contribute to the noise. Consequently, as the upper bound, for the term that corresponds to α can be achieved for $n_z = 1$, one can obtain the following upper bound for the noise-to-signal ratio r,

$$r \leq \frac{(N-n)n + N^2(\varepsilon/2)^2}{(N-n)^2(1-2(\varepsilon/2)^2)}. \tag{5.21}$$

Investigating this equation it can be seen that the two different sources of error compete in producing noise. For the case with small fraction of excitations in the initial state, $\frac{n}{N} \ll 1$, such that $\varepsilon^2 > \frac{4n}{N}$ then the error in π pulse is the dominant term in the noise. Otherwise, in case of $\frac{4n}{N} > \varepsilon^2$ the imperfection in the initial state plays an important role in increasing the upper bound of the noise-to-signal ratio. For instance, 2% of the atoms not in the ground state, which is a typical value [22], will cause a 2% error. The error in the π pulse would have to be as large as $\varepsilon = 0.4$ in order to be comparable in importance.

5.6 Semi-classical treatment of multiple rephasing pulses

So far we have studied the application of a single π pulse. Much longer storage times are achievable by applying sequences of π pulses. This is also known as bang-bang control. We analyze this case using the semi-classical approach. We have seen before that semi-classical and quantum treatment lead to identical conclusions for small errors. The intensity of the signal after applying m pairs of π pulses is given by,

$$I_{echo} \approx I_0 N^2 \xi^2 (1 - (2m^2 - m + 1)\varepsilon^2/2). \tag{5.22}$$

The intensity that is associated to the noise also can be approximated by $I_{noise} \approx I_0 N m^2 \varepsilon^2/2$. Thus, after applying sequence of the rephasing pulses, the noise-to-signal ratio reads

$$r \approx m^2 \varepsilon^2/2, \tag{5.23}$$

for $m\varepsilon \ll 1$. For instance, with typical 1% error in the π pulse one can benefit from 30 pairs of rephasing pulses, while still achieving an efficiency factor of 91% and a noise-to-signal ratio of

0.04. If the pulses are 4 msec apart as in Ref. [14], 30 pairs of pulses correspond to a storage time of 240 msec. Ref. [127] managed to increase the T_2 time to 1 sec, by proper alignment of the magnetic field, that is much longer than 80 msec in Ref. [14]. This field configuration would allow one to put the rephasing pulses further apart. For example, one can consider the rephasing pulses 40 msec apart, giving a 2.4 sec storage time with an efficiency factor of 91% and a noise-to-signal ratio of 0.04.

5.7 Discussion and Conclusion

We have shown that realistic imperfections in the π pulses only have small effects on the retrieval efficiency of quantum memories, and that the corresponding noise is also acceptable. The latter fact is due to collective interference. While the emission of the read photon is strongly enhanced in the direction given by the phase matching condition, the noise due to pulse imperfections is non-directional. As a consequence, even the use of great numbers of π pulses (bang-bang control) is realistic at the quantum level. This settles the question raised by Ref. [128].

We have also studied errors due to imperfect optical pumping, i.e. imperfect initial state preparation. We find that these errors are likely to dominate over π pulse errors in many circumstances, but that they can also be kept at an acceptable level.

Our discussion was phrased in terms of the DLCZ protocol [3] for concreteness. However, the same results apply to other ensemble-based quantum memory protocols including those based on electromagnetically induced transparency [115], off-resonant Raman transitions [116], controlled reversible inhomogeneous broadening [117], and atomic frequency combs [24].

In conclusion, the prospects for the use of spin-echo techniques in light-matter interfaces at the quantum level are very good. We hope that our work will further encourage experimental work in this direction.

Acknowledgments. This work was supported by an NSERC Discovery Grant, an AITF New Faculty Award, the EU project Q-essence, the Swiss NCCR Quantum Photonics, and iCORE. We

thank M. Afzelius, N. Gisin and E. Saglamyurek for useful discussions.

5.8 Appendix-Spatial inhomogeneity in the rf pulse

As we discussed, the main error in rf pulses is the variance in the intensity of the rf pulse that leads to inhomogeneity of the rf pulse across the sample [127]. Consequently, the error would be different for the atoms at the different positions. Here we extend our analysis to study such errors.

We study the spatial inhomogeneity in the rf pulse by considering $e^{\sum_{k=1}^{N} i\varepsilon_k/2\vec{\sigma}^{(k)}.\hat{n}^{(k)}\otimes\mathbb{1}}$ as the operator which represents the error. Therefore, based on eq. (5.13) the final state is,

$$\mid \psi_f(\vec{\Delta}k_1,\vec{\Delta}k_2,\varepsilon)\rangle = \frac{1}{\sqrt{N}}J_+(\vec{\Delta}k_2)e^{i\hat{\Omega}\tau_2}e^{i\pi/2J_x}e^{\sum_{k=1}^{N} i\varepsilon_k/2\vec{\sigma}^{(k)}.\hat{n}^{(k)}\otimes\mathbb{1}}e^{i\hat{\Omega}\tau_1}J_+(\vec{\Delta}k_1)\mid gg...g\rangle. \quad (5.24)$$

We can follow the same approach as we used in the paper to simplify the final state that eases the rest of the calculation. Therefore, the final state $\mid \psi_f(\vec{\Delta}k_1,\vec{\Delta}k_2,\varepsilon)\rangle$ up to a unitary operator and a global phase is

$$\frac{1}{\sqrt{N}}J_-(\vec{\Delta}k_2)e^{-i\hat{\Omega}\tau_2}e^{\sum_{k=1}^{N} i\xi_k\vec{\sigma}^{(k)}.\hat{n}^{(k)}\otimes\mathbb{1}}e^{i\hat{\Omega}\tau_1}J_+(\vec{\Delta}k_1)\mid gg...g\rangle. \quad (5.25)$$

Considering the π pulse at the middle of the process, $\tau=\tau_1=\tau_2$, and by conducting some algebra one can derive that $e^{-i\hat{\Omega}\tau}e^{\sum_{k=1}^{N} i\xi_k\vec{\sigma}^{(k)}.\hat{n}^{(k)}\otimes\mathbb{1}}e^{i\hat{\Omega}\tau}=e^{\sum_{k=1}^{N} i\xi_k\vec{\sigma}^{(k)}.\hat{n}'^{(k)}\otimes\mathbb{1}}$, which shows rotation in a new direction $\hat{n}'^{(k)}=(n_x^{(k)}\cos\Delta_k\tau+n_y^{(k)}\sin\Delta_k\tau)\hat{x}+(-n_x^{(k)}\sin\Delta_k\tau+n_y^{(k)}\cos\Delta_k\tau)\hat{y}+n_z^{(k)}\hat{z}$. Finally, by applying the unitary $e^{\sum_{k=1}^{N} i\xi_k\vec{\sigma}^{(k)}.\hat{n}'^{(k)}\otimes\mathbb{1}}$ the final state can be simplified to

$$\mid \psi_f(\vec{\Delta}k_1,\vec{\Delta}k_2,\varepsilon)\rangle = \hat{\mathscr{O}}J_+\mid gg...g\rangle, \quad (5.26)$$

where the operator $\hat{\mathscr{O}}$, which acts on k^{th} atom is given by,

$$\hat{\mathscr{O}}=\frac{1}{\sqrt{N}}\sum_{k=1}^{N}e^{i\vec{\Delta}k_2.\vec{X}_k}(\alpha^{(k)}\sigma_-^{(k)}+\beta^{(k)}e^{i\Delta_k\tau}\sigma_z^{(k)}+\gamma^{(k)}e^{2i\Delta_k\tau}\sigma_+^{(k)})\otimes\mathbb{1}, \quad (5.27)$$

and $\alpha^{(k)}=\cos^2(\varepsilon_k/2)+2i\sin(\varepsilon_k/2)\cos(\varepsilon_k/2)-{n_z^{(k)}}^2\sin^2(\varepsilon_k/2)$, $\beta^{(k)}=-i\sin(\varepsilon_k/2)\cos(\varepsilon_k/2)(n_x^{(k)}-in_y^{(k)})+n_z^{(k)}\sin^2(\varepsilon_k/2)(n_x^{(k)}-in_y^{(k)})$ and $\gamma^{(k)}=\sin^2(\varepsilon_k/2)(n_x^{(k)}-in_y^{(k)})^2$. Finally, the state can be

simplified to

$$|\psi_f(\vec{\Delta k}_1,\vec{\Delta k}_2,\varepsilon)\rangle = \frac{1}{\sqrt{N}}\sum_{j=1}^{N}\alpha^{(j)}e^{i(\vec{\Delta k}_1+\vec{\Delta k}_2).\vec{X}_j}\mid g..g\rangle \tag{5.28}$$
$$+\frac{1}{\sqrt{N}}\sum_{j,k=1}^{N}(-1)^{\delta_{jk}}\beta^{(k)}e^{i\Delta_k\tau}e^{i(\vec{\Delta k}_1).\vec{X}_j}e^{i(\vec{\Delta k}_2).\vec{X}_k}\mid g..s^{(j)}..g\rangle$$
$$+\frac{1}{\sqrt{N}}(\sum_{j,k=1,j\neq k}^{N}\gamma^{(k)}e^{2i\Delta_k\tau}e^{i(\vec{\Delta k}_1).\vec{X}_j}e^{i(\vec{\Delta k}_2).\vec{X}_k})|g..s^{(j)}..s^{(k)}..g\rangle.$$

Fortunately, having different number of excitations in the final state simplifies the calculation of the norm.

As we discussed, the first term contributes in directional emission of the readout photon. Hence, the $\alpha^{(k)}$s play role in finding the intensity of the echo. In other words, shining the read laser with $\vec{k}_r = -\vec{k}_w$ result in the emission of a readout photon that is peaked around $\vec{k}_{ro} = -\vec{k}_s$. The non-directional noise in the re-emission can be attributed to the terms corresponding to $\beta^{(k)}$ and $\gamma^{(k)}$ coefficients, because average over the position of the atoms leads to randomly distributed re-emission. It can be shown that the following gives norm of the $\mid \psi_f\rangle$ in eq. (5.28),

$$A^2 = \frac{1}{N}\mid\sum_{j=1}^{N}\alpha^{(j)}e^{i(\vec{\Delta k}_1+\vec{\Delta k}_2).\vec{X}_j}\mid^2 + \frac{1}{N}\sum_{j=1}^{N}\mid\sum_{k=1}^{N}(-1)^{\delta_{jk}}e^{i\Delta_k\tau}\beta^{(k)}e^{i(\vec{\Delta k}_1).\vec{X}_j}e^{i(\vec{\Delta k}_2).\vec{X}_k}\mid^2 \tag{5.29}$$
$$+\frac{1}{N}\sum_{j,k=1,j\neq k}^{N}\mid\gamma^{(k)}\mid^2 .$$

In order to analyze the efficiency reduction the lower bound of echo intensity have to be studied. Considering the phase-matching condition it can be shown that $I_{echo} \propto \frac{1}{N}|\sum_{j=1}^{N}\alpha^{(j)}|^2$. For small errors, $\varepsilon_j \ll 1$ and keeping terms to $\mathcal{O}(\varepsilon^3)$, it can be shown that the following lower bound can be achieved for $n_z^{(j)} = 0$

$$\frac{1}{N}|\sum_{j=1}^{N}\alpha^{(j)}|^2 \leq N(1-2(\varepsilon_{max}2/)^2), \tag{5.30}$$

where ε_{max} is the largest error and N is number of the atoms. With the aim of studying the intensity of the noise that is proportional to the $\frac{1}{N}\sum_{j=1}^{N}\mid\sum_{k=1}^{N}(-1)^{\delta_{jk}}e^{i\Delta_k\tau}\beta^{(k)}e^{i(\vec{\Delta k}_1).\vec{X}_j}e^{i(\vec{\Delta k}_2).\vec{X}_k}\mid^2$ $+\frac{1}{N}\sum_{j,k=1,j\neq k}^{N}\mid\gamma^{(k)}\mid^2$ for the small errors, $\varepsilon_j \ll 1$, one needs to consider the $e^{i\Delta_k\tau}$ as a random phase, that takes place for long enough times that τ is comparable with the $\frac{1}{\Gamma}$. It can be shown

that for random ϕ_k, $|\sum_k e^{i\phi_k}\beta^{(k)}|^2 = |\sum_{k,l}\beta^{(k)}\beta^{(l)^*}e^{i(\phi_k-\phi_l)}|^2 = \sum_k|\beta^{(k)}|^2$, because $\langle e^{i(\phi_k-\phi_l)}\rangle = \delta_{kl}$. Hence, one can conclude that $|\sum_{k=1}^{N}(-1)^{\delta_{jk}}e^{i\Delta_k\tau}\beta^{(k)}e^{i(\vec{\Delta k}_1).\vec{X}_j}e^{i(\vec{\Delta k}_2).\vec{X}_k}|^2$ can be approximated as $\sum_{k=1}^{N}|(-1)^{\delta_{jk}}\beta^{(k)}e^{i(\vec{\Delta k}_1).\vec{X}_j}e^{i(\vec{\Delta k}_2).\vec{X}_k}|^2 = \sum_{k=1}^{N}|(-1)^{\delta_{jk}}\beta^{(k)}|^2$. By taking these considerations into account and keeping terms up to $\mathscr{O}(\varepsilon^4)$ give the noise intensity upper bound as

$$\begin{aligned} I_{noise} &\leq N\max(n_z^{(k)^2}(n_x^{(k)^2}+n_y^{(k)^2})(\varepsilon_k/2)^4+(n_x^{(k)^2}+n_y^{(k)^2})(\varepsilon_k/2)^2) \\ &+\frac{N^2-N}{N}\max((\varepsilon_k/2)^4|(n_x^{(k)}-in_y^{(k)})^2|^2) \\ &= N(\varepsilon_{max}/2)^2+\mathscr{O}(\varepsilon^4), \end{aligned} \tag{5.31}$$

which implies that a uniformly directed error with $n_z = 0$ gives the upper bound for the noise. Obviously, the second term in the noise intensity is proportional to ε^4 that is negligible for the small errors. Then it leads to $I_{noise} \leq N(\varepsilon_{max}/2)^2$. This shows that the fully quantum mechanical treatment for an inhomogeneous error is in good agreement with the results for global errors derived in the paper.

Chapter 6

Conclusion

The emergence of companies that are focused on quantum technologies are an indication of advances of practical applications. The fast progress within the past decade in quantum memories promises significant developments in the near future to realize the first real-world implementations of long-distance quantum communication based on quantum repeaters. For this purpose, developments of quantum memory protocols and physical systems are essential to approach combination of higher efficiencies, multimode capacity and longer storage times.

The present thesis contributed to developments of quantum memories by proposing new quantum memory protocols, see Chapter (2,3). Furthermore, nitrogen vacancy (NV) centers are studied for a new implementation that can lead to the first micron-scale quantum memory. The precision requirements for the spin echo technique is also studied, due to the importance of long storage time in quantum repeaters.

In summary, the controllable-dipole quantum memory showed that a scheme equivalent to the Raman-type quantum memory can be implemented without application of an optical control field. The scheme proposed a way to store quantum states of light in a two-level system by direct control of the transition dipole moment and without an engineered inhomogeneous broadening. The proposal has been analyzed for the in-cavity and free-space cases. For the experimental implementation, Tm^{3+}:YAG has been proposed, in which the transition dipole moment can be turned on and off by changes to the angle of the external magnetic field.

The quantum memory protocol based on the refractive index modulation has also been proposed in the present thesis. Interestingly, this scheme resembles the gradient echo memory (GEM). As opposed to the GEM protocol, there is no modulation on the energy of the relevant atomic transition. It has been shown that a time-dependent modulation of the refractive index of the host

medium implies a position-dependent frequency of the photon along the propagation direction. Lithium niobate is an attractive candidate for refractive index modulation as it is one of the main materials that are used the electro-optical modulators. Tm^{3+} doped lithium niobate waveguide already has been used to implement the AFC protocol [50]. Implementing electrodes along the waveguide allows to implement this proposal. This can be an implementation of a GEM-like protocol without difficulties due to application of a position dependent field.

An ensemble of nitrogen vacancy (NV) centers that are coupled to a cavity is examined as a potential physical system for implementation of quantum memories. As the NV ensembles suffer from a large excited state inhomogeneous broadening, the Raman-type scheme can be used to circumvent the broadening for storage of optical photons. This proposal allows to implement micron-scale quantum memories that can be incorporated with sources and detectors for the implementation of an on-chip quantum register.

Finally, precision requirements for the spin echo technique, which is essential for extending the storage time in many solid-state quantum memories are studied. In Chapter (5), it has been shown how the imperfection in the initially prepared atomic state and the error in the applied π-pulses for the spin echo technique can contribute to the noise. Based on the results, for a limited error in the π-pulses, multiple π-pulses can be used to extend the storage time by about 2 orders of magnitude.

In the present thesis, limited but effective steps have been taken toward more practical solid-state quantum memories for future applications. However, different aspects of quantum memories are expected to develop in the future. See the next chapter for a brief description of some of the foreseeable directions for future studies.

Chapter 7

Outlook

In my opinion, there are several direction for future studies in the area of quantum memories that will involve further theoretical and experimental efforts. These future studies may include new physical implementations, new functionalities for quantum memories, developments of quantum repeaters and combination of quantum repeaters with satellite quantum communications.

As has been discussed in this thesis, NV centers are a new possibility for small-scale integrable quantum memories. In addition to the NV centers, hollow-core photonic crystal fibers possess incredible optical depths that can be employed for efficient quantum memories. Rare-earth ions doped in ceramic is another promising new physical system. More experimental investigations of these physical systems are expected in the near future.

Apart from storage in and retrieval from a quantum memory, it is possible to use quantum memories for straightforward processing tasks inside the memory. More specifically, I will be contributing to proposals for a quantum non-demolition (QND) photon-counting measurement based on storage and in-memory interference between atomic excitations. In addition, AFC quantum memory has the potential to be used for storing and interfering multiple pulses in different frequency modes.

One of the main goals for development of quantum memories is the implementation of quantum repeaters for distributing entanglement over long distances. Based on the developments during the last few years, there are several groups that are expected to realize quantum repeaters. The first real-world demonstrations will have limited performance; however, further progress is expected to approach practical stages.

Recently, quantum communication with satellites has become an ongoing effort in several groups around the world including one in Canada [132]. This is motivated by the experimental

demonstration of quantum communication on earth over a distance of 144km. This experiment can be done between ground stations and moving satellites as the absorption loss is significantly lower at higher heights above the earth's surface. In longer terms, this scheme can be combined with quantum repeaters for global entanglement distribution.

Bibliography

[1] E. Knill, R. Laflamme and G. J. Milburn, Nature(London) **409**, 46 (2001).

[2] H.-J. Briegel, W. Dür, J.I. Cirac and P. Zoller, Phys. Rev. Lett. **81**, 5932 (1998).

[3] L.-M. Duan, M. Lukin, J.I. Cirac, and P. Zoller, Nature(London) **414**, 413 (2001).

[4] K. Heshami, A. Green, Y. Han, A. Rispe, E. Saglamyurek, N. Sinclair, W. Tittel and C. Simon, *Controllable-dipole quantum memory*, Physical Review A **86**, 013813 (2012).

[5] J. Clark, K. Heshami and C. Simon, Phys Rev A **86**, 013833 (2012).

[6] K. Heshami, C. Healey, B. Khanaliloo, V. Acosta, C. Santori, P. Barclay and C. Simon, In preparation (2013).

[7] K. Heshami, N. Sangouard, J. Minar, H. de Riedmatten and C. Simon, Physical Review A **83**, 032315 (2011).

[8] D. Deutsch, Proc. R. Soc. Lond. A **400**, 97 (1985).

[9] P.W. Shor, Foundations of Computer Science, 1994 Proceedings., 35th Annual Symposium on, 124 (1994).

[10] C.H. Bennett, G. Brassard, Proc. of IEEE Int. Conference on Computers, Systems and Signal Processing **175**, (1984).

[11] J. Nunn, N.K. Langford, W.S. Kolthammer, T.F.M. Champion, M.R. Sprague, P.S. Michelberger, X.-M. Jin, D.G. England and I.A. Walmsley, preprint arxiv:12081534 (2012).

[12] N. Sangouard, C. Simon, H. de Riedmatten, and N. Gisin, Rev. Mod. Phys. **83**, 33 (2011).

[13] M. Razavi, M. Piani and N. Lütkenhaus, Phys. Rev. A **80**, 032301 (2009).

[14] J. J. Longdell, E. Fraval, M. J. Sellars, and N. B. Manson, Phys. Rev. Lett. **95**, 063601 (2005).

[15] A.V. Gorshkov, A. André, M.D. Lukin, and A.S. Sørensen, Phys. Rev. A **76**, 033805 (2007).

[16] J. Nunn *et al.*, Phys. Rev. A **75**, 011401(R) (2007).

[17] J. Nunn, K. Reim, K.C. Lee, V.O. Lorenz, B.J. Sussman, I.A. Walmsley and D. Jaksch, Phys. Rev. Lett. **101**, 260502 (2008).

[18] S.A. Moiseev and S. Kröll, Phys. Rev. Lett. **87**, 173601 (2001).

[19] B. Kraus *et al.*, Phys. Rev. A **73**, 020302(R) (2006).

[20] N. Sangouard, C. Simon, M. Afzelius, and N. Gisin, Phys. Rev.A **75**, 032327 (2007).

[21] M. Hosseini *et al.*, Nature **461**, 241 (2009).

[22] M. P. Hedges, M. J. Sellars, Y.-M. Li, and J. J. Longdell, Nature **465**, 1052 (2010).

[23] M. Hosseini, G. Campbell, B.M. Sparkes, P.K. Lam and B.C. Buchler, Nature Physics **7**, 794 (2011).

[24] M. Afzelius, C. Simon, H. de Riedmatten, and N. Gisin, Phys. Rev. A **79**, 052329 (2009).

[25] M. Afzelius *et al* , Phys. Rev. Lett. **104**, 040503 (2010).

[26] M.U. Staudt, S.R. Hastings-Simon, M. Nilsson, M. Afzelius, V. Scarani, R. Ricken, H. Suche, W. Sohler, W. Tittel and N. Gisin, Phys. Rev. Lett. **98**, 113601 (2007).

[27] Hamidreza Kaviani, MSc Thesis, University of Calgary, December 2012.

[28] G. Hétet, D. Wilkowski and T. Chaneliére, preprint arxiv:12080677 (2012).

[29] I. Iakoupov and A.S. Sørensen, preprint arxiv:13010705 (2013).

[30] W. Tittel, M. Afzelius, T. Chaneliére, R.L. Cone, S. Kröll, S.A. Moiseev and M. Sellars, Laser and Photon. Rev. **4**, 244 (2010).

[31] E. Fraval, Ph.D. Thesis, Australian National University (2006).

[32] R.L. Ahlefeldt, A. Smith, and M.J. Sellars, Phys. Rev. B **80**, 205106 (2009).

[33] J.R. Maze, A. Gali, E. Togan, Y. Chu, A. Trifonov, E. Kaxiras and M.D. Lukin, New J. Phys. **13**, 025025 (2011).

[34] H.J. Mamin, M. Kim, M.H. Sherwood, C.T. Rettner, K. Ohno, D.D. Awschalom and D. Rugar, Science **339**, 557 (2013).

[35] J.R. Maze, P.L. Stanwix, J.S. Hodges, S. Hong, J.M. Taylor, P. Cappellaro, L. Jiang, M.V. Gurudev Dutt, E. Togan, A.S. Zibrov, A. Yacoby, R.L. Walsworth and M.D. Lukin, Nature(London) **455**, 644 (2008).

[36] Y. Kubo, I. Diniz, A. Dewes, V. Jacques, A. Dréau, J.-F. Roch, A. Auffeves, D. Vion, D. Esteve, and P. Bertet, Phys. Rev. A **85**, 012333 (2012).

[37] Brian Julsgaard, Cécile Grezes, Patrice Bertet and Klaus Mølmer, preprint arxiv:13011500 (2013).

[38] M. Afzelius, N. Sangouard, G. Johansson, M.U. Staudt and C.M. Wilson, preprint arxiv: 13011858 (2013).

[39] N. Bar-Gill, L.M. Pham, A. Jarmola, D. Budker, R.L. Walsworth, preprint arxiv:12117094 (2012).

[40] P.C. Maurer, G. Kucsko, C. Latta, L. Jiang, N.Y. Yao, S.D. Bennett, F. Pastawski, D. Hunger, N. Chisholm, M. Markham, D.J. Twitchen, J. I. Cirac, M. D. Lukin, Science **336**, 1283 (2012).

[41] K.F. Reim *et al.*, Nat. Phot. **4**, 218 (2010).

[42] X.-H. Bao, A. Reingruber, P. Dietrich, J. Rui, A. Dück, T. Strassel,L. Li, N.-L. Liu, B. Zhao and J.-W. Pan, Nature Physics **8**, 517 (2012).

[43] H. P. Specht, C. Nölleke, A. Reiserer, M. Uphoff, E. Figueroa, S. Ritter and G. Rempe, Nature(London) **473**, 190 (2011).

[44] M. Bajcsy, S. Hofferberth, V. Balic, T. Peyronel, M. Hafezi, A.S. Zibrov, V. Vuletic, and M.D. Lukin, Phys. Rev. Lett. **102**, 203902 (2009).

[45] M.R. Sprague, D.G. England, A. Abdolvand, J. Nunn, X.-M. Jin, W. S. Kolthammer, M. Barbieri, B. Rigal, P.S. Michelberger, T.F.M. Champion, P.St.J. Russell, I.A. Walmsley, preprint arxiv:12120396 (2012).

[46] M.U. Staudt, S.R. Hastings-Simon, M. Afzelius, D. Jaccard, W. Tittel, N. Gisin, Optics Communications **266** 720 (2006).

[47] A. Ferrier, C.W. Thiel, B. Tumino, M.O. Ramirez, L.E. Bausá, R.L. Cone, A. Ikesue and Ph. Goldner, Phys. Rev. B **87**, 041102(R) (2013).

[48] M. Sabooni, Q. Li, S. Kröll, L. Rippe, preprint arXiv:1301.0636 (2013).

[49] M. Afzelius and C. Simon, Phys. Rev. A **82**, 022310 (2010).

[50] E. Saglamyurek *et al.*, Nature (London) **469**, 512 (2011).

[51] M. Bonarota, J.-L. Le Gouët and T Chaneliére, New J. Phys. **13**, 013013 (2011).

[52] C. Clausen, I. Usmani, F. Bussiéres, N. Sangouard, M. Afzelius, H. de Riedmatten and N. Gisin, Nature (Londin) **469**, 508 (2011).

[53] M. Hosseini, B.M. Sparkes, G. Campbell, P.K. Lam and B.C. Buchler, Nature Communications **2**, 174 (2011).

[54] S. Chen, Y.-A. Chen, T. Strassel, Z.-S. Yuan, B. Zhao, J. Schmiedmayer, and J.-W. Pan, Phys. Rev. Lett. **97**, 173004 (2006).

[55] W.J. Munro, A.M. Stephens, S.J. Devitt, K.A. Harrison and K. Nemoto, Nature Photonics **6**, 777 (2012).

[56] A.I. Lvovsky, B.C. Sanders, and W. Tittel, Nat. Phot. **3**, 706 (2009).

[57] K. Hammerer, A.S. Sørensen, and E.S. Polzik, Rev. Mod. Phys. **82**, 1041 (2010).

[58] C. Simon *et al.*, Eur. Phys. J. D **58**, 1 (2010).

[59] M.D. Lukin, Rev. Mod. Phys. **75**, 457 (2003).

[60] A.V. Gorshkov, A. André, M. Fleischhauer, A.S. Sørensen, and M.D. Lukin, Phys. Rev. Lett. **98**, 123601 (2007).

[61] G. Hétet, J.J. Longdell, A.L. Alexander, P.K. Lam, and M.J. Sellars, Phys. Rev. Lett. **100**, 023601 (2008).

[62] O. Guillot-Noël, Ph. Goldner, E. Antic-Fidancev, and J.L. Le Gouët, Phys. Rev. B **71**, 174409 (2005).

[63] A. Louchet, J. S. Habib, V. Crozatier, I. Lorgeré, F. Goldfarb, F. Bretenaker, and J.L. Le Gouët, Phys. Rev. B **75** 035131 (2007).

[64] M. Afzelius *et al.*, J. Lumin. **130**, 1566 (2010).

[65] Ph. Tamarat *et al.*, New J. Phys. **10**, 045004 (2008).

[66] A.V. Gorshkov, A. André, M.D. Lukin, and A.S. Sørensen, Phys. Rev. A **76**, 033804 (2007).

[67] J. Simon, H. Tanji, J.K. Thompson, and V. Vuletic, Phys. Rev. Lett. **98**, 183601 (2007).

[68] A. Kalachev and O. Kocharovskaya, Phys. Rev. A **83**, 053849 (2011).

[69] Apart from saturation effects, the equations given below could also describe a single two-level system coupled to a cavity, as e.g. in H.P. Specht *et al.*, Nature **473**, 190 (2011).

[70] A. Kalachev, Phys. Rev. A. **78**, 043812 (2008).

[71] Q. Y. He, M. D. Reid, and P. D. Drummond, Optics Express **17**, 9662 (2009).

[72] M.O. Scully and M.S. Zubairy, *Quantum Optics* (Cambridge University Press, Cambridge, 1997).

[73] T.A. Salaoru and J.R. Woodward, Rev. Sci. Instr. **78**, 036104 (2007).

[74] A.V. Gorshkov, A. André, M.D. Lukin, and A.S. Sørensen, Phys. Rev. A **76**, 033805 (2007).

[75] S.A. Moiseev and W. Tittel, New J. Phys. **13**, 063035 (2011).

[76] $\mathscr{L}^{-1}\{F(s).G(s)\} = \int_0^z dz' f(z')g(z-z')$.

[77] M.G. Raymer, J. Mostowski, Phys. Rev. A **24**, 1980 (1981).

[78] R. M. Macfarlane, Opt. Lett. **18**, 1958 (1993).

[79] B. Lauritzen *et al.*, Phys. Rev. Lett. **104**, 080502 (2010).

[80] P. Kok *et al.*, Rev. Mod. Phys. **79**, 135 (2007).

[81] D.F. Phillips, A. Fleischhauer, A. Mair, and R.L. Walsworth, Phys. Rev. Lett. **86**, 783 (2001).

[82] K.F. Reim *et al.*, Nature Photonics **4**, 218 (2010).

[83] K. Heshami *et al.*, Phys. Rev. A **86**, 013813 (2012).

[84] S.A. Moiseev and S. Kröll, Phys. Rev. Lett. **87**, 173601 (2001); B. Kraus *et al.*, Phys. Rev. A **73**, 020302(R) (2006).

[85] G. Hétet, J.J. Longdell, A.L. Alexander, P.K. Lam, and M.J. Sellars, Phys. Rev. Lett. **100**, 023601 (2008).

[86] A. Kalachev and O. Kocharovskaya, Phys. Rev. A **83**, 053849 (2011).

[87] J.J. Longdell, G. Hétet and P.K. Lam, M.J. Sellars Phys. Rev. A **78**, 032337 (2008).

[88] E. Fraval, M.J. Sellars, and J.J. Longdell, Phys. Rev. Lett. **95**, 030506 (2005).

[89] Dr. Daniel Oblak, private communication.

[90] K.K. Wong, *Properties of Lithium Niobate* (INSPEC, London, 2002).

[91] R.S. Weis and T.K. Gaylord, Appl. Phys. A **37**, 191 (1985).

[92] A. Kalachev and O. Kocharovskaya, J. Mod. Opt. **58**, 1971(2011).

[93] N. Sinclair *et al.*, Journal of Luminescence **130** 1586 (2010).

[94] C.W. Thiel, Y. Sun, T. Böttger, W.R. Babbitt and R.L. Cone, Journal of Luminescence **130** 1598 (2010).

[95] N. Bar-Gill, L.M. Pham, A. Jarmola, D. Budker, R.L. Walsworth, preprint arxiv:12117094 (2012).

[96] Y. Kubo, *et al*, Phys. Rev. A **85**, 012333 (2012).

[97] E. Saglamyurek *et al*, Nature(London) **469**, 512 (2011).

[98] P.R. Hemmer, A.V. Turukhin, M.S. Shahriar and J.A. Musser, Optics Letters **26**, 361 (2001).

[99] K.F. Reim, J. Nunn, V.O. Lorenz, B.J. Sussman, K.C. Lee, N.K. Langford, D. Jaksch and I.A. Walmsley, Nature Photonics **4**, 218 (2010).

[100] E. Togan, Y. Chu, A.S. Trifonov, L. Jiang, J. Maze, L. Childress, M.V.G. Dutt, A.S. Sørensen, P.R. Hemmer, A.S. Zibrov and M.D. Lukin, Nature(London) **466**, 730 (2010).

[101] C. Santori, D. Fattal, S.M. Spillane, M. Fiorentino, R.G. Beausoleil, A.D. Greentree, P. Olivero, M. Draganski, J.R. Rabeau, P. Reichart, B.C. Gibson, S. Rubanov, D.N. Jamieson, and S. Prawer, Optics Express **14**, 7986 (2006).

[102] N.B. Manson and R.L. McMurtrie, J. of Luminescence **127**, 98 (2007).

[103] Ph. Tamarat, N.B. Manson, J.P. Harrison, R.L. McMurtrie, A. Nizovtsev, C. Santori, R.G. Beausoleil, P. Neumann, T. Gaebel, F. Jelezko, P. Hemmer and J. Wrachtrup, New J. Phys. **10** 045004 (2008).

[104] It has to be noted that the non-spin-conserving coupling in the lower branch allows to consider a scheme similar to our proposal that includes $^3A_{20}$ ground state [101], in which the fields are negatively detuned from the lower branch. This will require a separate investigation that considers the branching ratios under a specific strain.

[105] A.V. Gorshkov, A. André, M.D. Lukin, and A.S. Sørensen, Phys. Rev. A **76**, 033804 (2007).

[106] K. Heshami, A. Green, Y. Han, A. Rispe, E. Saglamyurek, N. Sinclair, W. Tittel, and C. Simon, Phys. Rev. A **86**, 013813 (2012).

[107] S. Felton, A.M. Edmonds, M.E. Newton, P.M. Martineau, D. Fisher, D.J. Twitchen, and J.M. Baker, Phys. Rev. B **79**, 075203 (2009).

[108] V. Acosta *et al.*, in preparation (2013).

[109] P.E. Barclay, K.-M. Fu, C. Santori, and R.G. Beausoleil, Optics Express **17**, 9588 (2009).

[110] A. Faraon, P.E. Barclay, C. Santori, K.-M.C. Fu and R.G. Beausoleil, Nature Photonics **5**, 301 (2011).

[111] C. Santori, P.E. Barclay, K.-M.C. Fu, R.G. Beausoleil, S. Spillane and M. Fisch, Nanotechnology **21**, 274008 (2010).

[112] K. Heshami, N. Sangouard, J. Minár, H. de Riedmatten, and C. Simon, Phys. Rev. A **83**, 032315 (2011).

[113] A. I. Lvovsky, B. C. Sanders and W. Tittel, Nat. Phot. **3**, 706 (2009); W. Tittel *et al.*, Las. Phot. Rev. **4**, 244 (2010).

[114] H. J. Kimble, Nature **453**, 1023 (2008).

[115] M. Fleischhauer and M.D. Lukin, Phys. Rev. Lett. **84**, 5094 (2000); T. Chaneliere *et al.*, Nature **438**, 833 (2005); M.D. Eisaman *et al.*, Nature **438**, 837 (2005).

[116] J. Nunn *et al.*, Phys. Rev. A **75**, 011401 (2007); K.F. Reim *et al.*, Nat. Phot. **4**, 218 (2010).

[117] S.A. Moiseev and S. Kröll, Phys. Rev. Lett. **87**, 173601 (2001); B. Kraus *et al.*, Phys. Rev. A **73**, 020302 (2006); A.L. Alexander, J.J. Longdell, M.J. Sellars, and N.B. Manson, Phys. Rev. Lett. **96**, 043602 (2006).

[118] H. de Riedmatten, M. Afzelius, M.U. Staudt, C. Simon, and N. Gisin, Nature **456**, 773 (2008).

[119] R. Zhang, S. R. Garner, and L. V. Hau, Phys. Rev. Lett. **103**, 233602 (2009).

[120] J. Laurat *et al.*, Opt. Express **14**, 6912 (2006).

[121] I. Novikova *et al.*, Phys. Rev. Lett. **98**, 243602 (2007).

[122] A. Amari *et al.*, J. Lumin. **130**, 1579 (2010).

[123] B. Zhao, Y.-A. Chen, X.-H. Bao, T. Strassel, C.-S. Chuu, X.-M. Jin,J. Schmiedmayer, Z.-S. Yuan, S. Chen and J.-W. Pan, Nat. Phys. **5**, 95 (2009).

[124] R. Zhao, Y. O. Dudin, S. D. Jenkins, C. J. Campbell, D. N. Matsukevich, T. A. B. Kennedy and A. Kuzmich, Nat. Phys. **5**, 100 - 104 (2009).

[125] E. Fraval, M. J. Sellars, and J. J. Longdell, Phys. Rev. Lett. **92**, 077601 (2004).

[126] G. Heinze, A. Rudolf, F. Beil, and T. Halfmann, Phys. Rev. A **81**, 011401(R) (2010).

[127] S. E. Beavan, E. Fraval, M. J. Sellars, and J. J. Longdell, Phys. Rev. A **80**, 032308 (2009).

[128] M. Johnsson and K. Mølmer, Phys. Rev. A **70**, 032320 (2004).

[129] E. Fraval, M. J. Sellars, and J. J. Longdell, Phys. Rev. Lett. **95**, 030506 (2005).

[130] All of the operators in the power are local and they commute. Therefore, $e^{i\pi\sum_{j=1}^{N}\sigma_x^{(j)}\otimes\mathbb{1}} = \prod_{j=1}^{N} e^{i\pi\sigma_x^{(j)}\otimes\mathbb{1}}$. It can be shown that $e^{A\otimes\mathbb{1}} = e^A \otimes \mathbb{1}$ and $e^{\mathbb{1}\otimes B} = \mathbb{1}\otimes e^B$ for any operator A and B.

[131] C. Ottaviani *et al.*, Phys. Rev. A **79**, 063828 (2009); M.O. Scully and M.S. Zubairy, Science **301**, 181 (2003).

[132] D. Rideout *et al.*, Class. Quantum Grav. **29**, 224011 (2012).